

12

AFWAL-TR-83-3060



FATIGUE/IMPACT STUDIES IN
LAMINATED COMPOSITES

V. Sarma Avva
Professor of Mechanical Engineering
North Carolina A&T State University
Greensboro, NC 27411

May 1983

Final Report for Period 10 September 1980 to 31 December 1982

Approved for public release; distribution unlimited.

FLIGHT DYNAMICS LABORATORY
AIR FORCE WRIGHT AERONAUTICAL LABORATORIES
AIR FORCE SYSTEMS COMMAND
WRIGHT-PATTERSON AIR FORCE BASE, OHIO 45433

DTIC
ELECTE
S JUL 9 1984 D
B

AD-A142 841

DTIC FILE COPY

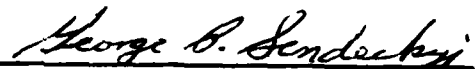
84 05 04 005

NOTICE

When Government drawings, specifications, or other data are used for any purpose other than in connection with a definitely related Government procurement operation, the United States Government thereby incurs no responsibility nor any obligation whatsoever; and the fact that the government may have formulated, furnished, or in any way supplied the said drawings, specifications, or other data, is not to be regarded by implication or otherwise as in any manner licensing the holder or any other person or corporation, or conveying any rights or permission to manufacture use, or sell any patented invention that may in any way be related thereto.

This report has been reviewed by the Office of Public Affairs (ASD/PA) and is releasable to the National Technical Information Service (NTIS). At NTIS, it will be available to the general public, including foreign nations.

This technical report has been reviewed and is approved for publication.



GEORGE P. SENDECKY, Aero. Engr.
Fatigue, Fracture & Reliability Gp.



DAVEY E. SMITH, Chief
Structural Integrity Branch
Structures & Dynamics Division

FOR THE COMMANDER:



RALPH L. KUSTER, JR., Col, USAF
Chief, Structures & Dynamics Division

"If your address has changed, if you wish to be removed from our mailing list, or if the addressee is no longer employed by your organization please notify AFWAL/EDGE, W-PAFB, OH 45433 to help us maintain a current mailing list".

Copies of this report should not be returned unless return is required by security considerations, contractual obligations, or notice on a specific document.

Unclassified

SECURITY CLASSIFICATION OF THIS PAGE (When Data Entered)

REPORT DOCUMENTATION PAGE		READ INSTRUCTIONS BEFORE COMPLETING FORM
1. REPORT NUMBER AFWAL-TR-83-3060	2. GOVT ACCESSION NO. AD-A292 844	3. RECIPIENT'S CATALOG NUMBER
4. TITLE (and Subtitle) Fatigue/Impact Studies in Laminated Composites	5. TYPE OF REPORT & PERIOD COVERED Final Report 80 Sept. 10 to 82 Dec. 31	
7. AUTHOR(s) V. Sarma Avva (formerly A. V. Sharma)	6. CONTRACT OR GRANT NUMBER(s) F33615-80-K-3243	
9. PERFORMING ORGANIZATION NAME AND ADDRESS Department of Mechanical Engineering North Carolina A&T State University 1601 E. Market St., Greensboro, NC 27411	10. PROGRAM ELEMENT, PROJECT, TASK AREA & WORK UNIT NUMBERS PE: 62101F 24010152	
11. CONTROLLING OFFICE NAME AND ADDRESS USAF/AFSC; Flight Dynamics Laboratory, Air Force Wright Aeronautical Laboratories W-PAFB, OH 45433	12. REPORT DATE May 1983	13. NUMBER OF PAGES 152
14. MONITORING AGENCY NAME & ADDRESS (if different from Controlling Office)	15. SECURITY CLASS. (of this report) Unclassified	
16. DISTRIBUTION STATEMENT (of this Report) Approved for public release; distribution unlimited.		
17. DISTRIBUTION STATEMENT (of the abstract entered in Block 20, if different from Report)		
18. SUPPLEMENTARY NOTES		
19. KEY WORDS (Continue on reverse side if necessary and identify by block number) Fatigue and Impact Models, Experimental, Residual Strength, Composites, Graphite/Epoxy, X-Radiography, Damage Documentation, Failure Threshold.		
20. ABSTRACT (Continue on reverse side if necessary and identify by block number) This study primarily addresses the behavior of the laminated fiber composite materials subjected to low velocity projectile impact and or cyclic loading. In particular, the following cases have been studied. 1. The strength degradation of a composite laminate subjected to low velocity projectile impact is studied. The variation of the residual strength of the laminate as a function of the kinetic energy of the impacting projectile (over)		

DD FORM 1473
1 JAN 73

Unclassified

SECURITY CLASSIFICATION OF THIS PAGE (When Data Entered)

Unclassified

SECURITY CLASSIFICATION OF THIS PAGE(When Data Entered)

20. Abstract (continued) - 2

is evaluated thereby establishing a failure threshold curve for a specific laminate - T300/934, $(\pm 45, 0, 90)_{2s}$.

2. The behavior of the same laminate, with and without a centrally-drilled hole, under tensile fatigue loads is assessed experimentally. The resulting σ -N (fatigue stress-number of cycles) curves are shown.

3. The behavior of the laminates subjected to several combinations of fatigue and impact loads is evaluated. The effect of the order of applying the fatigue and impact loads on the strength and the life of the laminates is also determined.

4. The experimental results are compared with results obtained by using some of the existing analytical models applicable to the study of fatigue and impact behavior of the composite laminates.

5. Analyses of the damage resulting from the impact and fatigue loads in the composite laminates are also documented.

Based on the experimental work performed using a graphite/epoxy composite material system with an orientation and a stacking sequence of $(\pm 45, 0, 90)_{2s}$, the following conclusions may be drawn.

1. The residual strength of the impact-damaged laminates can be predicted using an analytical model. The correlation between the experimental and the analytical results was found to be good. Extensive experimental data is not necessary to use the analytical model.

2. Both the power law and the wearout models appear to be useful in predicting the fatigue life of the composite laminates. However, because of the slope parameter, the wearout model appears to have a slight edge over the power law model, particularly at low fatigue life and higher applied stress. The analytical and the experimental results were found to correlate well.

3. The strength degradation due to cyclic loading in notched laminates was found to be extremely small up to a million cycles. The residual strength of the fatigue-damaged laminates was found to increase (in proportion to the applied maximum stress with $R = 0.1$) after a million fatigue cycles.

4. Impact loading followed by cyclic loading was found to be more damaging (in reducing the life of the laminate) than the reversed sequence of loading.

5. The magnitude of the minimum projectile velocity causing catastrophic failure in the laminates tested was found as a function of the applied stress and the number of fatigue cycles.

6. The techniques used to document the damage in the impact- and fatigue-damaged specimens need further refinement.

7. The technique used to propel the projectile at a predetermined velocity needs further improvement.

(continued on additional page)

Unclassified

SECURITY CLASSIFICATION OF THIS PAGE(When Data Entered)

20. Abstract (continued) - 3

8. The development of an analytical model is recommended to predict the minimum impact energy precipitating in a catastrophic failure of the composite materials subjected to cyclical loads.

Accession For	
NTIS GRA&I	<input checked="" type="checkbox"/>
DTIC TAB	<input type="checkbox"/>
Unannounced	<input type="checkbox"/>
Justification _____	
By _____	
Distribution/	
Availability Codes	
Dist	Avail and/or Special
A-1	

BASE COPY INSPECTED

FOREWORD

This final technical report was prepared by V. Sarma Avva (formerly A. V. Sharma), Department of Mechanical Engineering, North Carolina Agricultural and Technical State University for the Flight Dynamics Laboratory, Air Force Wright Aeronautical Laboratories, Air Force Systems Command, Department of the Air Force, Wright-Patterson Air Force Base, Ohio 45433 under a Contract No. F33615-80-K-3243, Project 2401, Work Unit 24010152. The Air Force Program Monitor was Dr. George P. Sendeckyj, AFWAL/FIBE.

Principal Investigator: V. Sarma Avva

Graduate Assistants: J. Rao Vala, M. Jeyaseelan

Technician's Help: Charlie Pinnix

TABLE OF CONTENTS

SECTION	PAGE
I. INTRODUCTION	1
II. LITERATURE REVIEW	3
III. STATEMENT OF WORK	12
IV. ANALYTICAL MODELS	14
1. Residual Strength Model (Impact)	14
2. Fatigue Strength Model	16
V. SPECIMEN DESCRIPTION AND SELECTION	18
VI. EXPERIMENTAL ARRANGEMENT AND TEST PROCEDURE	24
1. Tensile Strength Test	24
2. Impact Tests	24
3. Fatigue Tests With Unnotched Specimens	26
4. Fatigue Tests With Notched Specimens	27
5. Fatigue/Impact Tests	28
6. X-Ray Radiography	29
VII. EXPERIMENTAL DATA	31
1. Tension Tests	31
2. Impact Tests	31
3. Fatigue Tests (Without Notch)	40
4. Fatigue Tests (With Notch)	40
5. Fatigue/Impact Tests (Without Notch)	40
VIII. RESULTS AND ANALYSES	60
1. Static Tension Tests (With and Without Notch)	60
2. Impact Tests	60
3. Fatigue Tests (Unnotched)	77
4. Fatigue Tests (Notched)	106
5. Fatigue/Impact Tests	112
a. Impact/Fatigue Tests	112
b. Fatigue/Impact Tests	117
IX. CONCLUSIONS AND RECOMMENDATIONS	119
REFERENCES	121

TABLE OF CONTENTS (continued)

SECTION	PAGE
APPENDIX A: IMPACT MODEL	125
APPENDIX B: FATIGUE MODEL	129

LIST OF ILLUSTRATIONS

NO.	PAGE
1. Specimen Configuration	19
2. Projectile Firing and Velocity Detecting Mechanism	25
3. Photograph of an Unnotched Laminate Failure Under Ultimate Static Tensile Load	61
4. Photograph of an Unnotched Laminate Failure Under Ultimate Static Tensile Load	62
5. Photograph of a Notched Laminate Failure Under Ultimate Static Tensile Load	63
6. Applied Stress Vs. Kinetic Energy of Projectile	64
7. Normalized Stress Vs. Kinetic Energy of Projectile	65
8. Photograph of an Impact-Damaged Specimen, No. 8-22, Applied Load, P = 14,000 lb.; Velocity, v = 85 fps	67
9. Photograph of an Impact-Damaged Specimen, No. 3-12, Applied Load, P = 8,160 lb.; Velocity, v = 110 fps	68
10. Photograph of an Impact-Damaged Specimen, No. 6-17, Applied Load, P = 6,600 lb.; Velocity, v = 226 fps	69
11. Photograph of an Impact-Damaged Specimen, No. 3-4, Applied Load, P = 6,860 lb.; Velocity, v = 335 fps	70
12. Photograph of an Impact-Damaged Specimen, No. 6-11, Applied Load, P = 6,600 lb.; Velocity, v = 226 fps	71
13. Photograph of an Impact-Damaged Specimen, No. 13-32, Applied Load, P = 6,860 lb.; Velocity, v = 335 fps	72
14. Photograph of an Impact-Damaged Specimen, No. 4-7, Applied Load, P = 6,350 lb.; Velocity, v = 71 fps	73
15. Photograph of an Impact-Damaged Specimen, No. 11-13, Applied Load, P = 6,220 lb.; Velocity, v = 353 fps	74
16. Projectile Rebound Velocity Vs. Forward Velocity	76
17. Laminate Stress Vs. Kinetic Energy of Projectile/Unit Thickness; Comparison of Experimental and Analytical Results	84

LIST OF ILLUSTRATIONS (continued)

No.	PAGE
18. σ -N Curve for an Unnotched T300/934 Laminate, R = 0.1, f = 10 Hz	86
19. σ -N Curve for an Unnotched Laminate - Analytical and Experimental Results	89
20. Log-Log Plot of σ -N Data for an Unnotched Laminate: Wearout Model and Experimental Results	90
21. Probability of Survival Vs. σ_e , Equivalent Static Strength Curve: Wearout Model-Analytical and Experimental	91
22. Probability of Survival Vs. σ_e , Equivalent Static Strength Curve: Power Law Model-Analytical and Experimental	92
23. Radiograph: Progressive Damage Documentation, Specimen No. 8-32, $\sigma = 0$, R = 0, N = 0	94
24. Radiograph: Progressive Damage Documentation, Specimen No. 8-32, $\sigma = 34.09$ ksi, R = 0.1, N = 200,000 cycles	94
25. Radiograph: Progressive Damage Documentation, Specimen No. 8-32, $\sigma = 34.09$ ksi, R = 0.1, N = 400,000 cycles	95
26. Radiograph: Progressive Damage Documentation, Specimen No. 8-32, $\sigma = 34.09$ ksi, R = 0.1, N = 600,000 cycles	95
27. Radiograph: Progressive Damage Documentation, Specimen No. 8-32, $\sigma = 34.09$ ksi, R = 0.1, N = 800,000 cycles	96
28. Radiograph: Progressive Damage Documentation, Specimen No. 8-32, $\sigma = 34.09$ ksi, R = 0.1, N = 1,000,000 cycles	96
29. Radiograph: Progressive Damage Documentation, Specimen No. 10-26, $\sigma = 0$, R = 0, N = 0	97
30. Radiograph: Progressive Damage Documentation, Specimen No. 10-26, $\sigma = 35.81$ ksi, R = 0.1, N = 200,000 cycles	97
31. Radiograph: Progressive Damage Documentation, Specimen No. 10-26, $\sigma = 35.81$ ksi, R = 0.1, N = 400,000 cycles	98
32. Radiograph: Progressive Damage Documentation, Specimen No. 10-26 $\sigma = 35.81$ ksi, R = 0.1, N = 600,000 cycles	98

LIST OF ILLUSTRATIONS (continued)

NO.	PAGE
33. Radiograph: Progressive Damage Documentation, Specimen No. 10-26, $\sigma = 35.81$ ksi, $R = 0.1$, $N = 800,000$ cycles	99
34. Radiograph: Progressive Damage Documentation, Specimen No. 10-26, $\sigma = 35.81$ ksi, $R = 0.1$, $N = 1,000,000$ cycles	99
35. Radiograph: Progressive Damage Documentation, Specimen No. 5-10, $\sigma = 0$, $R = 0$, $N = 0$	100
36. Radiograph: Progressive Damage Documentation, Specimen No. 5-10, $\sigma = 63.74$ ksi, $R = 0.1$, $N = 5,000$ cycles	100
37. Radiograph: Progressive Damage Documentation, Specimen No. 5-10, $\sigma = 63.74$ ksi, $R = 0.1$, $N = 15,000$ cycles	101
38. Radiograph: Progressive Damage Documentation, Specimen No. 5-10, $\sigma = 63.74$ ksi, $R = 0.1$, $N = 30,000$ cycles	101
39. Radiograph: Progressive Damage Documentator, Specimen No. 5-10, $\sigma = 63.74$ ksi, $R = 0.1$, $N = 45,000$ cycles	102
40. Radiograph: Progressive Damage Documentator, Specimen No. 5-10, $\sigma = 63.74$ ksi, $R = 0.1$, $N = 70,000$ cycles	102
41. Radiograph: Progressive Damage Documentation, Specimen No. 5-10, $\sigma = 63.74$ ksi, $R = 0.1$, $N = 120,000$ cycles	103
42. Radiograph: Progressive Damage Documentation, Specimen No. 6-5, $\sigma = 0$, $R = 0$, $N = 0$	104
43. Radiograph: Progressive Damage Documentation, Specimen No. 6-5, $\sigma = 66.67$ ksi, $R = 0.1$, $N = 5,000$ cycles	104
44. Radiograph: Progressive Damage Documentation, Specimen No. 6-5, $\sigma = 66.67$ ksi, $R = 0.1$, $N = 10,000$ cycles	105
45. Radiograph: Progressive Damage Documentation, Specimen No. 6-5, $\sigma = 66.67$ ksi, $R = 0.1$, $N = 15,000$ cycles	105
46. σ -N Curve for a Notched T300/934 Laminate, $R = 0.1$, $f = 10$ Hz.	108

LIST OF TABLES

NO.		PAGE
1.	Specimen Selection Chart: Impact Tests	20
2.	Specimen Selection Chart: Fatigue Tests (Without Notch)	21
3.	Specimen Selection Chart: Fatigue Tests (With Notch)	22
4.	Specimen Selection Chart: Fatigue/Impact Tests	23
5.	Ultimate Stress-Strain Data (Without Notch)	32
6.	Ultimate Stress-Strain Data (With Notch)	33
7.	Impact Test Data	34
8.	Fatigue Test Data (Without Notch)	41
9.	Fatigue Test Data (With Notch)	47
10.	Impact/Fatigue Test Data	52
11.	Fatigue/Impact Test Data	57
12.	Impact Test Data (K.E./Unit Thickness)	78
13.	Impact Tests: Percentage Error - Analytical/Experimental	85

SECTION I
INTRODUCTION

The evaluation of the fatigue behavior of the high performance fiber composites is a complex process. The term fatigue may be defined as "a change of materials properties such as strength, stiffness, and life during the cyclic, periodic, or extended application of external environments such as loads, strains, temperature, moisture, radiation, and the like" (1)*. The fatigue strength is one of the essential properties needed in the design of light weight, high strength components fabricated with the fiber composites. Various factors such as the ply-orientation and stacking sequence, fabrication variables, etc., would affect the fatigue strength of the laminated composites. In addition, artificially implanted flaws or mechanically damaged laminates would lead to reduced laminate strength (2). The fatigue strength, in general, would vary with the cyclical loading. Further, the fatigue strength of a typical composite laminate (with an implanted flaw such as a smooth circular hole through the entire thickness) as a function of the number of cycles to failure will also degrade. In general, the fatigue failures would be accompanied by progressive delaminations, fiber-splitting, and (in compression mode) fiber-buckling (3).

Just like the fatigue strength, the residual strength of the laminated composites subjected to low velocity projectile

*Numbers in parentheses designate References at end of the report.

impact is also one of the important factors to be considered in the design of components with fiber composites. Low velocity impact damage could take place in composites due to runway debris, foreign objects such as hand tools etc. Such damage may or may not be clearly visible and yet, it results in a loss of the laminate strength. The impact-damaged laminates under controlled conditions exhibit many characteristics similar to the fatigue-damaged composites. Strength reduction is one of the common features. The damaged laminate under the fatigue or impact loads typically exhibits delaminations, debonding, fiber breakage, interfacial phenomena, etc. There are many experimental techniques presently available to study the characteristics of the damaged laminates. There are also some analytical models to predict the behavior of the laminates subjected to impact and fatigue loads.

The behavior of the laminated composite materials subjected to a combination of low velocity projectile impact and axial fatigue loads is not fully understood. The order in which these two loads (impact and fatigue) are applied to the laminate could have an effect on the residual strength of the composite material. Further, the presence of implanted flaws (in the form of a hole) in the laminate subjected to fatigue loads could have some identifiable common characteristics with the behavior of the impact-damaged laminates exposed to cyclical loads.

SECTION II
LITERATURE REVIEW

The use of laminated composites as primary structural materials has generated the need to characterize the response of these materials under all anticipated loading conditions such as impact loads, cyclical loads, etc. One of the major problems encountered in the structural application of composite materials is their low impact resistance. These materials are being applied to jet engine fan and compressor blades as well as to aircraft structures, all of which are subjected to some kind of hard body (stones, rivets, ice balls, dropping of hand tools, etc.) and soft body (birds) impact. Consequently, it is of interest to study the impact damage caused by low velocity projectiles to composite materials.

Two modes of failure are typically observed when a composite material is impacted by a foreign object. Hard objects mainly cause local damage which in turn may result in significant strength degradation upon subsequent fatigue loading. On the other hand, a soft body impact might directly cause an overall structural failure due to large deformations at the blade root. However, for certain impact parameters (mass, materials, velocity and geometry), a soft body may cause local damage only (such as in the leading edge of a blade) exhibiting a loss of mass without gross failure at the root. Small object impact on composites causes mainly local damage which is limited by and large to the immediate impact areas. This type of damage appears in the form

of indentation, lateral and axial cracks, perforations, delaminations and spallation. The type of damage depends largely on the material type and thickness of the laminate, mass and striking velocity of the impactor. The major effect with these types of damage is a reduction in the strength of the impacted laminate.

For low impact velocities, no strength degradation is observed. The range of these impact velocities for which no damage is produced can be very small for the case of a hard object impacting a brittle material (4) and much larger for small soft object impacts (5). When a specimen is subjected to a localized hard particle impact at a velocity and then loaded to failure, the resulting strength will be less than the original strength. The same result can be achieved by implanting a flaw through the thickness and stressing it to failure. Using fracture mechanics, a theoretical model was developed (6) to evaluate the residual strength of impact-damaged laminates. In developing this model, it was assumed that the difference between the energy density required to break an undamaged and an impact-damaged specimen is directly proportional to the kinetic energy imparted to the specimen. The models, developed by Waddoups, et. al., (7) and Husman, et. al., (6) to predict the residual strength of impact-damaged specimens appear to be similar if the concept of crack in (7) is replaced with a circular hole (6). Another relationship between the residual strength and the kinetic energy was developed (8). This relationship using

the concept of notched strength was proposed by Whitney and Nuismer (8). Various theoretical approaches to study the behavior of the notched composites based on linear elastic fracture mechanics and other methods have been reviewed by Yeow, et. al. (9). Experimental verification of theoretical models was also common in many of the studies reviewed in (9). The experimental studies (10-13) typically deal with the effect of implanted flaws such as holes and slots of known dimensions in composite materials as a function of variables such as lamina configuration (ply orientation and stacking sequence), fiber/matrix combination, specimen width to projectile diameter ratio, etc.

The use of reinforced materials in applications subjected to dynamic loads depends to a large extent on their ability to withstand the cyclic loading which is one of the most important reasons to investigate the fatigue behavior of composite materials. A considerable amount of research work has been done on isotropic materials to understand their fatigue behavior. It may be described as the growth of a single dominant crack initiated by a dislocation or pre-existing void in the material at the micro-structural level. The knowledge so gained from the fatigue behavior of isotropic materials is not sufficient to understand the failure mechanisms in fiber-reinforced composite materials as they are inhomogeneous and anisotropic. The fatigue strength in composites depends on the type of material, fiber orientation, stacking sequence, test frequency, stress ratio, etc., which

restricts the generalization of the fatigue behavior even for a given combination of composite material.

Several investigators (14-16) reported that the frequency of testing has significant effect on the fatigue response of some composites. On studying the tests conducted at various frequencies, it was suggested that multidirectional carbon- and boron-epoxies with some zero degree fibers can be tested up to 20 Hz. For composites containing fibers with a lower modulus, a test frequency of 10 Hz was recommended. According to Hahn and Kim (15), at higher stress levels, the fiber breakage and matrix cracking leads to fracture. At lower stresses, the micro-cracks in the matrix grow perpendicular to the loading direction causing several random fiber breakages (17). Such a failure is the result of reduction in the effective cross-sectional area. The crack created by a fiber break tends to grow into the matrix at a higher loading rate (18). Thus, the composite strength may decrease with increasing loading rate (19). The subsequent crack growth also depends on the level of the applied stress at which the fiber breaks. If the fiber breaks at a low stress level due to defects or weaknesses (20, 21), the crack is more likely to lead to interfacial debonding than to extend into the matrix (19). Consequently, when a composite system contains many weak fibers, substantial number of fibers break before the failure of the composite takes place. There would be a larger number of fiber breaks in longer specimens than in shorter

specimens at the same level of applied stress. Hence, longer specimens tend to exhibit brush-like failure when compared to shorter specimens. The fatigue cracks in composites can initiate at the free surface as in metals and additionally at fiber breaks or fiber ends (22 - 24). Some of the fibers can break at as low as half of the ultimate strength (24). At higher volume fractions of fibers, there are more fiber breaks and hence more crack initiation sites. However, at the same time, more fibers act as crack arrestors and more effective retardation of crack growth will be realized (25.)

If the matrix has higher stiffness and yield strength yet is highly ductile, the stress transfer from broken fibers to the neighboring unbroken ones is more effective and the fracture surface becomes fairly planar with no signs of longitudinal cracking in the matrix (23). For the same reason the possibility of interfacial debonding increases. Since the fiber fracture is brittle when it happens, the net effect can be an increased crack growth rate and the composite becomes more fatigue sensitive than the matrix. For composites in which the matrix is well within the elastic range up to the composite failure, the fatigue damage in the matrix will be negligible, except at the sites of fiber breaks. Consequently, the modulus and the strength do not decrease until the fracture is imminent (26, 27).

Several investigators (28 - 30) have shown a possible relationship between the static strength and the fatigue life. The relationship is such that, among similar elements, a stronger element also has a longer life. In multidirectional composite laminates, depending upon the stacking sequence and delaminations (31 - 34), the final failure under tensile loading is invariably preceded by the failure of weaker plies. In general, the delamination surfaces consist of two distinct areas - one shiny and the other dull. It was reported (35) that SEM (Scanning Electron Microscope) photographs of delaminated surface revealed that the shiny areas have bare fibers on the surface while the dull areas have only traces of fibers in the epoxy. Apparently, the bare fibers act like convex mirrors, thereby producing macroscopically shiny surfaces. On the other hand, fiber traces are similar to concave mirrors and hence limit the reflection of light.

Three dimensional fatigue failure criterion for unidirectional composites under a state of cyclic stresses was discussed by Z. Hashin (36). Two distinct failure modes, fiber mode and matrix mode were modelled separately. In many applications, it is sufficient to deal with plane stress but the need for three dimensional state of stress arises predominantly near holes in the laminate and at the laminate edges. Fatigue failure criteria for three dimensional cyclic stress are of particular importance for fatigue failure analysis of notched laminates. The state of stress in the laminate near the notch is three dimensional and

can only be obtained by numerical methods such as finite element methods. The failure criteria developed (36) can be used to predict the location of the first failure, the mode and the number of cycles of failure. In Z. Hashin's analysis (36), the separation of bond between the two laminae due to shear and normal stress was not considered.

Many theoretical models have been developed to predict the fatigue life, such as the wearout and power law models (37), which will control the deterministic equation of the σ -N diagram. A residual strength model was suggested (38) in which it was shown that a specimen will decrease in its strength corresponding to its fatigue life cycles. The decrease in the residual strength has been used as a measure of fatigue life. The application of the wearout and power law models is shown in the subsequent sections of this report.

The analysis of a composite specimen with a centrally drilled hole involves two parts, viz., static failure analysis and fatigue failure analysis. The static failure model, at the laminate level, is divided (39) into three regions: (i) a central core region which is the projection of the notch in loading direction; (ii) an overstressed region of average stress concentration, adjacent to the core region; and (iii) an average stress region. This model adequately predicts (40) the gross heterogeneous behavior of the laminate in the overstressed and average stress regions. The stress state in the vicinity of the notch, though,

indicates the presence of high interlaminar stresses. In some laminates, these interlaminar stresses are large enough to cause a delamination or peeling off of one ply from another (41).

A "mechanistic wearout" concept used in earlier studies (41) underlines the basic philosophy of the laminate fatigue behavior. On fatigue loading, material property degradation is predominant in the vicinity of the notch due to stress concentration effects. An experimental characterization of the lamina fatigue data helps estimate the degradation in laminate properties due to cyclic loading. The material property degradation on fatigue loading, when incorporated into the static failure model described earlier, could lead to fatigue failure modes and strengths that are very different from the static predictions (40).

Schutz, et. al. (42) reported that a typical feature of specimens with holes is the occurrence of longitudinal cracks originating at the hole, whereupon the fracture can run partly along these longitudinal cracks. These cracks are visible only for load cycle numbers greater than 10^3 . Some of the conclusions from this study (42) are: (1) stress concentration in specimens containing open holes reduces the static tensile strength by comparison with plain specimens, (2) stress concentration reduces the fatigue strength in the short-life region, and in the long-life region, its effect disappears. Ramkumar (40) reports that the residual strength after 10^7 cycles was greater than or equal to the virgin strength. The increase in strength with fatigue

probably is due to stress redistribution that accompanies fatigue damage.

SECTION III

STATEMENT OF WORK

This study primarily addresses the behavior of the laminated fiber composite materials subjected to low velocity projectile impact and cyclical loading. In particular, the following cases have been studied:

1. The strength degradation of a composite laminate subjected to low velocity projectile impact is studied. The variation of the residual strength of the laminate as a function of the kinetic energy of the impacting projectile is evaluated thereby establishing a failure threshold curve for a specific laminate.
2. The behavior of the same laminate, with and without a centrally drilled hole, under tensile fatigue loads is assessed experimentally. The resulting σ -N (fatigue stress-number of cycles) curves are shown.
3. The behavior of the laminate subjected to several combinations of fatigue and impact loads is evaluated. The effect of the order of applying the fatigue and impact loads on the strength and the life of the laminates is also determined.
4. The experimental results are compared with results obtained by using some of the existing

analytical models applicable to the study of fatigue and impact behavior of the composite laminates.

5. Analyses of the damage resulting from the impact and fatigue loads in the composite laminates are also documented.

SECTION IV
ANALYTICAL MODELS

Two types of analytical models are presented here briefly. These models are not new. However, the results obtained using these models are compared with the experimental data.

1. Residual Strength Model

At very low impact energy levels, many laminated composite materials do not show any significant static strength degradation. Since significant damage does not occur at velocities less than the threshold damage velocity, it may be assumed that the damage is proportional to the difference between the kinetic energy of impact and the threshold damage kinetic energy. The preceding statement may be expressed as (43)

$$c = k (W - W_0) \quad (a)$$

where c = damage as an effective through the thickness crack of length $2c$
 k = constant depending on the material and the laminate
 W = kinetic energy of impact per unit thickness
 W_0 = threshold damage kinetic energy per unit thickness

The average stress criterion developed by Whitney and Nuismer (8) for an isotropic laminate is given by

$$(\sigma_N^\infty / \sigma_0) = [(1 - \tau_1) / (1 + \tau_1)]^{1/2} \quad (b)$$

where σ_N^∞ = failure stress of an infinite plate containing a crack (notch) of length $2c$
 σ_0 = failure stress of an unnotched plate
 τ_1 = $c / (c + a_0)$
 a_0 = characteristic dimension adjacent to discontinuity.

Substituting for τ_1 in equation (b),

$$(\sigma_N^\infty / \sigma_0) = [(a_0) / (2c + a_0)]^{1/2} \quad (c)$$

Equations (a) and (c) can be combined resulting in the following:

$$(\sigma_N^\infty / \sigma_0) = 1 / [(2k/a_0)(W-W_0) + 1]^{1/2} \quad (d)$$

Assuming $\sigma_N^\infty = \sigma_r$, residual strength of the specimen and $(k/a_0) = K$, a constant, the equation (d) can be re-written in the following form:

$$(\sigma_r / \sigma_0) = [2K(W-W_0) + 1]^{-1/2} \quad (e)$$

The above relationship can be used to predict the residual strength of a laminate for different values of kinetic energy. In order to determine the values of $2K$ and W_0 , equation (e) is re-written in linear form as:

$$y = ax + b$$

where $y = (\sigma_r / \sigma_0)^2$

$$x = W$$

$$a = 2K$$

$$b = (1 - 2KW_0)$$

The ultimate strength σ_0 and the post-impact residual strength σ_r at different velocities are determined by performing tests on a few specimens. Using linear regression analysis, a best fit is obtained for the data and the values for $2K$ and W_0 are thus determined. These values are used in equation (e) to predict the residual strength at any velocity of impact. Additional details on the application of this model can be found in a report by Avva (44). The numerical results pertaining to this report are given in Appendix A.

2. Fatigue Strength Model

A new procedure for fitting fatigue models to experimental data was developed by Sendeckyj (37). This procedure consists of transforming the fatigue data into equivalent static strength data using a deterministic equation with unknown parameters. The maximum-likelihood estimate of the shape parameter (in a two-parameter Weibull distribution) can be obtained using iterative procedures. The wearout model adopted by Sendeckyj (37) is given by the following deterministic equation

$$\sigma_e = \sigma_a [(\sigma_r/\sigma_a)^{1/s} + (n-1)C]^s \quad (a)$$

where σ_e , σ_a , σ_r , and n are the equivalent static strength, maximum applied cyclic stress, residual strength, and number of cycles, respectively. The parameter s is the absolute value of the asymptotic slope at long life on a log-log plot of the σ - N curve. The parameter C is a measure of the extent of the "flat" region on the σ - N curve at high applied cyclic stress levels. The probability that the static strength is higher than σ_e is given by

$$P(\sigma_e) = \exp[-(\sigma_e/\beta)^\alpha] \quad (b)$$

where α and β are the Weibull shape and scale parameters, respectively. The implications of the parameters s and C were discussed in detail in Reference (37). If the value of $C = 1$ in equation (a), the power law fatigue failure criterion is obtained. Thus,

$$\sigma_e = \sigma_a [(\sigma_r/\sigma_a)^{1/s} + (n-1)]^s \quad (c)$$

The reduction of experimental data and the calculations leading to the determination of the parameters in equations (a) to (c) were performed using a computer program written for this purpose (37). The numerical results are shown in Appendix B.

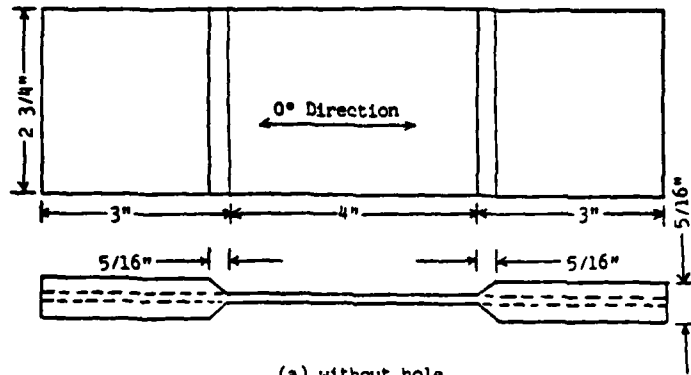
SECTION V
SPECIMEN DESCRIPTION AND SELECTION

The material combination for the fabrication of specimens was Thornel 300/Fiberite 934 with a stacking sequence of $(\pm 45, 0, 90)_{2s}$. Each lamina had a nominal cured thickness of 0.005". Specimens were provided with tapered tabs of glass/epoxy or glass-phenolic with a geometry as shown in Figure 1.

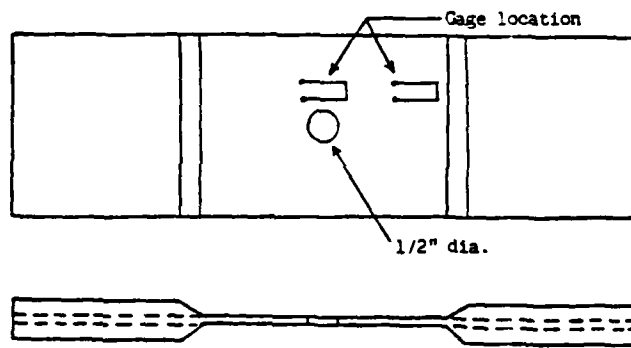
The fabricator supplied 400 specimens cut from 13 different large panels. The location of each specimen in the panel X is shown below:

X-1	X-2	X-3	X-4	X-5	X-6	X-7	X-8	X-9	X-10	X-11
X-12	X-13	X-14	X-15	X-16	X-17	X-18	X-19	X-20	X-21	X-22
X-23	X-24	X-25	X-26	X-27	X-28	X-29	X-30	X-31	X-32	X-33

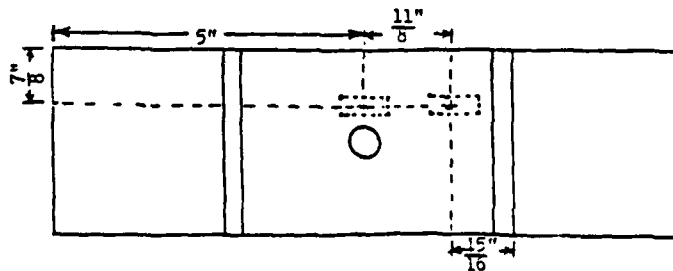
Some of the specimens were (apparently) retained by the fabricator to comply with quality assurance specifications. The specimens were initially selected for each of the proposed tests using the standard randomization techniques and table of random digits. Approximately 50 - 70 specimens were used in each of the four major test phases. Every data point was generated from testing approximately five specimens. Charts of panel number and specimen number within the panel for a particular test phase are shown in Tables 1 through 4. As testing was progressing, some specimens were found to be warped subsequent to receiving them from the fabricator. Such specimens were replaced with others using the same randomization techniques as indicated earlier.



(a) without hole



(b) with hole



Measurements Group, Inc., Gage: CEA-06-2°OUW-350

(c) Gage location and designation

Figure 1. Specimen Configuration.

TABLE 1. IMPACT ENERGY TEST

Proposed Test Condition No.	Specimens tested (X-N) [X - Panel Number] [N - Specimen Number]
1	4 - 12, 7 - 17, 10 - 23, 12 - 4, 13 - 8
2	4 - 27, 7 - 5, 8 - 19, 11 - 6, 13 - 2
3	1 - 4, 2 - 24, 4 - 7, 7 - 29, 10 - 8
4	1 - 24, 4 - 4, 7 - 13, 9 - 9, 13 - 32
5	1 - 10, 6 - 11, 8 - 24, 11 - 25, 12 - 15
6	1 - 14, 4 - 18, 6 - 14, 7 - 14, 13 - 7
7	2 - 6, 3 - 12, 9 - 8, 10 - 17, 11 - 27
8	2 - 19, 5 - 28, 7 - 32, 10 - 18, 11 - 13
9	1 - 12, 3 - 4, 7 - 5, 9 - 33, 13 - 30
10	1 - 22, 3 - 26, 4 - 15, 11 - 7, 13 - 26
11	3 - 7, 4 - 23, 5 - 5, 7 - 31, 8 - 3
12	4 - 10, 6 - 4, 8 - 22, 9 - 32, 13 - 25
13	2 - 25, 3 - 31, 6 - 17, 10 - 33, 12 - 9

TABLE 2. FATIGUE TEST WITHOUT AN IMPLANTED FLAW

Proposed Test Condition No.	Specimen Tested (X-N) [X - Panel Number] [N - Specimen Number]
1	9 - 13, 7 - 24, 11 - 19, 5 - 9, 12 - 10
2	12 - 18, 1 - 29, 9 - 4, 10 - 31, 3 - 9
3	4 - 16, 12 - 19, 10 - 24, 7 - 28, 6 - 13
4	3 - 14, 7 - 19, 9 - 12, 5 - 27, 10 - 32
5	9 - 26, 7 - 7, 1 - 25, 3 - 30, 13 - 10
6	2 - 18, 10 - 25, 6 - 32, 7 - 22, 9 - 19
7	11 - 24, 5 - 29, 9 - 16, 12 - 28, 8 - 32
8	4 - 32, 6 - 24, 13 - 5, 5 - 10, 1 - 8
9	8 - 2, 5 - 14, 2 - 33, 9 - 27, 3 - 15
10	12 - 21, 2 - 23, 6 - 5, 11 - 28, 8 - 11
11	9 - 30, 4 - 11, 8 - 13, 7 - 10, 11 - 29
12	13 - 16, 11 - 26, 3 - 5, 7 - 16, 2 - 11
13	5 - 23, 4 - 20, 10 - 22, 6 - 20, 12 - 7

TABLE 3. FATIGUE TEST WITH AN IMPLANTED FLAW

Proposed Test Condition No.	Specimen Tested (X-N) [X - Panel Number] [N - Specimen Number]
1	4 - 17, 7 - 27, 6 - 9, 2 - 5, 13 - 24
2	1 - 26, 3 - 25, 9 - 15, 6 - 21, 13 - 6
3	3 - 29, 8 - 31, 10 - 20, 2 - 22, 1 - 2
4	6 - 12, 5 - 15, 8 - 17, 2 - 20, 12 - 2
5	7 - 12, 8 - 4, 12 - 8, 13 - 20, 4 - 22
6	6 - 7, 3 - 27, 8 - 23, 11 - 22, 9 - 10
7	10 - 2, 5 - 7, 12 - 5, 2 - 26, 9 - 21
8	10 - 6, 13 - 27, 11 - 20, 3 - 8, 6 - 15
9	7 - 15, 2 - 29, 12 - 14, 9 - 11, 11 - 10
10	5 - 33, 9 - 6, 3 - 20, 2 - 17, 8 - 7
11	1 - 32, 4 - 10, 13 - 19, 3 - 28, 11 - 10
12	4 - 31, 1 - 3, 2 - 28, 11 - 21, 10 - 16
13	9 - 17, 2 - 21, 11 - 10, 5 - 4, 3 - 17

TABLE 4. FATIGUE/IMPACT TESTS

Proposed Test Condition No.	Specimen Tested (X-N) [X-Panel Number] [N-Specimen Number]
1	12 - 26, 2 - 8, 6 - 2, 8 - 10, 13 - 31
2	9 - 5, 1 - 16, 6 - 19, 3 - 10, 5 - 11
3	13 - 9, 9 - 31, 6 - 10, 2 - 7, 10 - 30
4	3 - 28, 10 - 7, 8 - 15, 6 - 8, 2 - 14
5	13 - 15, 1 - 28, 3 - 32, 6 - 3, 8 - 8
6	6 - 31, 7 - 8, 5 - 13, 3 - 24, 10 - 11
7	5 - 25, 6 - 30, 2 - 2, 7 - 12, 10 - 9
8	9 - 22, 12 - 16, 8 - 29, 5 - 12, 3 - 17
9	13 - 12, 13 - 3, 1 - 32, 6 - 29, 8 - 6
10	6 - 26, 6 - 27, 5 - 26, 6 - 28
11	13 - 4, 5 - 6, 10 - 27, 3 - 17, 6 - 33
12	1 - 33, 13 - 13, 1 - 9, 2 - 3, 5 - 2
13	9 - 24, 7 - 3, 9 - 20, 10 - 16, 13 - 14

SECTION VI

EXPERIMENTAL ARRANGEMENT AND TEST PROCEDURE

The tests were carried out using a closed-loop hydraulic testing machine of 55 kips loading capacity. The grips were hydraulically operated. The testing machine has provision for three modes of operation, viz., load, strain and stroke. If it is desired, the mode of operation can be changed any time during the operation. There are four ranges in which each mode can be operated, viz., 100%, 50%, 20% and 10%. Depending upon the maximum expected operating value of load or stroke, an appropriate range can be selected.

A brief description of the tests performed is given here.

1. Tensile Strength Test

Static ultimate strength and strain values of the laminate were determined using 11 specimens. The dimensions (thickness and width) of each of the selected specimens were measured at least at three different points on the specimens. Foil type strain gages were bonded, back to back, in the center of the specimen to measure the load-induced axial strains. Standard strain gage bonding techniques were used. The load and the corresponding strains were recorded using an x-y plotter. The tension test was continued until failure took place. The tensile load was applied at a rate of 2% strain per minute.

2. Impact Test

A schematic view of the projectile firing mechanism is shown in Figure 2. An air supply line is connected to a reservoir through

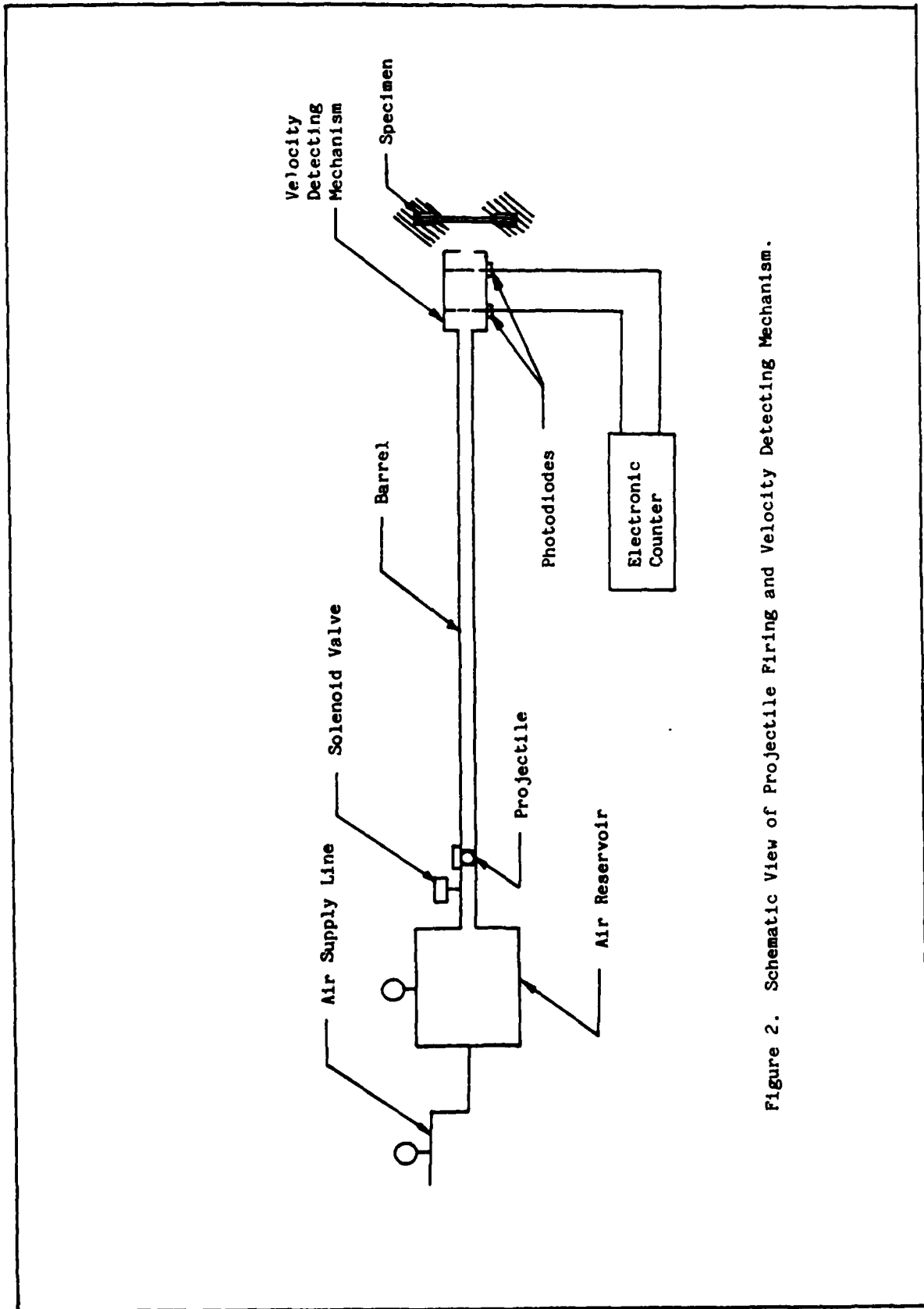


Figure 2. Schematic View of Projectile Firing and Velocity Detecting Mechanism.

a butterfly valve. A (gun) barrel connected to the reservoir acts as a smooth guide to the projectile. Two photo-diodes located at 15.24 cm (6 in.) apart at the other end of the barrel are connected to an electronic counter. As the projectile travels through the barrel, light beams emitted by the photo-diodes are interrupted. An electronic counter starts when the first light beam is interrupted by the projectile and stops when the second light beam is interrupted. Thus, the counter records the time taken by the projectile to travel a distance of 15.24 cm (6 in.) and hence the average forward velocity of the projectile can be determined. A solenoid valve is used to release the compressed air from the reservoir which in turn propels the projectile through the barrel. The projectile is an aluminum sphere 1.27 cm (0.5 in.) in diameter. These tests were conducted to determine the failure threshold level of the composite laminate. The specimens were subjected to different pre-loads in tension and were then impacted by the projectile at different velocities. Some of the specimens failed catastrophically upon impact. Those specimens that survived the impact were subjected to continued loading until failure occurred and the residual strength was found.

3. Fatigue Tests with Unnotched Specimens

The tension-tension fatigue tests were conducted at a frequency of 10 Hz (haversine function) and a stress ratio (ratio of minimum stress to the maximum applied stress on a specimen)

of 0.1. The σ -N diagram was generated by using fatigue lives at ten different stress levels. At each stress level, about five specimens were tested out of which two specimens were radiographed at regular intervals - after a predetermined number of cycles - for damage analyses till the failure of the specimen or completion of 10^6 cycles took place. All the specimens that have completed a million load cycle were considered as runouts and were tested for their residual strength.

4. Fatigue Tests With Notched Specimens

Five specimens were used to evaluate the static ultimate tensile strength of the notched laminate. A clean, smooth hole of 0.5 in. diameter (same diameter as that of the aluminum projectile used) was drilled in the geometric center of each of the specimens. Radiographs of the specimens after drilling the hole were taken to ensure that the drilling-induced damage around the hole was not "abnormal."

Two strain gages (see Fig. 1-c), one near the hole and another near the tab, were bonded on each side of the specimen using M-Bond 200 adhesive. The strain gages were connected to the x-y recorders through a Wheatstone bridge and an amplifier for strain measurements. After checking for the continuity of the circuits and balancing, the specimen was held between the hydraulic grips. A strain rate of 0.02 inch/inch/min. was adopted using the stroke mode of operation. The specimen was loaded using the ramp function and the maximum load at failure observed in the Random

Access Memory of the data display was counterchecked with that recorded by the x-y recorders.

The fatigue tests on the notched specimens were conducted under the same conditions as those of the unnotched specimens. Some of these tests were interrupted after attaining a predetermined number of cycles of operation for the purpose of documenting the progressive damage that may be taking place within the specimens. All the specimens which completed 10^6 cycles before failure took place were considered as runouts and were tested for their residual strength.

5. Fatigue/Impact Tests

The objective in these tests, as indicated earlier, was to study the behavior of the composite laminate subjected to impact loads followed by cyclic loads and vice-versa. The cyclic frequency of loading and the stress amplitude ratio were the same as before. The specimen was preloaded statically to a (maximum) stress value (with $R = 0.1$) and was then impacted at a predetermined velocity. If it had survived the impact, it was then subjected to cyclic loading until fatigue failure took place. On the other hand, if the specimen failed upon impact, the magnitude of the static tensile stress was reduced and the process was repeated. Sometimes, the velocity of the impacting projectile was reduced while maintaining the cyclic stress amplitude the same as before. In the fatigue-impact tests, the specimen was subjected to a specified number of fatigue cycles and was then impacted to

determine the minimum velocity which can cause catastrophic failure (failure on impact) of the specimen. At any one stress amplitude level (with $R = 0.1$) past the predetermined number of fatigue cycles, the velocity of the impacting projectile was either increased or decreased to affect a catastrophic failure. This procedure was repeated at different maximum stress levels ($R = 0.1$) and fatigue lives in establishing the minimum projectile velocity at which the catastrophic failure in the laminate takes place.

6. X-Ray Radiography

The damage resulting from the applied (impact/fatigue) loads was documented using photography and X-ray radiography. Radiographs of the specimens were taken at regular intervals using Faxitron X-ray System. The film used was Kodak M-5 type which was cut into 4 in. x 5 in. size and placed on a lead plate. The specimen was placed on top of the film and the compartment door was closed. A distance of 73 cms. from the X-ray source to the specimen was maintained. After setting the suitable values of the X-ray tube voltage and the exposure time, the X-ray machine was switched on. A combination of 25 kV tube voltage and 45 secs. exposure time was found to give satisfactory results. The Faxitron X-ray System can be operated either in manual or in an auto mode. When the films were developed in the darkroom, they were soaked in the developer solution for 5 minutes, then for about 30 seconds in short-stop and then for 90 seconds in fixer.

Then they were washed with plenty of water and dried.

The penetrant used to enhance the radiographs is a solution of 60 gms of zinc iodide, 8 ml of water, 10 ml of isopropyl alcohol and 10 ml of photoflow. The penetrant was allowed to soak through the damaged areas of the laminate for about 30 minutes. The excess solution was removed from the surfaces of the specimen with absorbent towels and the radiographs were then taken.

SECTION VII
EXPERIMENTAL DATA

1. Tension Tests

The experimental data from the tension tests are shown in Table 5. Eleven specimens were tested in generating the data as shown. The average numerical values are:

Area of the Cross-Section:	0.224 in ²
Ultimate Load, P_U :	18.539 kips
Ultimate Strength, σ_U :	82.763 ksi
Ultimate Strain, ϵ_U :	0.011
In-plane (axial) Modulus of Elasticity, E_{11} :	7.524 msi

The tensile stress and strain values of the notched specimens are shown in Table 6. These strain values (in the direction of the load) were measured near (see Fig. 1-c) the hole and slightly away from the end tabs. The modulus of elasticity values shown in Table 6 are based on the far-field (near the tabs) stress-strain values. Using this modulus and the measured strain value near the hole (in the direction of the load), the maximum stress in the vicinity of the hole was calculated. The ratio of the maximum stress near the hole to the far-field stress value was found to be about 1.4 (stress concentration factor).

2. Impact Tests

The projectile impact test data shown in Table 7 was obtained by varying the magnitude of the preload and the projectile impact energy. The failure threshold curve shown in Fig. 6 was developed using this data. The energy of impact as

TABLE 5: ULTIMATE STRESS-STRAIN DATA

Material: T300/934
 Laminate Orientation: (+45,0,90)2s
 Specimen Size: 3" x 10" x 16 plies (with tapered tabs)

Specimen No.	Area of Cross-Sect. in ² m ² (10 ⁻⁴)	Ultimate Load (P _u) kips/kN	Ultimate Strength (σ _u) ksi/MPa	Ultimate Strain (ε _u)	Modulus of Elasticity (E) msi/GPa
12-11	0.223 1.439	17.69 78.69	77.96 537.56	0.012	6.61 45.58
12-33	0.223 1.439	18.88 83.98	83.21 573.71	0.009	8.95 61.72
12-27	0.223 1.439	21.14 94.03	93.17 642.38	0.014	6.85 47.23
10-23	0.223 1.439	18.00 80.06	80.03 551.75	0.010	7.75 53.44
11-05	0.228 1.471	16.66 74.10	73.04 503.58	0.010	7.61 52.49
13-08	0.222 1.432	19.50 86.74	87.70 604.64	0.011	7.82 53.92
7-26	0.225 1.452	17.91 79.66	79.50 548.14	0.011	7.51 51.76
9-30	0.235 1.516	16.88 75.06	71.84 495.31	0.010	7.26 50.03
12-10	0.225 1.452	19.75 87.85	94.05 648.44	0.011	8.20 56.51
7-24	0.221 1.426	20.40 90.74	92.27 636.15	0.012	7.89 54.37
5-09	0.223 1.439	17.13 76.17	76.69 528.77	0.010	7.99 55.08
7-31*	0.218 1.407	8.36 37.19	38.42 264.89	-	-

*Specimen with clean hole

TABLE 6: ULTIMATE (TENSILE) STRESS-STRAIN DATA
(Specimen with an implanted hole)

Material: Graphite/Epoxy Composite (T300/934)

Laminate Orientation: $(\pm 45, 0, 90)_2s$

Specimen Size: 2.75" x 10" x 0.081" (16 plies)

Specimen No.	Area of Cross-Sect. in. ² $m^2 (10^{-4})$	Ultimate Load (P _u) kips/kN	Ultimate Strength (σ_u) ksi/MPa	Ultimate Strain (ϵ_u) (10^{-2})	Ultimate Strain near the hole (ϵ_u^h) (10^{-2})	Ultimate Stress near the hole (σ_u^h) ksi/MPa	Modulus of Elasticity (E_{11}) msi/GPa
7-31	0.218 1.407	8.36 37.19	38.35 264.32	-	-	-	-
1-26	0.229 1.478	8.38 37.27	36.59 252.17	0.445	0.641	52.69 363.30	8.22 56.68
13-6	0.231 1.490	8.63 38.39	37.36 257.65	0.427	0.641	56.09 386.74	8.75 60.33
3-25	0.221 1.426	9.14 40.65	41.36 285.06	0.463	0.650	58.05 400.25	8.93 61.57
8-31	0.221 1.426	8.19 36.43	37.06 255.47	0.436	0.596	50.66 349.30	8.50 58.61

σ_u = Far-field stress closer to the end tabs; ϵ_u = Strain corresponding to σ_u .

ϵ_u^h = Strain in the vicinity of the hole (load direction);

σ_u^h = Stress in the vicinity of the hole corresponding to ϵ_u^h .

TABLE 7: EXPERIMENTAL DATA: IMPACT TEST

Specimen No.	Area of Cross-Sect. in^2 $\text{m}^2(10^{-4})$	Velocity of Impact (v_i) ft/sec, m/sec	Energy of Impact, (K.E.) in-lb, Joules	Load at Impact (P_i) kips/kN	Strength at Impact (σ_i) ksi/MPa	Residual Load (P_R) kips/kN	Residual Strength (σ_R) ksi/MPa
11-25	0.213 1.375	170 51.82	36.0 4.07	4.68 20.79	21.93 151.19	9.61 42.75	45.08 310.78
12-15	0.218 1.407	158 48.16	31.0 3.51	6.18 27.50	28.36 195.55	9.65 42.92	44.27 305.20
06-14	0.218 1.407	139 42.37	24.0 2.72	10.18 45.28	46.76 322.41	-	-
07-14	0.218 1.407	130 39.62	21.0 2.37	11.15 49.60	51.24 353.29	-	-
13-07	0.217 1.400	280 77.42	99.0 11.19	10.18 45.28	46.05 323.75	-	-
04-23	0.222 1.432	254 70.23	81.0 9.15	10.00 44.48	45.00 310.29	-	-
07-05	0.218 1.407	81 24.69	8.0 0.90	11.00 48.93	50.53 348.38	18.74 83.37	86.10 593.63
08-19	0.218 1.407	80 24.38	8.0 0.90	9.00 40.03	41.34 285.04	16.43 73.08	75.47 520.35
11-06	0.218 1.407	72 21.95	7.0 0.79	13.10 58.27	60.091 414.31	-	-
05-05	0.218 1.407	284 86.56	102 11.52	7.00 31.14	32.15 221.69	-	-

TABLE 7 (continued) - b

Specimen No.	Area of Crqss-Sect. in ² (10 ⁻⁴) m ²	Velocity of Impact (v _i) ft/sec, m/sec	Energy of Impact, (K.E.) in-lb, Joules	Load at Impact (P _i) kips/kN	Strength at Impact (σ _i) ksi/MPa	Residual Load (P _R) kips/kN	Residual Strength (σ _R) ksi/MPa
12-09	0.220 1.419	400 121.92	202 22.82	4.15 18.47	18.90 130.33	7.31 32.52	33.27 229.41
13-32	0.222 1.432	185 56.39	43 4.86	6.20 27.56	27.89 192.29	9.73 43.27	43.78 301.83
10-18	0.220 1.419	359 109.42	162.39 18.35	4.10 18.22	18.66 128.63	7.26 32.29	33.07 228.02
04-18	0.245 1.581	271 82.60	92.54 10.46	5.19 23.09	21.20 146.17	6.26 27.82	25.55 176.17
02-06	0.231 1.490	325 99.06	133.09 15.04	5.86 26.07	25.35 174.76	7.21 32.06	31.18 214.95
07-32	0.220 1.419	297 90.53	111.14 12.56	4.70 20.91	21.41 147.63	7.71 34.31	35.14 242.23
05-28	0.231 1.490	359 109.42	162.39 13.53	3.20 14.23	13.84 95.43	7.92 35.22	34.25 236.13
09-09	0.218 1.407	203 61.87	51.92 5.87	5.20 22.77	23.53 162.20	9.24 41.09	42.45 292.68
06-11	0.227 1.465	270 82.30	91.85 10.38	4.10 18.24	18.06 124.53	7.51 33.40	33.10 228.05
01-14	0.232 1.497	264 80.47	87.82 9.92	5.78 25.69	24.94 171.92	-	-

TABLE 7 (continued) - c

Specimen No.	Area of Cross-Sect. in ² m ² (10 ⁻⁴)	Velocity of Impact (v _i) ft/sec, m/sec	Energy of Impact, (K.E.) in-lb, Joules	Load at Impact (P _i) kips/kN	Strength at Impact (σ _i) ksi/MPa	Residual Load (P _R) kips/kN	Residual Strength (σ _R) ksi/MPa
01-04	0.233 1.503	170 51.82	36.41 4.11	8.64 38.43	37.05 255.45	-	-
04-07	0.212 1.368	71 21.64	6.35 0.72	7.09 31.51	33.37 230.10	10.58 47.08	49.85 343.73
07-29	0.212 1.368	114 34.75	15.60 1.76	7.18 31.93	33.81 233.12	18.80 83.64	88.57 610.67
03-12	0.226 1.458	110 33.53	15.25 1.72	8.16 36.30	36.07 248.72	17.02 75.69	75.23 518.64
11-27	0.218 1.407	127 38.71	20.32 2.30	10.46 46.53	47.98 330.82	-	-
02-24	0.232 1.497	89 27.13	9.98 1.13	7.67 34.12	33.06 227.94	18.68 83.08	80.50 555.08
08-24	0.229 1.478	201 61.26	50.91 5.75	7.70 34.25	33.70 232.34	-	-
01-10	0.231 1.490	171 52.12	36.84 4.16	6.62 29.43	28.69 197.81	10.16 45.19	45.97 316.93
10-17	0.218 1.407	334 101.80	140.56 15.88	5.70 25.35	26.20 180.61	5.96 26.49	27.37 188.69
10-08	0.229 1.478	115 35.05	16.66 1.89	11.50 51.15	50.15 345.79	-	-

TABLE 7 (continued) - d

Specimen No.	Area of Cross-Sect. in ² m ² (10 ⁻⁴)	Velocity of Impact (v _i) ft/sec, m/sec	Energy of Impact, (K.E.) in-lb, Joules	Load at Impact (P _i) kips/kN	Strength at Impact (σ _i) ksi/MPa	Residual Load (P _R) kips/kN	Residual Strength (σ _R) ksi/MPa
04-04	0.217 1.400	166 50.60	34.72 3.92	7.40 32.92	34.10 235.12	7.90 35.16	36.42 251.14
07-13	0.223 1.439	195 59.44	47.91 5.41	7.25 32.25	32.50 224.06	-	-
08-22	0.227 1.465	85 25.91	9.10 1.03	14.00 62.27	61.76 425.79	-	-
11-07	0.221 1.426	268 81.69	90.50 10.21	6.07 26.99	27.52 189.74	6.39 28.41	28.97 199.72
01-22	0.224 1.445	317 96.62	126.62 14.31	5.60 24.91	25.00 172.37	4.80 21.34	21.42 147.68
04-15	0.218 1.407	398 121.31	199.59 22.55	5.87 26.30	26.95 185.82	-	-
06-04	0.221 1.426	57 17.37	4.09 0.46	14.50 64.50	65.76 453.40	17.86 79.44	80.99 558.43
07-33	0.224 1.445	215 65.53	58.24 6.58	6.55 29.13	29.25 201.70	7.44 33.07	33.21 228.95
09-17	0.221 1.426	187 57.00	44.06 4.98	7.19 31.96	32.47 223.85	-	-
03-04	0.223 1.439	226 68.88	64.36 7.27	6.60 29.36	29.58 203.97	8.39 37.34	37.62 259.41

TABLE 7 (cont) e

Specimen No.	A Cross Sect. in ² m ² (10 ⁻⁴)	Velocity of Impact (v _i) ft/sec, m/sec	Energy of Impact, (K.E.) in-lb, Joules	Load at Impact (P _i) kips/kN	Strength at Impact (σ _i) ksi/MPa	Residual Load (P _R) kips/kN	Residual Strength (σ _R) ksi/MPa
08-03	0.233 1.503	351 106.98	155.23 17.54	5.25 23.35	22.52 155.29	8.06 35.84	34.57 238.32
03-07	0.218 1.407	344 104.85	149.10 16.84	5.80 25.80	26.64 183.69	6.48 28.80	29.74 205.07
02-19	0.231 1.490	366 111.56	168.78 19.07	5.80 25.80	25.09 172.97	-	-
11-13	0.218 1.407	353 107.59	157.00 17.74	6.22 27.67	28.56 196.90	-	-
01-12	0.229 1.478	369 112.47	171.56 19.38	6.70 29.80	29.30 201.99	-	-
13-30	0.220 1.419	336 102.41	142.25 16.07	7.20 32.03	32.68 225.34	-	-
04-27	0.215 1.387	74 22.56	6.90 0.78	9.81 43.64	45.65 314.74	15.34 68.22	71.37 492.10
13-02	0.231 1.490	172 52.43	37.28 4.21	10.10 44.93	43.68 301.20	-	-
01-24	0.225 1.452	250 76.20	78.75 8.90	6.92 30.78	30.79 212.15	-	-
10-33	0.220 1.419	174 53.04	38.14 4.31	8.95 39.89	40.76 281.00	-	-

TABLE 7 (continued) - f

Specimen No.	Area of Cross-Sect. in ² m ² (10 ⁻⁴)	Velocity of Impact (v _i) ft/sec, m/sec	Energy of Impact, (K.E.) in-lb, Joules	Load at Impact (P _i) kips/kN	Strength at Impact (σ _i) ksi/MPa	Residual Load (P _R) kips/kN	Residual Strength (σ _R) ksi/MPa
06-17	0.226 1.458	335 102.11	141.40 15.98	6.86 30.50	30.36 209.35	-	-
09-32	0.221 1.426	250 76.2	78.75 8.90	6.82 30.33	30.90 213.03	-	-
03-26	0.226 1.458	386 117.65	187.73 21.21	5.52 24.55	24.43 168.45	6.58 29.26	29.12 200.77

shown in Table 7. Column 4, is based on the forward velocity of the impacting projectile.

3. Fatigue Tests (Without Notch)

The tension-tension fatigue test data are given in Table 8. With the magnitude of the static ultimate strength of the laminate in the background, the magnitudes of applied loads (minimum/maximum) for each of the specimens tested were selected to maintain a stress ratio of $R = 0.1$ at 10 Hz. As indicated earlier, about four to five test specimens were used per test condition. Those specimens that did not fail under tension-tension cyclic fatigue conditions after seeing one million cycles were tested to determine their residual strengths.

4. Fatigue Tests (With Notch)

The determination of residual strength of the specimens after undergoing a certain number of fatigue cycles was the objective of these tests. A total number of 38 specimens were tested at different stress levels and the results are given in Table 9. The variation of residual stress with the number of cycles was also studied.

5. Fatigue/Impact Tests (Without Notch)

The impact-fatigue tests were conducted with 35 specimens to determine the number of fatigue cycles a specimen can undergo after being impacted at a particular velocity and at a particular stress level. These results are given in Table 10. Three particular data points of these tests were chosen and the effect of

TABLE 8: Tension - Tension Fatigue Data (R = 0.1, Without Hole)

Specimen No.	Thickness t in. mx10 ⁻³	Width b in. mx10 ⁻³	Area A ₂ in. ² m ² x10 ⁻⁶	Max. Load P _{max} kips kN	Max. Stress σ _{max} ksi MPa	No. of Cycles N x10 ³	Residual Stress σ _r ksi MPa	Location of Failure* in. mx10 ⁻³	Comments, If Any, See Note No.
9-16	0.082 2.083	2.723 69.160	0.223 143.840	7.50 33.36	34.09 235.04	1000	71.18 490.78	0.33 8.38	
5-29	0.081 2.057	2.723 69.160	0.221 142.550	7.50 33.36	33.94 234.01	800			1
8-32	0.082 2.083	2.724 69.170	0.223 143.840	7.50 33.36	34.09 235.04	1000	93.20 642.60	2.50 63.50	
12-28	0.082 2.083	2.723 69.160	0.223 143.840	7.50 33.36	34.09 235.04	1000	84.81 584.74	1.88 47.75	
9-33	0.082 2.083	2.724 69.170	0.223 143.840	7.50 33.36	34.09 235.04	1000	87.25 601.59	2.25 57.15	
6-32	0.081 2.057	2.723 69.160	0.221 142.550	9.00 40.03	40.72 280.75	1000	73.67 507.90	1.75 44.45	2
7-22	0.082 2.083	2.723 69.160	0.223 143.840	9.00 40.03	40.36 278.27	1000	78.37 540.34	0.06 1.52	
9-26	0.082 2.083	2.723 69.160	0.223 143.840	9.00 40.03	40.72 280.75	1000	82.29 567.35	3.75 95.25	
1-15	0.082 2.083	2.724 69.170	0.224 144.480	9.00 40.03	40.18 277.03	1000	80.59 555.64	3.88 98.55	
10-3	0.082 2.083	2.721 69.110	0.223 143.840	9.00 40.03	40.36 278.27	1000	84.94 585.65	3.50 88.90	

*Measured from the end of the numbered tab taper

TABLE 8 (Continued) - b

Specimen No.	Thickness t in.-3 mx10 ⁻³	Width b in.-3 mx10 ⁻³	Area A ₂ in. ² m x10 ⁻⁶	Max. Load P _{max} kips kN	Max. Stress σ _{max} ksi MPa	No. of Cycles N x10 ³	Residual Stress σ _r ksi MPa	Location of Failure* in.-3 mx10 ⁻³	Comments, If Any, See Note No.
13-10	0.082 2.083	2.722 69.140	0.223 143.840	10.00 44.48	44.84 309.16	1000	58.87 405.80	3.50 88.90	3
1-25	0.082 2.083	2.721 69.110	0.223 143.840	10.00 44.48	44.84 309.16	1000	77.35 533.34	0.06 1.52	
7-7	0.083 2.110	2.722 69.140	0.226 145.770	10.00 44.48	44.25 305.08				4
1-6	0.083 2.110	2.724 69.170	0.226 145.770	10.00 44.48	44.25 305.08	1000	78.11 538.55	3.25 82.55	
8-33	0.082 2.083	2.724 69.170	0.223 143.840	10.00 44.48	44.84 309.16	1000	91.36 629.93	0.33 8.38	
3-18	0.082 2.083	2.725 69.220	0.223 143.840	12.00 53.38	53.81 371.02	1000	70.01 482.73	2.25 57.15	
1-7	0.082 2.083	2.724 69.170	0.223 143.840	12.00 53.38	53.81 371.02	531.5		3.00 76.20	
2-16	0.084 2.134	2.725 69.220	0.229 147.640	12.00 53.38	52.40 361.30	106.7		0.33 83.82	
7-25	0.082 2.083	2.723 69.160	0.223 143.840	12.00 53.38	53.81 371.02	1000	76.81 529.60	0.50 12.70	
10-26	0.082 2.083	2.724 69.170	0.223 143.840	12.00 53.38	53.81 371.02	1000	59.58 410.81	1.25 31.75	

*Measured from the end of the numbered tab taper

TABLE 8 (Continued) - c

Specimen No.	Thickness t in.-3 mx10 ⁻³	Width b in. mx10 ⁻³	Area A ₂ in. ² m ² x10 ⁻⁶	Max. Load P _{max} kips kN	Max. Stress σ _{max} ksi MPa	No. of Cycles N x10 ³	Residual Stress σ _r ksi MPa	Location of Failure* in. mx10 ⁻³	Comments, If Any, See Note No.
12-19	0.081 2.057	2.722 69.140	0.220 141.900	13.50 60.05	61.36 423.09	72.73		4.00 101.60	
6-13	0.083 2.110	2.723 69.160	0.226 145.770	13.50 60.05	59.73 411.85	187.23		3.63 92.20	
10-24	0.082 2.083	2.721 69.110	0.223 143.840	13.50 60.05	60.54 417.40	174.37		2.13 53.98	
7-28	0.083 2.110	2.722 69.140	0.226 145.770	13.50 60.05	59.73 411.85	264.53		2.25 57.15	
7-30	0.083 2.110	2.722 69.140	0.226 145.770	13.50 60.05	59.73 411.85	145.30		3.13 79.50	
5-10	0.082 2.083	2.725 69.220	0.223 144.130	14.00 62.78	63.74 439.47	122.60		0.75 19.05	
1-8	0.082 2.083	2.723 69.160	0.226 145.770	14.00 62.78	61.95 427.11	35.40		2.50 63.50	
6-24	0.082 2.083	2.723 69.160	0.226 145.770	14.00 62.78	61.95 427.11	28.62		2.50 63.50	
13-5	0.084 2.134	2.723 69.160	0.230 148.350	14.00 62.78	60.87 419.68	15.14		4.13 104.90	
4-32	0.081 2.057	2.723 69.160	0.221 142.550	14.00 62.78	63.35 436.77	4.13		0.13 31.75	5

*Measured from the end of the numbered tab taper

TABLE 8 (Continued) - d

Specimen No.	Thickness t in. mx10 ⁻³	Width b in. mx10 ⁻³	Area A ₂ in. ² m x10 ⁻⁶	Max. Load P _{max} kips kN	Max. Stress σ _{max} ksi MPa	No. of Cycles N x10 ³	Residual Stress σ _r ksi MPa	Location of Failure* in. mx10 ⁻³	Comments, If Any, See Note No.
6-5	0.083 2.110	2.724 69.170	0.225 145.130	15.00 66.72	66.67 459.67	18.23		3.75 95.25	
2-23	0.082 2.083	2.725 69.220	0.223 144.130	15.00 66.72	67.26 463.77	1.04		0.13 31.75	
2-11	0.082 2.083	2.723 69.160	0.223 144.130	15.00 66.72	67.26 463.77	23.40		1.00 25.40	
3-9	0.081 2.057	2.723 69.160	0.221 142.550	15.00 66.72	67.87 467.95	28.34		0.50 12.70	
9-4	0.081 2.057	2.723 69.160	0.221 142.550	15.00 66.72	67.87 467.95	8.63		0.33 8.38	
3-14	0.082 2.083	2.725 69.220	0.223 144.130	16.00 71.17	71.75 494.69	9.87		0.50 12.70	
7-19	0.082 2.083	2.725 69.220	0.223 144.130	16.00 71.17	71.75 494.69	2.26		2.75 69.85	
2-33	0.082 2.083	2.725 69.220	0.223 144.130	16.00 71.17	71.75 494.69	21.67		0.75 19.05	
10-32	0.082 2.083	2.722 69.140	0.223 144.130	16.00 71.17	71.75 494.69	5.44		0.33 8.38	
5-27	0.082 2.083	2.722 69.140	0.223 144.130	16.00 71.17	71.75 494.69	6.72		0.50 12.70	

*Measured from the end of the numbered tab taper

TABLE 8 (Continued) - e

Specimen No.	Thickness t in. mx10 ⁻³	Width b in. mx10 ⁻³	Area A ₂ in. ² m ² x10 ⁻⁶	Max. Load P _{max} kips kN	Max. Stress σ _{max} ksi MPa	No. of Cycles N x10 ³	Residual Stress σ _r ksi MPa	Location of Failure* in. mx10 ⁻³	Comments, If Any, See Note No.
13-16	0.081 2.057	2.724 69.170	0.221 142.550	17.00 75.62	76.92 530.37	0.16		3.13 79.50	
3-19	0.082 2.083	2.724 69.170	0.223 144.130	17.00 75.62	76.23 525.61	0.20		0.50 12.70	
7-16	0.082 2.083	2.723 69.160	0.223 144.130	17.00 75.62	76.23 525.61	1.00		2.63 66.80	
1-29	0.082 2.083	2.724 69.170	0.223 144.130	17.00 75.62	76.23 525.61	0.12		4.13 104.90	
3-5	0.082 2.083	2.724 69.170	0.223 144.130	17.00 75.62	76.23 525.61	0.17		4.00 101.60	
8-26	0.082 2.083	2.722 69.140	0.223 144.130	17.00 75.62	76.23 525.61	0.63		1.75 44.45	
9-18	0.083 2.110	2.724 69.170	0.226 145.770	17.00 75.62	75.22 518.62	0.20		0.06 1.52	
5-3	0.081 2.077	2.723 69.160	0.221 142.550	17.00 75.62	76.92 530.37	0.30		4.13 104.90	
9-2	0.081 2.057	2.724 69.170	0.221 142.550	17.00 75.62	76.92 530.37	0.01		0.13 3.30	
3-2	0.083 2.110	2.725 69.220	0.226 145.770	17.00 75.62	75.22 518.62	0.49		2.33 59.18	

*Measured from the end of the numbered tab taper

TABLE 8 (Continued) - f

Specimen No.	Thickness t in $\times 10^{-3}$	Width b in $\times 10^{-3}$	Area A_2 in ² $\times 10^{-6}$	Max. Load P max kips kN	Max. Stress σ max ksi MPa	No. of Cycles N $\times 10^3$	Residual Stress σ_r ksi MPa	Location of Failure# in $\times 10^{-3}$	Comments, If Any, See Note No.
5-14	0.082 2.083	2.723 69.160	0.223 144.130	18.00 80.06	80.72 556.54	1.00	0.06 1.52		
9-12	0.082 2.083	2.723 69.160	0.223 144.130	18.00 80.06	80.72 556.54	0.31	2.00 50.80		
3-23	0.081 2.057	2.722 69.140	0.220 142.210	18.00 80.06	81.82 564.13	0.33	3.75 95.25		
3-15	0.083 2.110	2.724 69.170	0.226 145.770	18.00 80.06	79.65 549.17	0.01	0.06 1.52		
9-27	0.081 2.057	2.724 69.170	0.221 142.550	18.00 80.06	81.45 561.58	0.71	4.13 104.90		

#Measured from the end of the numbered tab taper

COMMENTS:

1. The specimen was damaged during loading.
2. The specimen also failed at a distance of 3 in. from the numbered tab.
3. The failure of the specimen occurred along the external notch created while unloading the specimen.
4. Failed due to an inappropriate existing function generator setting.
5. Slight bend in the plane of the specimen was noted.

TABLE 9: TENSION - TENSION FATIGUE DATA (R = 0.1 with a hole of 0.5 in. dia.)

Specimen No.	Thickness t in. $\text{m} \times 10^{-3}$	Width b in. $\text{m} \times 10^{-3}$	Area A in. ² $\text{m}^2 \times 10^{-6}$	Max. Load P max kips kN	Max. Stress σ_{max} ksi MPa	No. of Cycles N $\times 10^3$	Residual Stress σ_r ksi MPa	Location of Failure* in. $\text{m} \times 10^{-3}$	Comments, if any, see note No.
7-15	0.081 2.057	2.723 69.164	0.221 142.545	4.50 20.02	20.36 140.38	200	40.70 280.63	2.13 54.10	
7-12	0.081 2.057	2.722 69.139	0.221 142.545	4.50 20.02	20.36 140.38	400	40.62 280.07	2.13 54.10	
8-7	0.081 2.057	2.722 69.139	0.221 142.545	4.50 20.02	20.36 140.38	600	41.88 288.76	2.13 54.10	
5-33	0.081 2.057	2.722 69.139	0.221 142.545	4.50 20.02	20.36 140.38	800	39.95 275.46	2.13 54.10	
9-15	0.084 2.134	2.722 69.139	0.229 147.705	4.50 20.02	19.65 135.49	1000	40.30 277.87	2.13 54.10	
13-27	0.081 2.057	2.722 69.139	0.221 142.545	4.50 20.02	20.36 140.38	581.71	-	2.38 60.45	1
12-5	0.081 2.057	2.722 69.139	0.221 142.545	4.50 20.02	20.36 140.38	1000	44.00 303.38	2.13 54.10	
6-12	0.080 2.032	2.722 69.139	0.218 140.610	4.50 20.02	20.64 142.31	1000	39.94 275.39	2.00 50.80	
2-20	0.083 2.108	2.723 69.164	0.226 145.770	4.50 20.02	19.91 137.28	1000	39.78 274.28	2.13 54.10	
2-5	0.083 2.108	2.722 69.139	0.226 145.770	4.50 20.02	19.91 137.28	1000	39.78 274.28	2.13 54.10	

*Measured from the end of the numbered tab taper

TABLE 9 (Continued) - b

Specimen No.	Thickness t in. $\text{m} \times 10^{-3}$	Width b in. $\text{m} \times 10^{-3}$	Area A in.^2 $\text{m}^2 \times 10^{-6}$	Max. Load P _{max} kips kN	Max. Stress σ_{max} ksi MPa	No. of Cycles N $\times 10^3$	Residual Stress σ_r ksi MPa	Location of Failure* in. $\text{m} \times 10^{-3}$	Comments, if any, see note No.
9-11	0.081 2.057	2.722 69.139	0.221 142.545	6.00 26.69	27.15 187.20	200	37.09 255.74	2.00 50.80	
12-8	0.081 2.057	2.721 69.113	0.220 141.900	6.00 26.69	27.27 188.03	400	45.81 315.86	2.13 54.10	
3-20	0.079 2.007	2.722 69.139	0.215 138.675	6.00 26.69	27.91 192.44	600	43.88 302.55	2.00 50.80	
13-20	0.081 2.057	2.722 69.139	0.221 142.545	6.00 26.69	27.15 187.20	800	44.79 308.83	2.25 57.15	
1-2	0.086 2.184	2.723 69.164	0.234 150.930	6.00 26.69	25.64 176.79	1000	40.85 281.66	2.25 57.15	
9-21	0.082 2.083	2.720 69.088	0.223 143.835	6.00 26.69	26.91 185.54	1000	43.08 297.04	2.13 54.10	
6-15	0.081 2.057	2.722 69.139	0.221 142.545	6.00 26.69	27.15 187.20	1000	45.39 312.96	2.13 54.10	
12-2	0.081 2.057	2.722 69.139	0.221 142.545	6.00 26.69	27.15 187.20	1000	42.41 292.42	2.13 54.10	
8-17	0.081 2.057	2.722 69.139	0.221 142.545	6.00 26.69	27.15 187.20	1000	44.53 307.03	2.00 50.80	

*Measured from the end of the numbered tab taper

TABLE 9 (Continued) - c

Specimen No.	Thickness t in. $\text{m} \times 10^{-3}$	Width b in. $\text{m} \times 10^{-3}$	Area A in.^2 $\text{m}^2 \times 10^{-6}$	Max. Load P _{max} kips kN	Max. Stress σ_{max} ksi MPa	No. of Cycles N $\times 10^3$	Residual Stress σ_r ksi MPa	Location of Failure* in. $\text{m} \times 10^{-3}$	Comments, if any, see note No.
9-7	0.082 2.083	2.722 69.139	0.223 143.835	8.00 35.58	35.87 247.32	200	43.37 299.04	2.00 50.80	
9-6	0.080 2.032	2.722 69.139	0.218 140.610	8.00 35.58	36.70 253.05	400	44.91 310.00	2.13 54.10	
8-4	0.080 2.032	2.722 69.139	0.218 140.610	8.00 35.58	36.70 253.05	600	46.59 321.24	2.00 50.80	
2-21	0.082 2.083	2.722 69.139	0.223 143.835	8.00 35.58	35.87 247.32	800	47.83 329.79	2.13 54.10	
10-20	0.081 2.057	2.720 69.088	0.220 141.900	8.00 35.58	36.36 250.70	0.12	-	2.25 57.15	2
6-7	0.082 2.083	2.724 69.190	0.223 143.835	8.00 35.58	35.87 247.32	1000	47.33 326.34	2.38 60.45	
6-21	0.082 2.083	2.721 69.113	0.223 143.835	8.00 35.58	35.87 247.32	1000	45.00 310.28	2.25 57.15	
10-6	0.081 2.057	2.722 69.139	0.221 142.545	8.00 35.58	36.36 250.70	200.36	-	2.13 54.10	3
3-8	0.080 2.032	2.722 69.139	0.218 140.610	8.00 35.58	36.70 253.05	0.45	-	2.13 54.10	4
10-2	0.081 2.057	2.722 69.139	0.221 142.545	8.00 35.58	36.20 249.60	1000	48.46 334.13	2.13 54.10	

*Measured from the end of the numbered tab taper

TABLE 9 (Continued) - d

Specimen No.	Thickness t in. mx10 ⁻³	Width b in. mx10 ⁻³	Area A in. ² m ² x10 ⁻⁶	Max. Load P _{max} kips kN	Max. Stress σ _{max} ksi MPa	No. of Cycles N x10 ³	Residual Stress σ _r ksi MPa	Location of Failure* in. mx10 ⁻³	Comments, if any, see note No.
5-15	0.082 2.083	2.722 69.139	0.223 143.835	8.00 35.58	35.87 247.32	1000	47.61 328.27	2.00 50.80	
4-22	0.076 1.930	2.722 69.139	0.207 133.515	8.00 35.58	38.65 266.49	-	-	2.13 54.10	5
2-17	0.083 2.108	2.722 69.139	0.226 145.770	8.00 35.58	35.40 244.08	0.950	-	2.13 54.10	6
6-9	0.080 2.032	2.723 69.164	0.218 140.610	8.00 35.58	36.70 253.05	1000	50.79 350.20	2.13 54.10	
9-10	0.082 2.083	2.722 69.139	0.223 143.635	8.50 37.81	38.12 262.84	1000	45.28 312.21	2.13 54.10	7
3-27	0.080 2.032	2.723 69.164	0.218 140.610	8.50 37.81	38.99 268.84	0.002	-	2.13 54.10	3
2-22	0.086 2.184	2.722 69.139	0.234 150.930	9.00 40.03	38.46 265.18	-	-	2.13 54.10	8
3-29	0.082 2.083	2.722 69.139	0.223 143.835	9.00 40.03	40.36 278.28	-	-	2.13 54.10	8
5-7	0.081 2.057	2.721 69.113	0.220 141.900	9.50 42.26	43.18 297.73	17.4	-	2.13 54.10	9

*Measured from the end of the numbered tab taper

TABLE 9 (Continued) - e

COMMENTS

1. The specimen broke in the middle due to some power failure problem in the machine.
2. The specimen broke after 120 cycles going into compression mode.
3. The specimen broke after 200,360 cycles because of wrong setting of span.
4. The specimen broke after 450 cycles.
5. The specimen broke as soon as the cyclic loading was started.
6. The specimen broke after 950 cycles.
7. The fatigue test was started with $P_{max} = 7,000$ lbs. and gradually increased to 8,500 lbs. By the time the maximum load was set to 8,500 lbs., the specimen had completed 16,000 cycles.
8. The specimen broke as soon as the cyclic loading was started.
9. The range of load was started with 750/7,500, gradually increased to 850/8,500, maintained till it reached 10,000 cycles. Then gradually increased to 900/9,000, maintained there till it reached 15,000 cycles, then again gradually increased to 950/9,500. The exact range of 950/9,500 was reached at 17,350th cycle and the specimen failed at 17,410th cycle.

TABLE 10: IMPACT/FATIGUE TEST DATA

Specimen No.	Area of Cross-Sect. in. 2 $2(10^{-4})$ m	Velocity of Impact (v_1) ft/sec, m/sec	Energy of Impact (K.E.) in-lb, Joules	Load at Impact (P_1) kips/kN	Strength at Impact (σ_1) ksi/MPa	Number of Cycles After Impact N	Comments, if any
11-10	0.210 1.355	309 94.18	120.30 13.59	6.00 26.69	28.60 197.20	-	Failure on impact
11-19	0.210 1.355	221 67.36	61.54 6.95	10.00 44.48	47.60 328.20	-	Failure on impact
11-8	0.210 1.355	100 30.48	12.60 1.42	10.00 44.48	47.60 328.20	3180	
11-24	0.207 1.335	211 64.31	56.10 6.34	6.00 26.69	29.00 199.96	1.82×10^6	
4-16	0.210 1.355	-	-	-	-	-	Failure on pre-loading
8-21	0.221 1.425	109 33.22	14.97 1.69	14.50 64.50	65.60 452.31	-	Failure on impact
7-3	0.215 1.387	100 30.48	12.60 1.42	15.00 66.72	69.80 481.27	-	Failure on impact
9-20	0.223 1.438	89 27.13	9.98 1.13	6.00 26.69	26.90 185.48	10^6	Residual Strength = 86.00 ksi
12-29	0.221 1.425	92 28.04	10.66 1.20	6.00 26.69	27.10 186.85	10^6	Residual Strength = 77.027 ksi
9-24	0.212 1.367	115 35.05	16.66 1.88	6.00 26.69	28.30 195.13	10^6	Residual Strength = 86.118 ksi

TABLE 10 (Continued) - b

Specimen No.	Area of Cross-Sect. in. ² $2(10^{-4})$ m	Velocity of Impact (v_1) ft/sec, m/sec	Energy of Impact, (K.E.) in-lb, Joules	Load at Impact (P_1) kips/kN	Strength at Impact (σ_1) ksi/MPa	Number of Cycles After Impact N	Comments, if any
13-14	0.218 1.406	101 30.78	12.85 1.45	10.00 44.48	45.90 316.48	3000	Residual Strength = 88.890 ksi
10-16	0.218 1.406	99 30.18	12.35 1.40	10.12 45.01	46.42 320.07	3000	Residual Strength = 78.555 ksi
1-9	0.218 1.406	127 38.71	20.32 2.30	10.09 44.88	46.28 319.10	-	Failure on impact
6-8	0.221 1.425	91 27.74	10.43 1.18	10.02 44.57	45.34 312.62	5 x 10 ⁵	Residual Strength = 82.367 ksi
2-8	0.221 1.425	123 37.49	19.06 2.15	12.10 53.82	54.75 377.50	-	Failure on impact
8-10	0.221 1.425	89 27.13	9.98 1.13	10.15 45.15	45.93 316.69	10 ⁶	Residual Strength = 83.357 ksi
12-26	0.218 1.406	104 31.70	13.63 1.54	12.20 54.27	55.96 385.84	-	Failure on impact
13-31	0.212 1.367	91 27.74	10.43 1.18	11.83 52.62	55.80 384.74	10 ⁶	Residual Strength = 77.656 ksi
6-2	0.204 1.316	93 28.35	10.90 1.23	12.00 53.38	58.82 405.56	-	Failure on impact
6-28	0.215 1.387	75 22.86	7.09 0.80	12.15 54.04	56.51 389.64	29610	

TABLE 10 (Continued) - c

Specimen No.	Area of Cross-Sect. in. ² m ² (10 ⁻⁴)	Velocity of Impact (v _i) ft/sec, m/sec	Energy of Impact, (K.E.) in-lb, Joules	Load at Impact (P _i) kips/kN	Strength at Impact (σ _i) ksi/MPa	Number of Cycles After Impact N	Comments, if any
6-27	0.218 1.406	70 21.34	6.17 0.70	11.25 50.04	51.61 355.85	10 ⁶	Residual Strength = 85.633 ksi
1-3	0.221 1.425	58 17.68	4.24 0.48	15.00 66.72	67.87 467.96	2170	
13-4	0.221 1.425	70 21.34	6.17 0.70	13.00 57.82	58.82 405.56	50190	
5-6	0.215 1.387	82 24.99	8.47 0.96	11.13 49.51	51.77 356.95	10 ⁶	Residual Strength = 79.074 ksi
6-33	0.215 1.387	158 48.16	31.45 3.55	11.50 51.15	53.49 368.81	2 x 10 ⁵	Residual Strength = 91.070 ksi
5-26	0.215 1.387	66 20.12	5.49 0.62	11.50 51.15	53.49 368.81	2 x 10 ⁵	Residual Strength = 88.307 ksi
5-12	0.212 1.367	47 14.33	2.78 0.31	14.50 64.50	68.40 471.62	19100	
9-22	0.218 1.406	61 18.59	4.69 0.53	14.50 64.50	66.51 458.59	41300	
2-7	0.226 1.458	42 12.80	2.22 0.25	16.50 73.39	73.01 503.40	5750	
8-29	0.215 1.387	57 17.37	4.09 0.46	17.00 75.62	79.07 545.19	1060	

TABLE 10 (Continued) - d*

Specimen No.	Area of Cross-Sect. in. ² $2(10^{-4})$ m ²	No. of Fatigue Cycles Before Impact	Load at Impact kips/kN (P_1)	Stress at Impact ksi/MPa (σ_1)	Velocity of Impact (v_1) ft/sec, m/sec	Energy of Impact (K.E.) in-lb, Joules	No. of Fatigue Cycles To Failure, After Impact	Comments, if any
3-13	0.218 1.406	2150	15.00 66.72	68.81 474.44	62 18.90	4.84 0.55	-	The specimen was tested for residual strength, after impact; $\sigma_r = 86.4$ ksi
6-10	0.218 1.406	29600	12.00 53.38	55.05 379.57	73 22.25	6.71 0.76	1.95×10^6	The test was stopped even though the specimen did not fail.
10-27	0.218 1.406	550	15.00 66.72	68.81 474.44	-	-	-	The specimen failed after 550 cycles, even before impact.
10-30	0.215 1.387	2150	15.00 66.72	69.77 481.06	59.5 18.14	4.46 0.50	36940	
3-17	0.215 1.387	50190	13.00 57.82	60.47 416.94	60 18.29	4.54 0.51	380,190	

*The columns on this page are slightly different from those on the three preceding pages. The loading sequence was reversed slightly. The specimens were cyclically loaded first (column 3, above) before they were subjected to impact loads. If the specimens survived the projectile impact, cycling was then resumed until failure took place.

reversing the sequence of the test (that is, cycle/impact/cycle) on the strength of the specimen was studied. The data pertaining to this reversed sequence of testing is shown on the last page of Table 10.

Some of the specimens were first subjected to cyclic loading and were then impacted with the projectile to determine the minimum projectile velocity (energy) precipitating a catastrophic failure of the laminate. Three different values of the number of cycles and two different stress levels were chosen from the knowledge of previous impact-fatigue test results (Table 10). A total of 22 specimens were tested and the results are shown in Table 11.

TABLE 11: FATIGUE/IMPACT TEST DATA

Specimen No.	Area of Cross-Sect. in. ² $2(10^{-4})$ m	No. of Fatigue Cycles	Load at Impact kips/kN (P _i)	Stress at Impact ksi/MPa (σ _i)	Velocity of Impact ft/sec, m/sec	Energy of Impact (K.E.) in-lb, Joules	Comments, if any
8-8	0.215 1.387	10 ⁶	10.00 44.48	46.51 320.68	111 33.83	15.52 1.75	Residual strength after impact = 50.4 ksi
6-3	0.215 1.387	10 ⁶	10.00 44.48	46.51 320.68	177 53.95	39.47 4.46	Very high velocity because of counter failure. Specimen failed on impact.
13-15	0.218 1.406	10 ⁵	10.00 44.48	45.87 316.27	130 39.62	21.29 2.41	Counter failure; specimen failed on impact.
3-32	0.218 1.406	10 ⁴	13.00 57.82	59.63 411.15	106 32.31	14.16 1.60	Failure on impact.
7-8	0.215 1.387	10 ⁶	10.00 44.48	46.51 320.68	129 39.32	20.97 2.40	Failure on impact.
5-13	0.218 1.406	10 ⁴	13.00 57.82	59.63 411.15	83 25.30	8.68 0.98	Residual strength after impact = 83.6 ksi.
3-24	0.218 1.406	10 ⁵	10.00 44.48	45.87 316.27	128 39.01	20.64 2.33	Failure on impact.
10-11	0.215 1.387	10 ⁵	10.00 44.48	46.51 320.68	124 37.80	19.37 2.19	Failure on impact.
3-28	0.212 1.367	10 ⁶	10.00 44.48	47.17 325.24	127 38.71	20.32 2.30	Failure on impact.
10-7	0.218 1.406	10 ⁶	10.00 44.48	45.87 316.27	121 36.88	18.45 2.08	Residual strength after impact = 47 ksi

TABLE 11 (Continued) - b

Specimen No.	Area of Cross-Sect. in. ² $2(10^{-4})$ m	No. of Fatigue Cycles	Load at Impact kips/kN (P_1)	Stress at Impact ksi/MPa (σ_1)	Velocity of Impact ft./sec, m/sec	Energy of Impact (K.E.) in-lb, Joules	Comments, if any
2-14	0.223 1.438	-	-	-	-	-	The specimen failed while loading.
1-32	0.220 1.419	10 ⁴	13.00 57.82	59.09 407.43	102 31.09	13.11 1.48	Failure on impact.
6-31	0.215 1.387	10 ⁴	13.00 57.82	60.47 416.94	110 33.53	15.25 1.72	Failure on impact.
13-12	0.215 1.387	10 ⁴	13.00 57.82	60.47 416.94	86 26.21	9.32 1.05	Failure on impact.
6-29	0.212 1.367	10 ⁴	13.00 57.82	61.32 422.80	87 26.52	9.54 1.08	Failure on impact
13-3	0.212 1.367	10 ⁵	10.00 44.48	47.17 325.24	133 40.54	22.29 2.52	Failure on impact
9-31	0.212 1.367	10 ⁴	13.00 57.82	61.32 422.80	80 24.38	8.06 0.91	Residual strength after impact = 80.2 ksi
1-16	0.226 1.458	10 ⁵	10.00 44.48	44.25 305.10	92 28.04	10.66 1.20	Residual strength after impact = 63.3 ksi
10-9	0.212 1.367	10 ⁵	10.00 44.48	47.17 325.24	102 31.09	13.11 1.48	Residual strength after impact = 58.6 ksi
6-30	0.218 1.406	10 ⁵	10.00 44.48	45.87 316.27	120 36.58	18.14 2.05	Failure on impact.

TABLE 11 (Continued) - c

Specimen No.	Area of Cross-Sect. in. ² $2(10^{-4})$ m ²	No. of Fatigue Cycles	Load at Impact kips/kN (P_1)	Stress at Impact ksi/MPa (σ_1)	Velocity of Impact ft/sec, m/sec	Energy of Impact (K.F.) in-lb, Joules	Comments, if any
6-19	0.212 1.367	10^5	10.00 44.48	47.17 325.24	104 31.70	13.63 1.54	Residual strength after impact = 56.2 ksi
13-13	0.218 1.406	10^5	10.00 44.48	45.87 316.27	113 34.44	16.09 1.82	Residual strength after impact = 55.4 ksi

SECTION VIII
RESULTS AND ANALYSES

1. Static Tension Tests

The experimental data pertaining to the evaluation of the static ultimate strength of the unnotched and notched laminates are shown in Tables 5 and 6, respectively. From this data, it may be seen that the scatter in the static strength values is not significant. The static strength and the corresponding strain for the unnotched laminate were found to be 82.76 ksi and 0.011, respectively. The far-field (closer to the end tabs) ultimate stress and strain values for the notched laminate were 38.14 ksi and 0.443×10^{-2} , respectively. The stress (calculated) and the strain (measured) values for the notched laminate near the hole in the direction of the load were found to be 54.37 ksi and 0.632×10^{-2} , respectively. The average static strength values were used in selecting the stress amplitude ratio (with $R = 0.1$, 10 Hz) for the fatigue tests. Three typical photographs of the laminates (unnotched and notched) failed under static tensile forces are shown in Figures 3, 4 and 5.

2. Impact Tests

Impact tests were conducted on $(\pm 45, 0, 90)_{2S}$ graphite/epoxy materials to understand the extent of damage and the resulting behavior of the laminates. The experimental data (Table 7) is plotted as shown in Figures 6 and 7. Figure 6 is a plot of the applied static tensile stress vs. the energy of the impacting projectile whereas Figure 7 shows normalized stress values plotted as a function of the impact energy. Typically, the data points shown in the above two figures refer to the



Front View

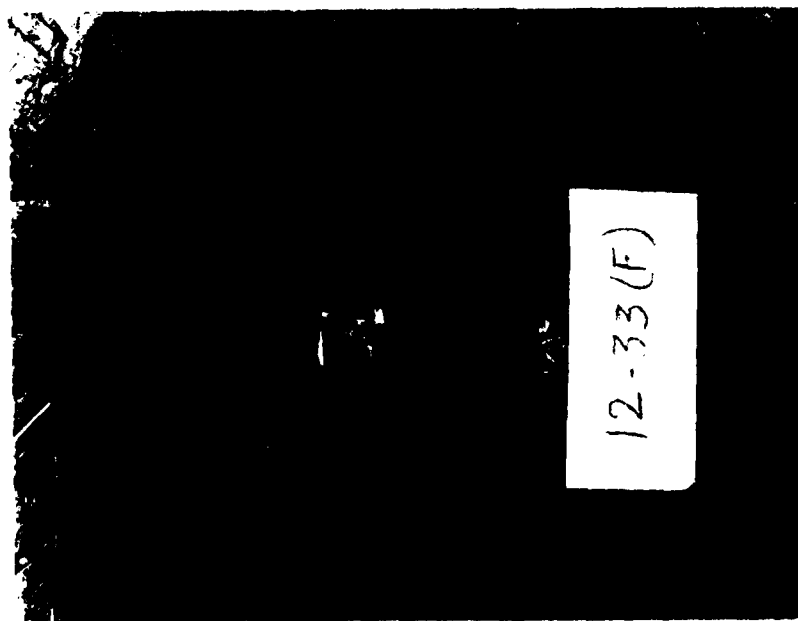


Rear View

Figure 3. Front and rear views of a failed specimen 12-27, graphite/epoxy composite tested for its static strength at a strain rate of 0.02/min.



Rear View



Front View

Figure 4. Front and rear views of a failed specimen 12-33, graphite/epoxy composite tested for its static strength at a strain rate of 0.02/min.

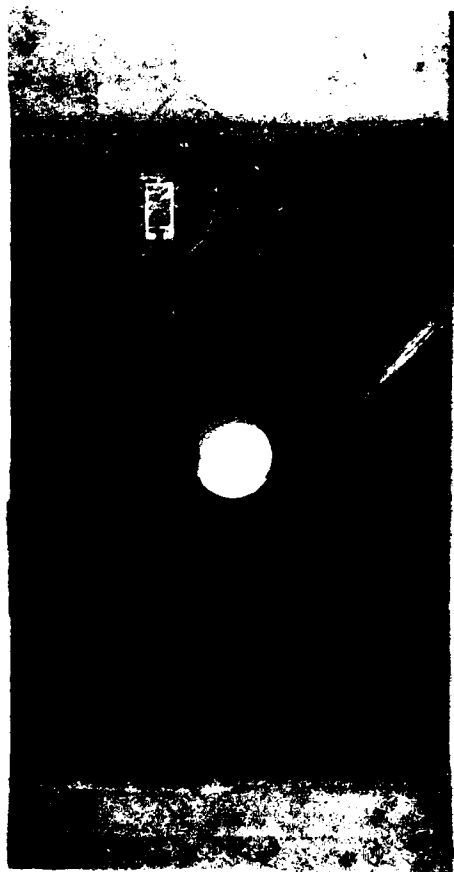


Figure 5. Typical failure of a notched specimen, No. 1-26; tested for ultimate stress/strain values. Note the location of the strain gages (two pairs, back-to-back).

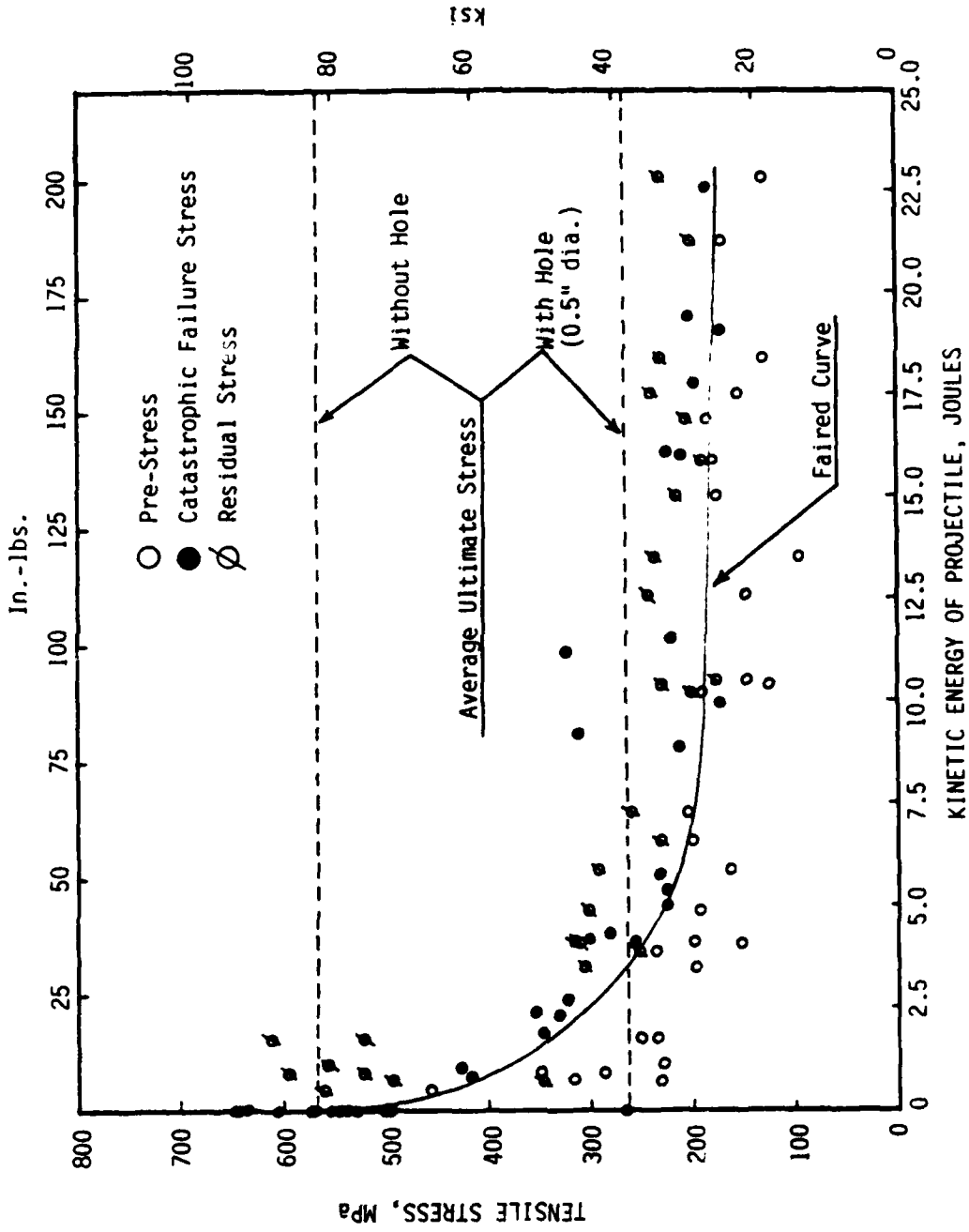


Figure 6. Graphite/Epoxy Composite, $(\pm 45, 0, 90)_{2s}$, Loaded in Tension; Tensile Stress Versus Kinetic Energy of Projectile

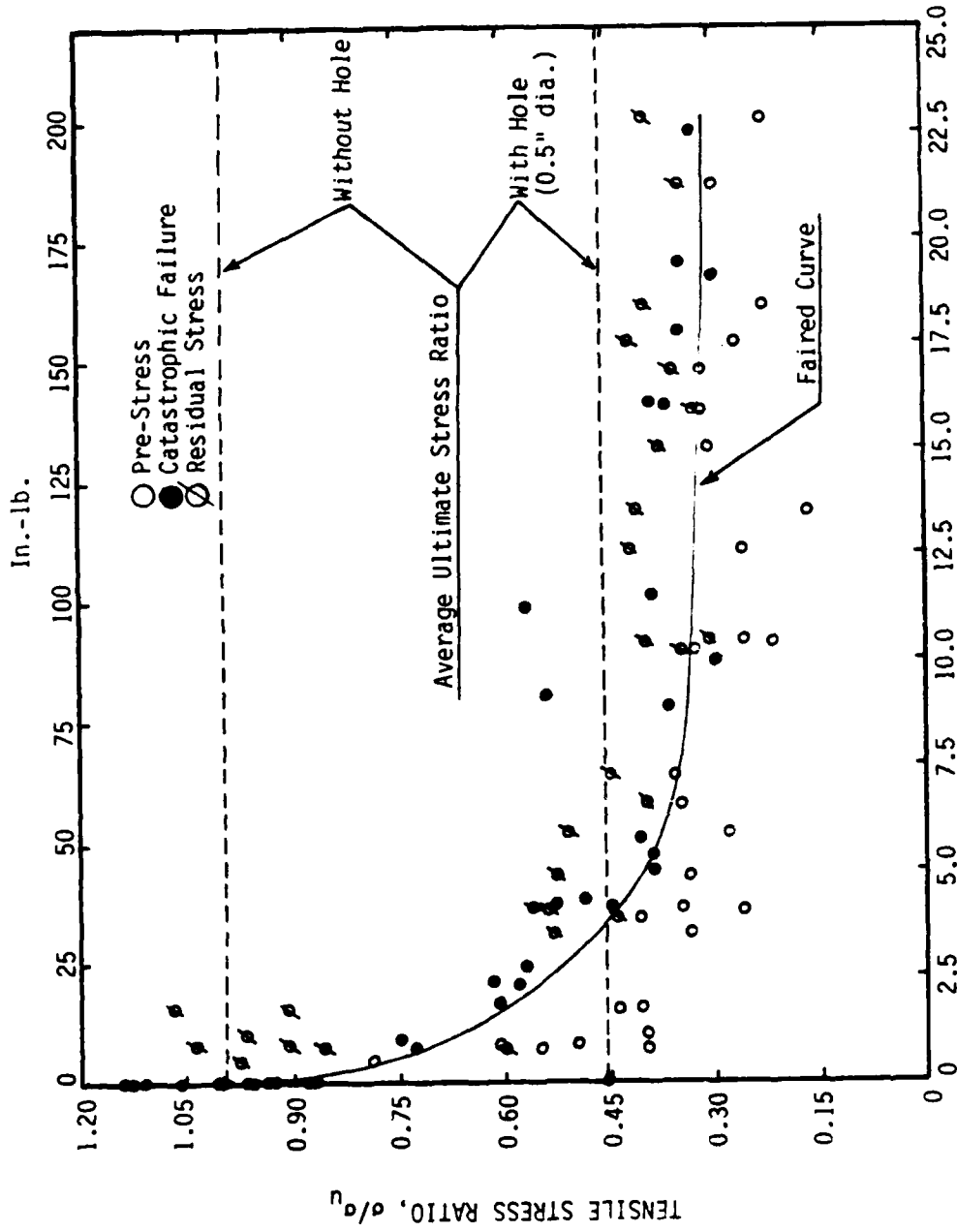
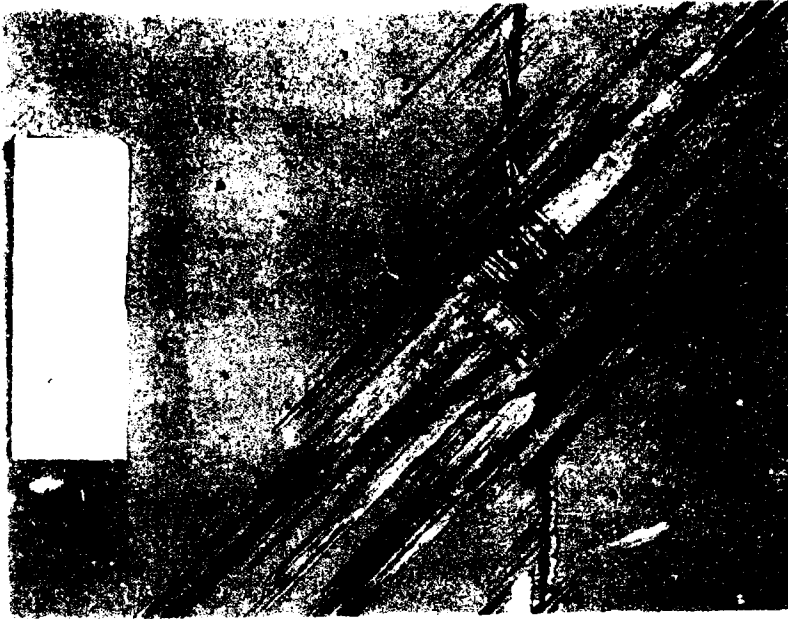


Figure 7. Graphite/Epoxy Composite, (+45,0,90)_{2s}, Loaded in Tension; stress Ratio Versus Kinetic Energy of Projectile.

prestress (this is the load applied to the specimen prior to impact - shown as an open circle), the catastrophic failure stress (this is the stress at which the specimen failed upon impact shown as solid circle), and the residual stress (this is the post-impact strength of the laminate that survived the projectile impact - shown as an open circle with a slash). For the purpose of comparison, the static ultimate strengths of the laminate, with and without hole, are also shown as broken horizontal lines in Figures 6 and 7. The solid curve shown is a faired curve drawn through appropriate test data points and is designated as a failure threshold curve for the laminate under consideration. In general, the failure threshold curve may be considered to form the boundary of the survival and the failure regions of the laminate subjected to impact. The percentage reduction in the strength of the laminate subjected to the projectile impact is shown in Figure 7. The data from this graph may be used to assess the residual strength of the laminate at various impact energy levels. Some typical patterns of laminate failures under impact loads are shown in Figures 8 through 15. By comparing these failure patterns with those shown in Figures 3 and 4, it may be noted that there is more extensive damage near the impact zone due to the projectile impact than that caused in the laminate due to failure under ultimate load. From Figure 6, it may be seen that the variation in the impact energy is small to cause catastrophic failure between stress levels from 200 MPa to 580 MPa. The slope of the failure threshold curve varies rapidly up to about 5 Joules and then tends to remain essentially constant with increasing impact energy of the

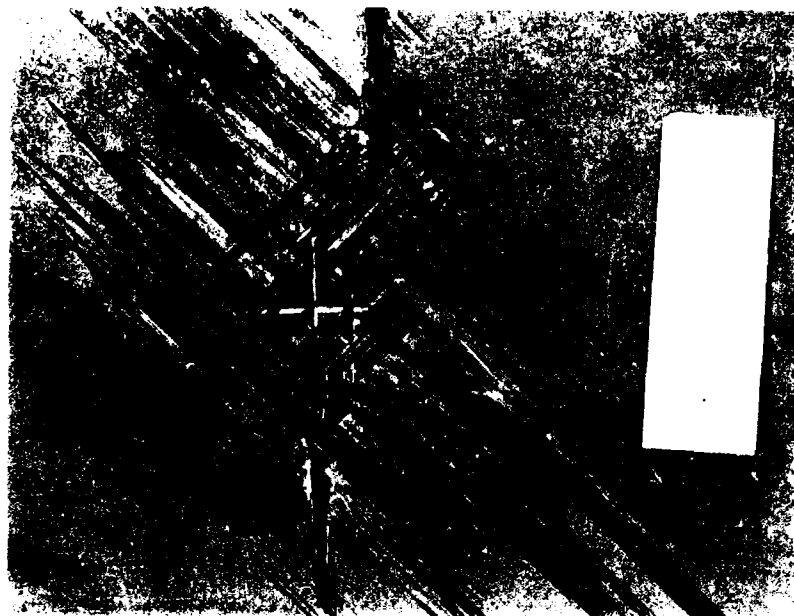


Rear View



Front View

Figure 8. Front and rear views of a catastrophically failed specimen at an impact velocity of 85 ft/sec. with a preload of 14000 lbs.

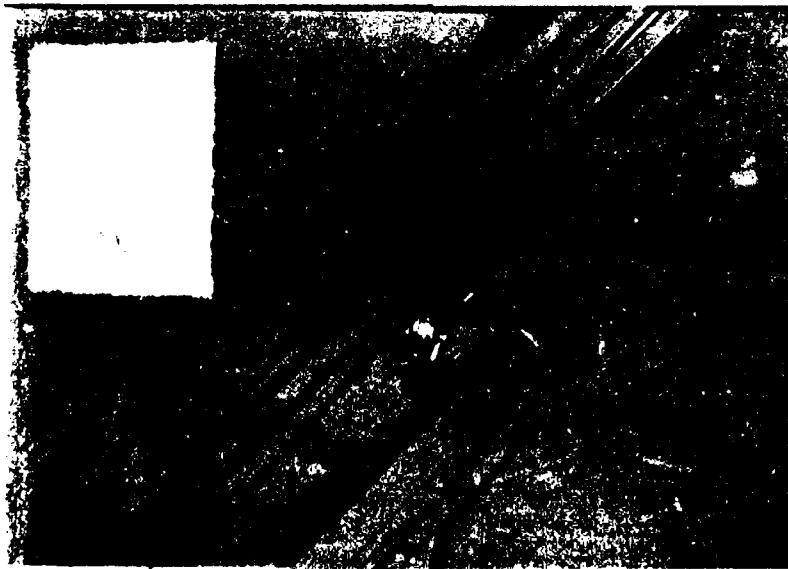


Rear View



Front View

Figure 9. Front and rear views of a failed specimen impacted at a velocity of 110 ft/sec. with a preload of 8160 lbs and stretched to failure at a strain rate of 0.02/min.

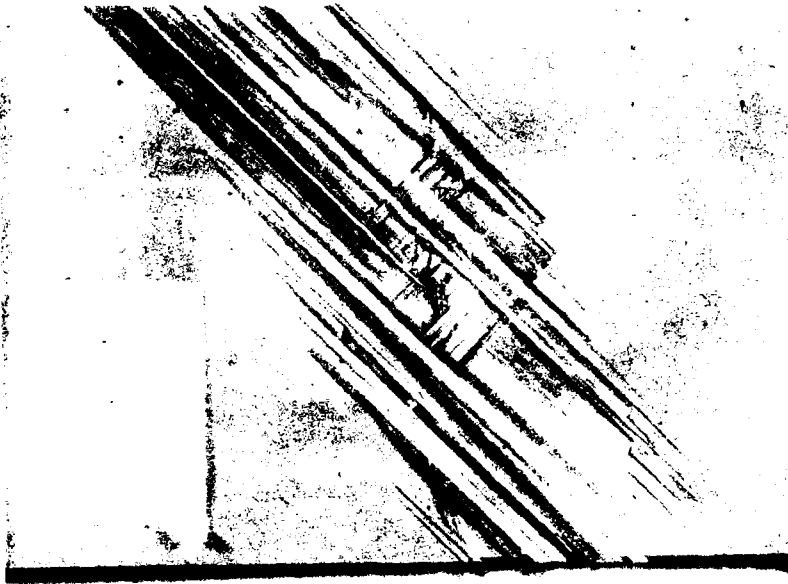


Front View

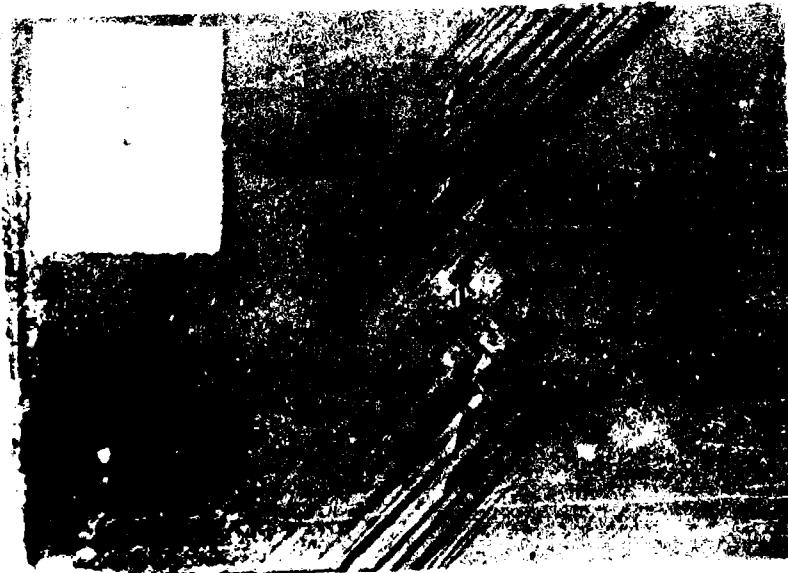


Rear View

Figure 10. Front and rear views of a specimen impacted at a velocity of 226 ft/sec. with a preload of 6600 lbs and then stretched to failure at a strain rate of 0.02/min.



Rear View



Front View

Figure 11. Front and rear views of a catastrophically failed specimen, impacted at a velocity of 335 ft/sec. with a preload of 6860 lbs.



Rear View

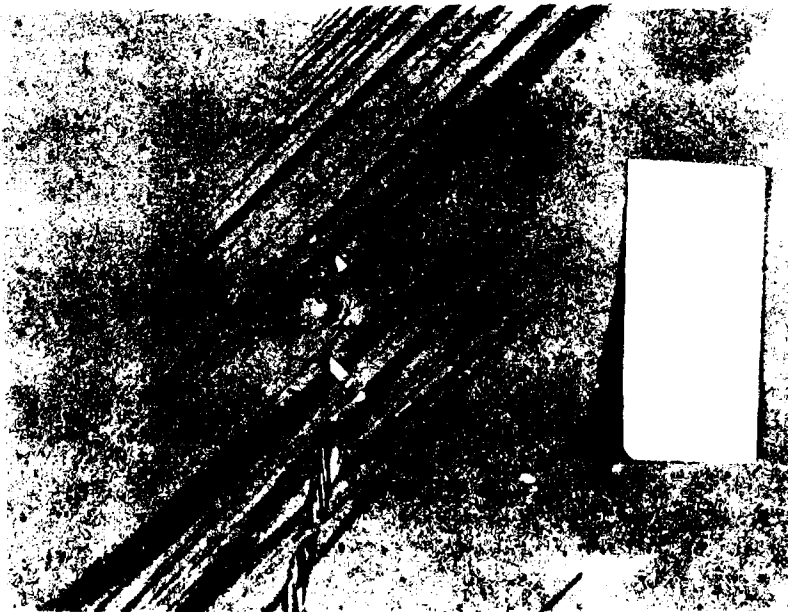


Front View

Figure 12. Front and rear views of a specimen impacted at a velocity of 226 ft/sec, with a preload of 6600 lbs, and stretched to failure at a strain rate of 0.02/min.

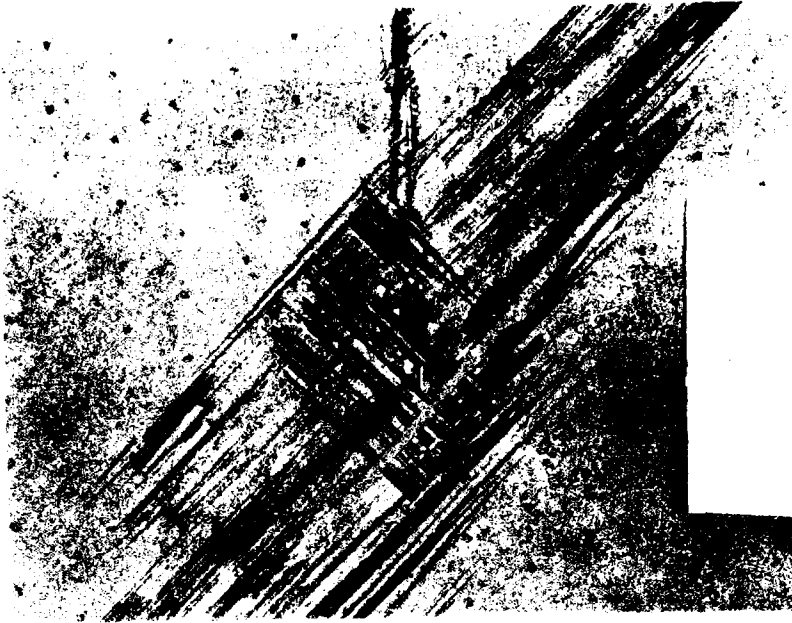


Rear View



Front View

Figure 13. Front and rear views of a catastrophically failed specimen when impacted at a velocity of 335 ft/sec. with a preload of 6860 lbs.



Rear View



Front View

Figure 14. Front and rear views of a specimen impacted at a velocity of 71 ft/sec. with a preload of 6350 lbs. and stretched to failure at a strain rate of 0.02/min.



Rear View



Front View

Figure 15. Front and rear views of a catastrophically failed specimen at a velocity of 353 ft./sec. with a preload of 6220 lbs.

projectile. In other words, the strength of the laminate degrades rapidly at higher preloads and lower impact energy. As the applied load is decreased while the energy of impact is increased, the failure threshold curve exhibits asymptotic behavior with respect to the energy axis. It may also be noted that the failure threshold curve is below the horizontal line representing the laminate strength with a clean hole. Such an observation should not be surprising since the projectile causes more damage to the laminate during and immediately after the penetration takes place than in a laminate with an implanted clean notch (hole). If the projectile could penetrate the laminate and produce literally a clean hole in it, then the failure threshold curve should coincide with the horizontal line representing the notched strength at higher energy levels.

Recently, an analytical model (44) was developed to predict the residual strength of the impact - damaged laminates. The validity of the model was verified experimentally and the comparison was found to be good. The data obtained from the present impact strength tests were tested with the above model. The details of the above model are shown in Appendix A. In order to use the above model for the present case, the rebound velocities need to be known. Since such an attempt (namely, measuring the rebound velocities) was not a part of the study, it was decided to approximate the rebound velocities for the purpose of this phase of the analysis. A faired graph, shown in Figure 16, from Reference (44) is reproduced here. Although the laminates tested in Reference (44) and the present study are different, one may note from

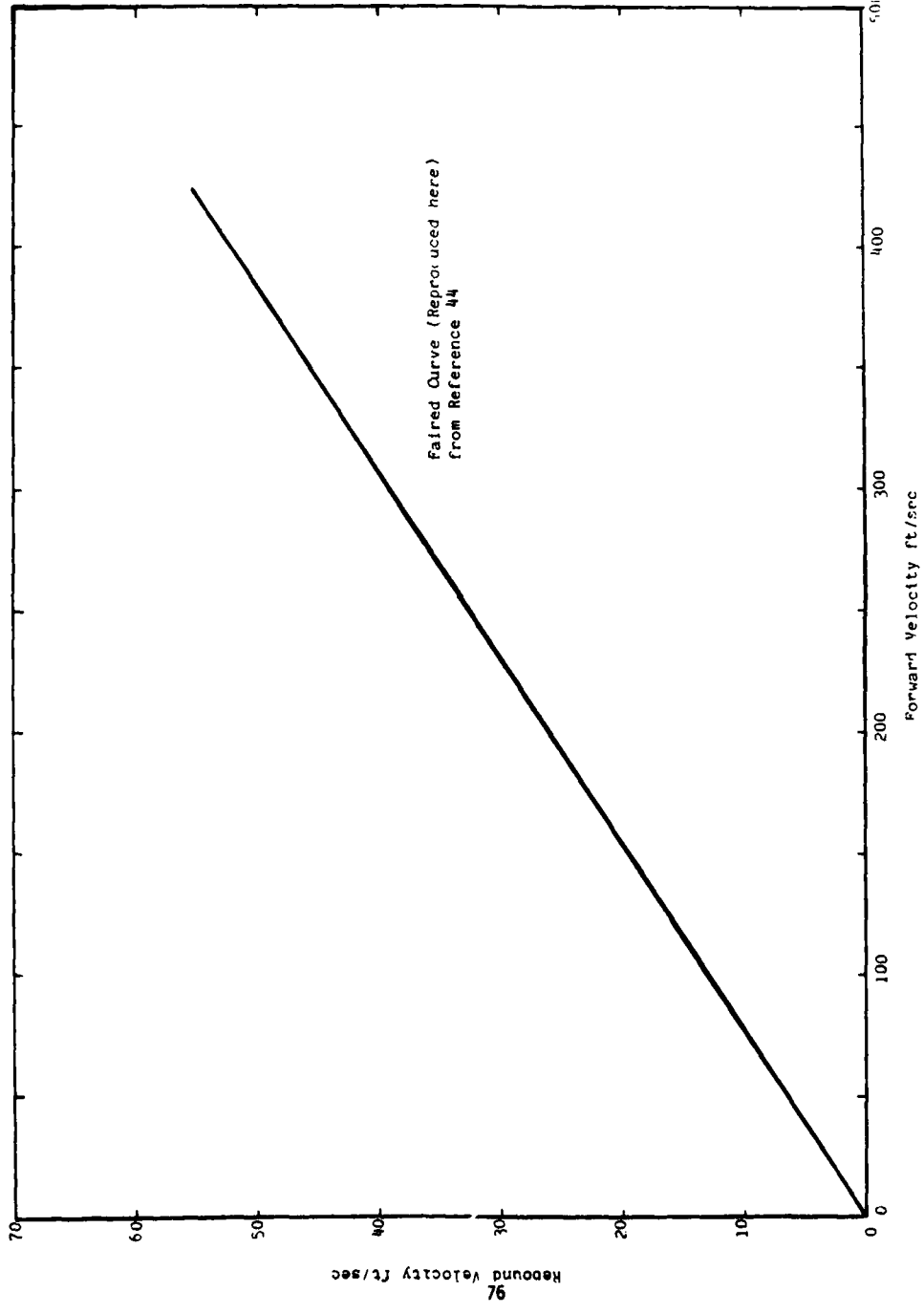


Figure 16. Forward Velocity vs Rebound Velocity.

Figure 16 that the magnitude of the rebound velocity is less than about 10% of the forward velocity. Consequently, the rebound velocities shown in Table 12 are assumed values. For the purpose of calculating the theoretical values using the above model, the error introduced through the assumed rebound velocities was considered to be small. With the help of the model and knowing the ultimate strength of the specimen and the energy imparted per unit thickness of the specimen, one can calculate the residual strength of the impact-damaged specimen. Figure 17 shows the theoretical and the experimental (faired) results plotted with σ_r/σ_0 as a function of impact energy/unit thickness. It may be observed from Figure 17 (and Table 13) that beyond an impact energy of 375 in-lb/in, the error involved between the two graphs is less than 10%.

3. Fatigue Tests With Unnotched Specimens

The experimental data is given in Table 8. The specimens were tested at eight test conditions (eight applied stress levels with $R = 0.1$ and a loading frequency of 10 Hz). The resulting data relating the applied cyclic stress with the logarithm of N , where N is the number of cycles, are plotted as shown in Figure 18. The solid curve in Figure 18 is a theoretical curve drawn using a wear-out model developed by Sendeckyj (37). The details of the wearout model are given briefly in Appendix B. It may be noted from Figure 18 that there is a reasonably good correlation between the theoretically predicted values and the experimental results. Based on this observation, the fatigue life of the laminate under consideration may be

TABLE 12: EXPERIMENTAL VALUES OF IMPACT TEST : Showing energy per unit thickness

Specimen No.	Thickness in. cm	Velocity of Impact ft/sec in/sec	Rebound Velocity ft/sec in/sec	Energy per unit thickness in. lb/in Joules/cm	Strength at Impact (σ_i) ksi MPa	Residual Strength ksi MPa	σ_i/σ_o (Exp.)	σ_r/σ_o (Exp.)
11-25	0.078	170	23.6	346	21.93	45.08	0.27	0.55
	0.198	51.82	7.2	15.39	151.19	310.78		
12-15	0.08	158	21.7	293	28.36	44.27	0.34	0.54
	0.203	48.16	6.6	13.03	195.55	305.20		
6-14	0.081	139	17.5	300	46.76	-	0.57	-
	0.206	42.37	5.3	13.34	322.41	-		
7-14	0.080	130	17.0	234	51.24	-	0.62	-
	0.203	39.62	5.2	10.41	353.29	-		
13-7	0.080	280	39.0	915	46.05	-	0.56	-
	0.203	85.34	11.9	40.70	323.75	-		
4-23	0.082	254	35.0	737	45.05	-	0.55	-
	0.208	77.42	10.7	32.78	310.29	-		
7-5	0.08	81	10.5	78	50.53	86.10	0.61	1.04
	0.203	24.69	3.2	3.47	348.18	593.63		
8-19	0.08	80	10.2	77	41.34	75.47	0.5	0.92
	0.203	24.38	3.1	3.43	285.04	520.35		
11-6	0.08	72	9.5	62	60.09	-	0.73	-
	0.203	21.95	2.9	2.76	414.31	-		
5-5	0.08	284	38.7	948	32.15	-	0.39	-
	0.203	86.56	11.8	42.17	221.69	-		

TABLE 12 (Continued) - b

Specimen No.	Thickness in. cm	Velocity of Impact ft/sec in/sec	Rebound Velocity ft/sec in/sec	Energy per unit thickness in. lb/in Joules/cm	Strength at Impact (σ_i) ksi MPa	Residual Strength ksi MPa	σ_i/σ_o (Exp.)	σ_r/σ_o (Exp.)
12-9	0.081 0.206	400 121.92	54.5 16.6	1857 82.60	18.9 130.33	33.27 229.41	0.23	0.40
13-32	0.082 0.208	185 56.39	24 7.3	398 17.7	27.89 192.29	43.78 301.82	0.34	0.53
10-18	0.081 0.206	359 109.2	45.5 13.9	1529 68.01	18.66 128.63	33.07 228.02	0.23	0.40
4-18	0.09 0.229	271 82.6	35.5 10.8	776 34.52	21.20 146.17	25.55 176.17	0.26	0.31
2-6	0.085 0.216	325 99.06	42.5 13.0	1183 52.62	25.35 174.76	31.18 214.95	0.31	0.38
7-32	0.081 0.206	297 96.53	38.5 11.7	1039 46.22	21.41 147.63	35.14 242.23	0.26	0.43
5-28	0.085 0.216	359 109.42	46.5 14.2	1448	13.84 95.43	34.25 236.13	0.17	0.42
9-9	0.08 0.203	203 61.87	26.5 8.1	491 21.84	23.53 162.20	42.45 292.68	0.29	0.52
6-11	0.083 0.211	270 82.3	35 10.7	838 37.28	18.06 124.53	33.10 228.05	0.22	0.40
1-14	0.085 0.216	264 80.47	34.5 10.5	781 34.74	24.94 171.92	-	0.30	-

TABLE 12 (Continued) - c

Specimen No.	Thickness in. cm	Velocity of Impact ft/sec in/sec	Rebound Velocity ft/sec in/sec	Energy per unit thickness in. lb/in Joules/cm	Strength at Impact (σ_i) ksi MPa	Residual Strength ksi MPa	σ_i/σ_o (Exp.)	σ_r/σ_o (Exp.)
1-4	0.086 0.218	170 51.82	22.5 6.9	319 14.19	37.05 255.45	-	0.45	-
4-7	0.078 0.198	71 21.64	9.5 2.9	61 2.71	33.37 230.10	49.85 343.73	0.41	0.6
7-29	0.084 0.213	114 34.75	14.7 4.5	148 6.53	33.81 233.12	88.57 610.67	0.41	1.07
3-12	0.083 0.211	110 33.53	14.2 4.3	139 6.18	36.07 248.72	75.23 518.64	0.44	0.91
8 11-27	0.08 0.203	127 38.71	16.5 5.0	192 8.54	47.908 330.82	-	0.58	-
2-24	0.085 0.216	89 27.13	11.7 3.6	89 3.96	33.06 227.94	80.50 555.08	0.40	0.98
8-24	0.084 0.213	201 61.26	26. 7.9	459 20.42	33.7 232.34	-	0.41	-
1-10	0.085 0.216	171 52.12	23.2 7.1	324 14.41	28.69 197.81	45.97 316.93	0.35	0.56
10-8	0.084 0.213	115 35.05	15 4.6	150 6.67	50.15 305.79	-	0.61	-
4-4	0.08 0.203	166 50.6	21.8 6.6	328 14.59	34.10 235.12	36.42 251.14	0.41	0.44

TABLE 12 (Continued) - d

Specimen No.	Thickness in. cm	Velocity of Impact		Rebound Velocity		Energy per unit thickness in. lb/in Joules/cm	Strength at Impact (σ_1)		Residual Strength ksi MPa	σ_1/σ_0 (Exp.)	σ_r/σ_0 (Exp.)
		ft/sec	in/sec	ft/sec	in/sec		ksi	MPa			
7-13	0.082 0.208	195	59.44	25.5	7.8	441	32.50	-	0.39	-	-
						19.62	224.06				
8-22	0.083 0.211	85	25.91	11	3.4	83	61.76	-	0.75	-	-
						3.69	425.79				
11-7	0.081 0.206	268	81.69	29.7	9.1	883	27.52	28.97	0.33	0.35	
						39.28	129.74		199.72		
1-22	0.082 0.208	317	96.62	41.2	12.6	1169	25	-	0.30	-	-
						52	172.37				
4-15	0.08 0.203	398	121.31	51.6	15.7	1890	26.95	-	0.33	-	-
						84.07	185.82				
6-4	0.081 0.206	57	17.37	7.8	2.4	38	65.76	80.97	0.8	0.98	
						1.69	453.40	558.43			
7-33	0.082 0.208	215	65.53	28	8.5	539	29.24	33.21	0.35	0.40	
						23.98	201.70	228.95			
9-17	0.081 0.206	187	57.00	24	7.3	413	32.47	-	0.39	-	-
						18.37	223.85				
3-4	0.082 0.208	226	68.88	29.2	8.9	595	29.58	37.62	0.36	0.46	
						26.47	203.97	259.41			
8-3	0.086 0.218	351	106.98	45.8	14.0	1467	22.52	34.57	0.27	0.42	
						65.26	155.29	238.32			

TABLE 12 (Continued) - e

Specimen No.	Thickness in. cm	Velocity of Impact ft/sec in/sec	Rebound Velocity ft/sec in/sec	Energy per unit thickness in. lb/in Joules/cm	Strength at Impact (σ_i) ksi MPa	Residual Strength ksi MPa	σ_i/σ_r (Exp.)	σ_r/σ_o (Exp.)
3-7	0.08	344	44.6	1412	26.64	29.74		
	0.203	104.85	13.6	62.81	183.69	205.07	0.32	0.36
2-19	0.085	366	47.5	1504	25.09	-	0.30	-
	0.216	111.56	14.5	66.9	172.97	-		
11-13	0.08	363	46.2	1482	23.56	-	0.35	-
	0.203	107.59	14.1	65.92	196.90	-		
1-12	0.084	369	45	1575	29.30	-	0.36	-
	0.213	112.47	13.7	70.06	201.99	-		
13-30	0.081	336	43.7	1329	32.68	-	0.4	-
	0.206	102.41	13.3	59.12	225.34	-		
4-27	0.079	74	9.8	66	45.65	71.37	0.55	0.87
	0.201	22.56	3.0	2.94	314.74	492.10		
13-2	0.085	172	22	334	43.68	-	0.53	-
	0.216	52.43	6.7	14.86	301.20	-		
1-24	0.083	250	32.5	718	30.79	-	0.37	-
	0.211	76.20	9.9	31.94	212.15	-		
6-17	0.083	335	43.7	1288	30.36	-	0.37	-
	0.211	102.11	13.3	57.29	209.35	-		
9-32	0.081	250	32.5	718	30.90	-	0.38	-
	0.206	76.2	9.9	31.94	312.03	-		

TABLE 12 (Continued) - f

Specimen No.	Thickness		Velocity of Impact		Rebound Velocity		Energy per unit thickness		Strength at Impact (σ_i)		Residual Strength		σ_i/σ_0 (Exp.)		σ_r/σ_0 (Exp.)	
	in.	cm	ft/sec	in/sec	ft/sec	in/sec	in. lb/in	Joules/cm	ksi	MPa	ksi	MPa	ksi	MPa		
3-26	0.083		386		46		1755		34.43		29.12		0.30		0.35	
	0.211		117.65		14.0		78.07		168.45		200.77					

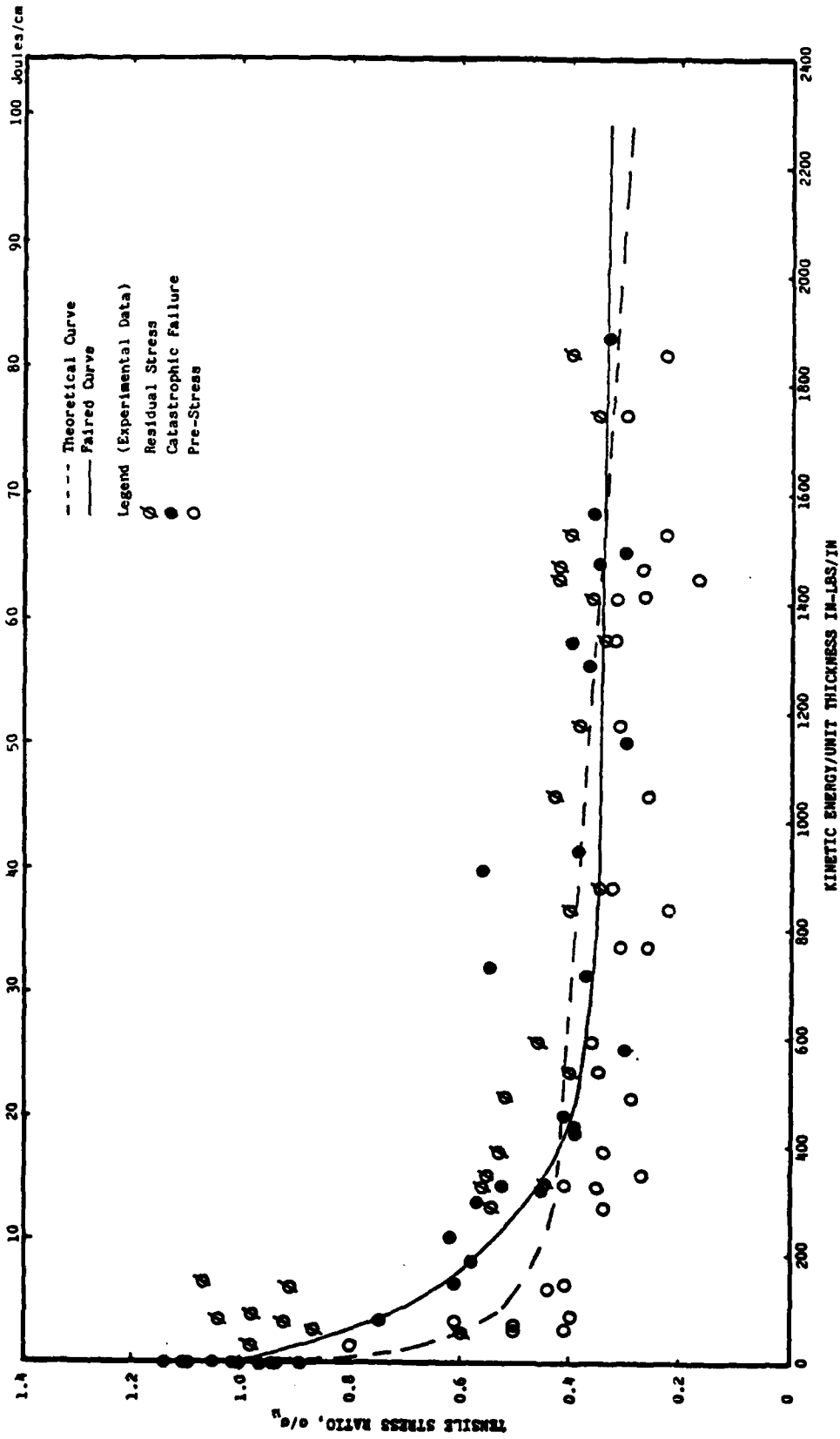


Figure 17. Graphite/Epoxy Composite, $(\pm 45, 0, 90)_{2a}$. Loaded in Tension, Stress Ratio Versus Kinetic Energy of Projectile.

TABLE 13. PERCENTAGE OF ERROR INVOLVED IN THEORETICAL AND EXPERIMENTAL VALUES*

Sl. No.	W (Net Energy)	σ_r/σ_0 (Exp.)	σ_r/σ_0 (Theo.)	Percentage Error
1	100	0.70	0.477	31.8
2	300	0.48	0.446	7.1
3	500	0.39	0.420	7.1
4	700	0.36	0.398	9.5
5	900	0.35	0.379	7.7
6	1100	0.340	0.348	2.3
7	1300	0.340	0.348	2.3
8	1500	0.34	0.336	1.2
9	1700	0.337	0.324	3.9
10	1900	0.336	6.314	6.5

*The values in the above table were generated by reading off of the (faired) theoretical and experimental graphs shown in Figure 17.

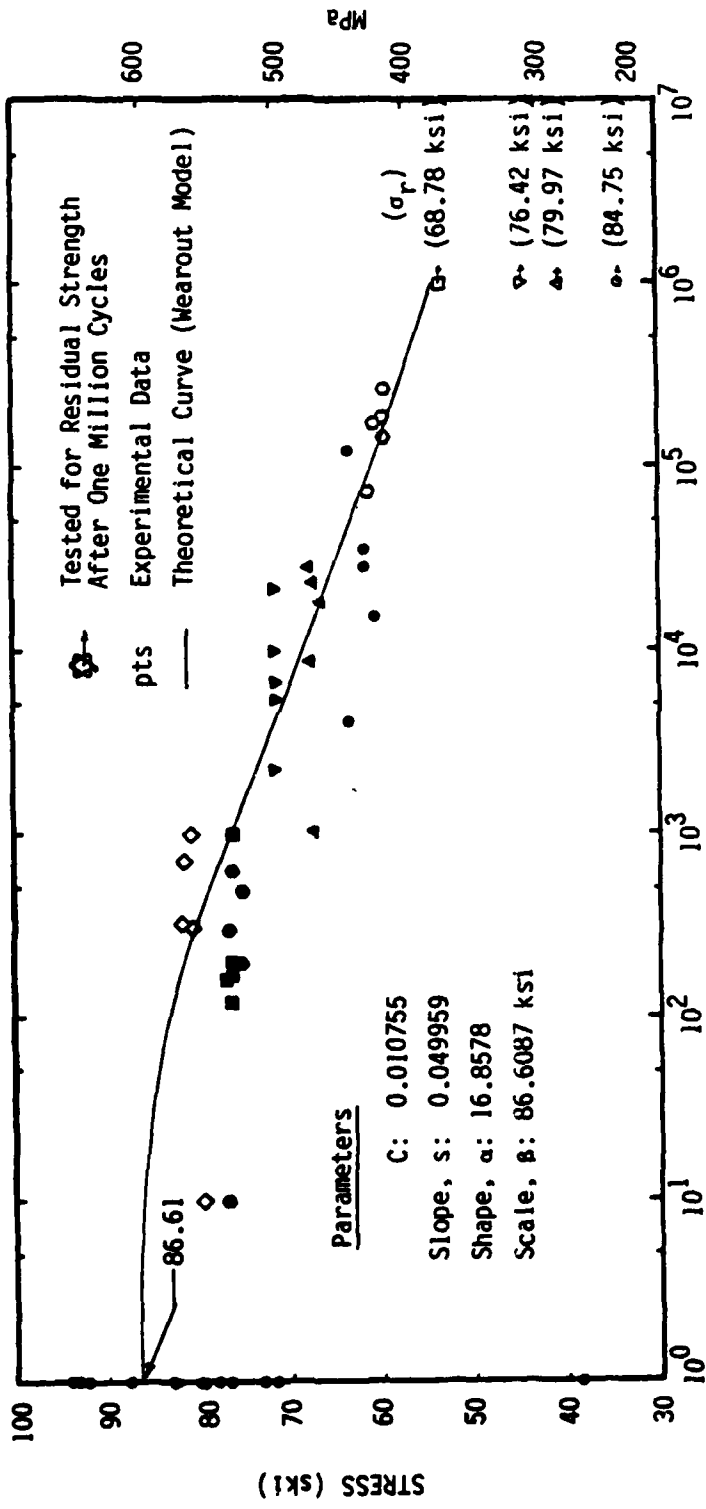


Figure 18. Tension-Tension Fatigue Test with $R = 0.1$ and Frequency of 10Hz; Graphite/Epoxy Composite ($\pm 45, 0, 90$)_{2s}; Maximum Stress Versus Fatigue Life. Residual Strength Values Shown on the Graph are Average Values.

predicted without conducting extensive tests. However, it should be noted that the fatigue life prediction for laminates should take into consideration several test parameters such as the frequency of loading, stacking sequences, etc., that are known to influence the fatigue life. The fatigue life of the laminate tested was found to be more than a million cycles, as shown in Figure 18 at an applied stress level equal to or less than about 54 ksi. This value is about 65% of the static ultimate strength.

Most of the tests conducted at or below an applied stress level of 54 ksi were terminated after reaching one million cycles and then loaded statically to determine the residual strength. The average values of the residual strength of the laminates tested at each applied stress level are also shown in Figure 18. At least four specimens were tested at each test condition in the determination of the average residual strength. If one assumes a stress under fatigue loading at about 46% of the static ultimate strength, then the design or working strength for this laminate is about 40 ksi. With this value in the background, one may observe from Figure 18 that the residual strength of the laminate at an applied stress level of 40 ksi is about 80 ksi, a value close to the static ultimate strength of 82.76 ksi, after a million cycles. In other words, it may be stated that this laminate would not degrade in its strength after experiencing a million cycles of fatigue loads at a design stress level of 40 ksi. It may also be observed from Figure 18 that the residual strength of the laminate increases with a decrease in the applied stress level at one million cycles.

For the purpose of comparison, theoretical values were also generated using a power law model (37). The theoretical values from the power law and the wearout models (Appendix B) as well as the test data are plotted as shown in Figure 19. From the σ -N plot shown in Figure 19, it appears that both the models can predict the fatigue lives. The σ -N curve of the wearout model is flat at higher applied stresses. The power law model shows a nonlinear behavior. The degree of flatness of the σ -N curve in the wearout model depends upon the value of the slope parameter (37). As the value of the slope parameter approaches zero, the size of the flat region increases. The experimental data and the theoretical values obtained from using the wearout model are plotted in a log-log space as shown in Figure 20. This plot shows a good correlation between the experimental and the theoretical data. Using the wearout and the power law models, the probability of survival vs. equivalent static strength curves are drawn as shown in Figures 21 and 22. A brief explanation to calculate the data points is given on p. 129. By comparing these graphs, it appears that the wearout model has less tendency to segregate the same stress-level-points which is a sign of even statistical distribution (37).

One of the objectives of the proposed work was to study the progressive damage propagation in the laminate due to fatigue loads. In order to observe the damage propagation, a non-destructive technique using X-ray radiography was used. This technique is known to be helpful

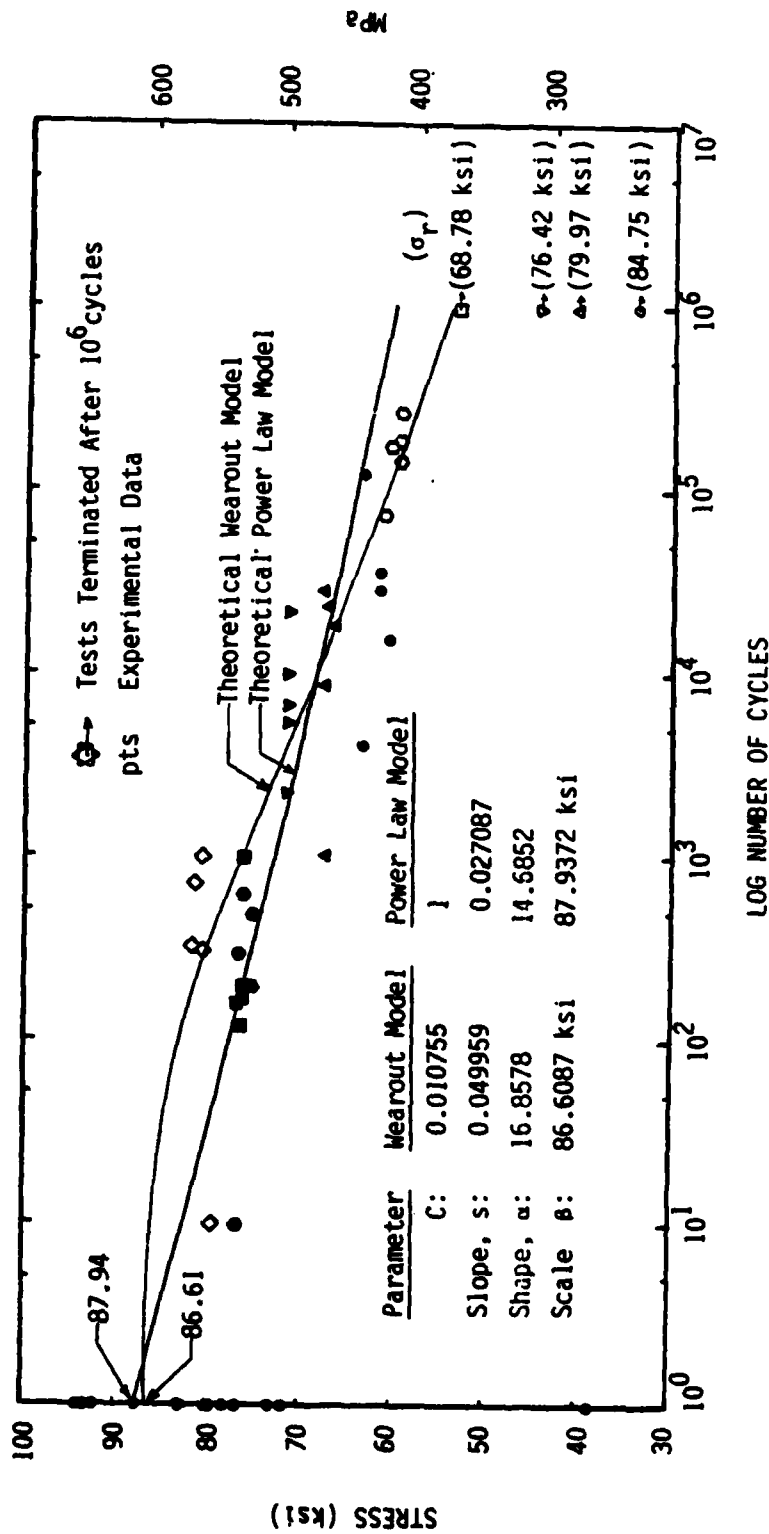


Figure 19. Tension-Tension Fatigue Test with $R = 0.1$ and a Frequency of 10Hz. Maximum Stress Versus Log Number of Cycles. Residual Strength Values Shown on the Graph are Average Values.

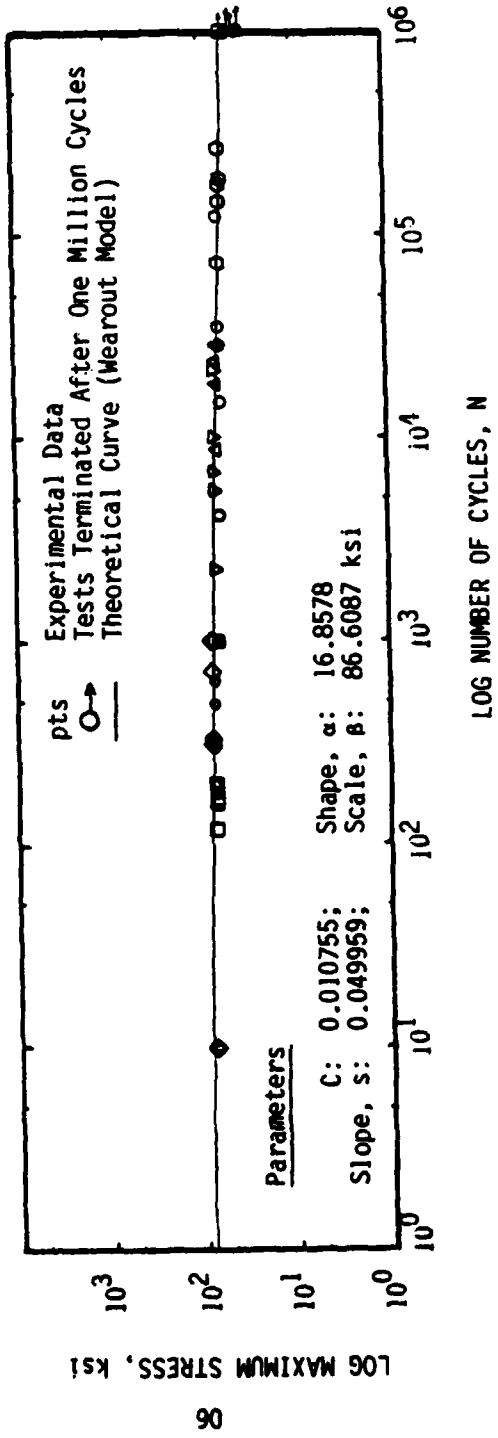


Figure 20. Tension-Tension Fatigue Test with $R = 0.1$ Frequency 10Hz; Graphite/Epoxy Composite ($\pm 45, 0, 90$)_{2s}; Log-Log Plot of Maximum Stress Versus Number of Cycles.

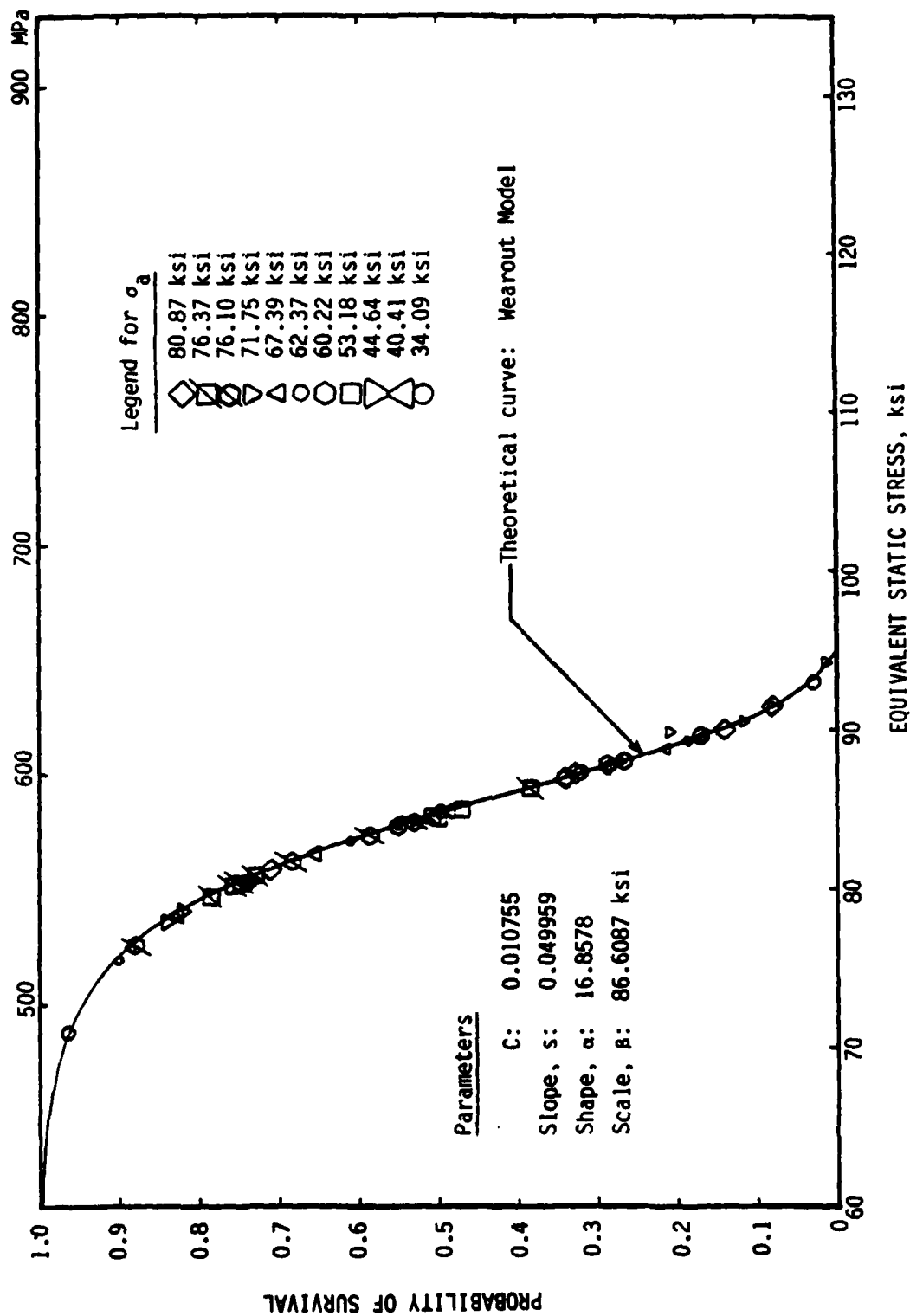


Figure 21. Probability of Survival for the Equivalent Static Strength Data Corresponding to Tension-Tension Fatigue Data, $(\pm 45, 0, 90)_{2s}$ Graphite/Epoxy Composite.

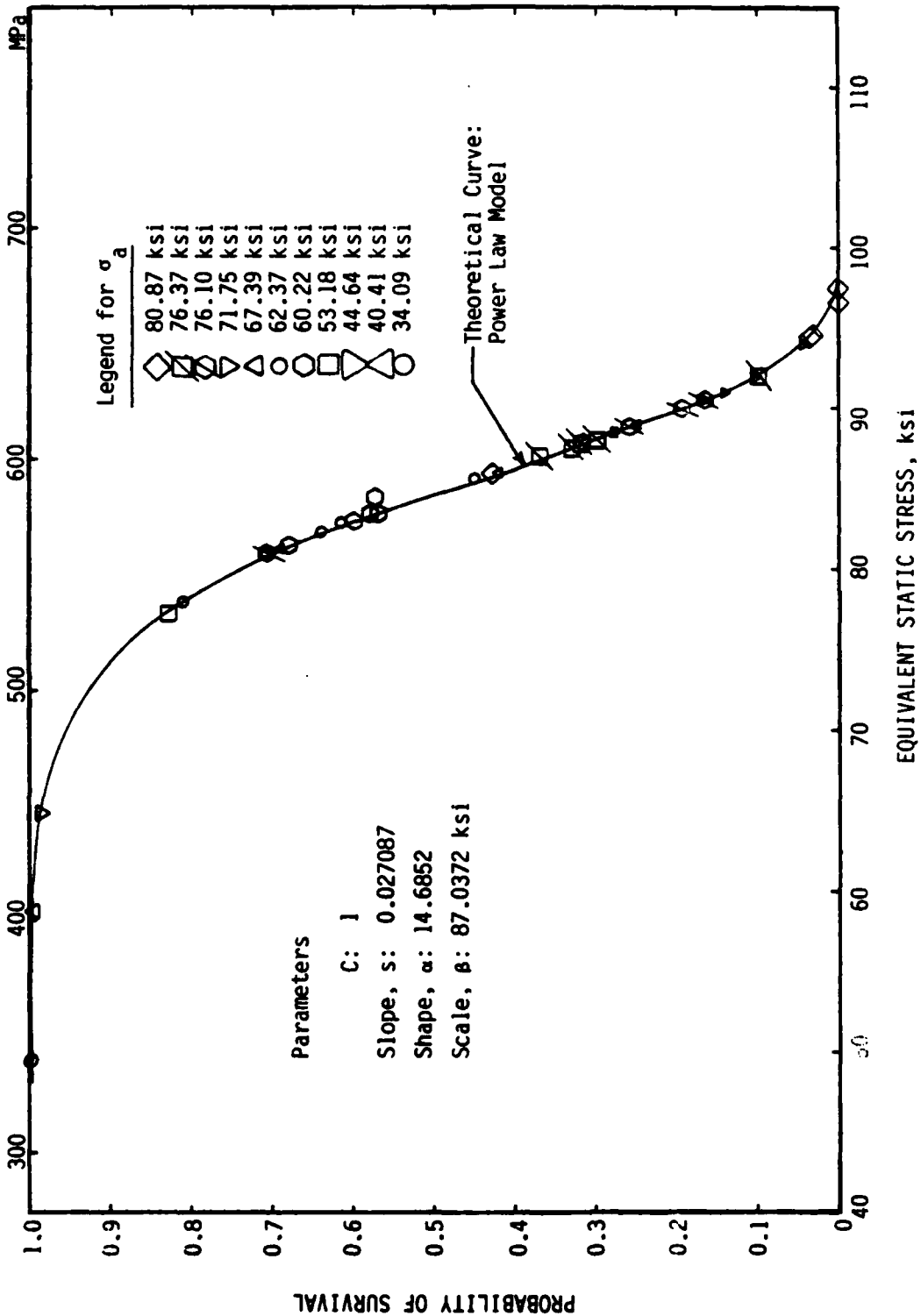


Figure 22. Probability of Survival for the Equivalent Static Strenth Data Corresponding to Tension-Tension Fatigue Data, ($\pm 45, 0, 90$)_{2s} Graphite/Epoxy Composite.

in documenting the fiber fracture, matrix failure and delaminations. Though the usage of TBE (Tetrabromoethane) is successful in enhancing the X-ray radiographs, its usage is restricted because of its toxic nature as well as an elaborate set-up requirement. Further, it appears to have an affinity to plasticize the epoxy (45). Because of these reasons, a zinc iodide solution has been used in enhancing the X-ray radiographs. The zinc iodide solution is not only cheaper but also is easier to handle.

The progressive damage documentations as shown in Figures 23 through 45 are considered to be typical of the numerous tests conducted under cyclical fatigue loads. It may be recalled that the laminate has a $(\pm 45, 0, 90)_{2S}$ orientation and stacking sequence. In general, the weaker 90° plies will fracture first and the load is transferred through the matrix to the other surviving fibers in the laminate. The $\pm 45^\circ$ fibers are expected to fail next with an increase in the applied loads. Eventually, the composite will fail as the applied stress exceeds the combined resistive stress of the 0° fibers. Initial fracture location in the 90° fibers appears to play a dominant role in the delamination process. This effect may be seen on a close observation of Figures 29 through 34. As the fatigue life increases, the extent of delaminations on both the free edges will be identical. Effect of the applied stresses on the fatigue failure at a particular fatigue life can be analyzed. Similarly, for a given stress level, fiber fracture and matrix failure at various fatigue lives can be analyzed. With this in the background, the radiographs at 34 ksi, 54 ksi, 64 ksi and 67 ksi

X - RAY RADIOGRAPHS OF SPECIMEN NUMBER 8-32



Figure 23

$\sigma = 0$, $R = 0$
 $N = 0$

Figure 24

$\sigma = 34.09$ ksi, $R = 0.1$
 $N = 200,000$ cycles

X-RAY RADIOGRAPHS OF SPECIMEN NUMBER 8-32



Figure 25

$\sigma = 34.09$ ksi, $R = 0.1$
 $N = 400,000$ cycles

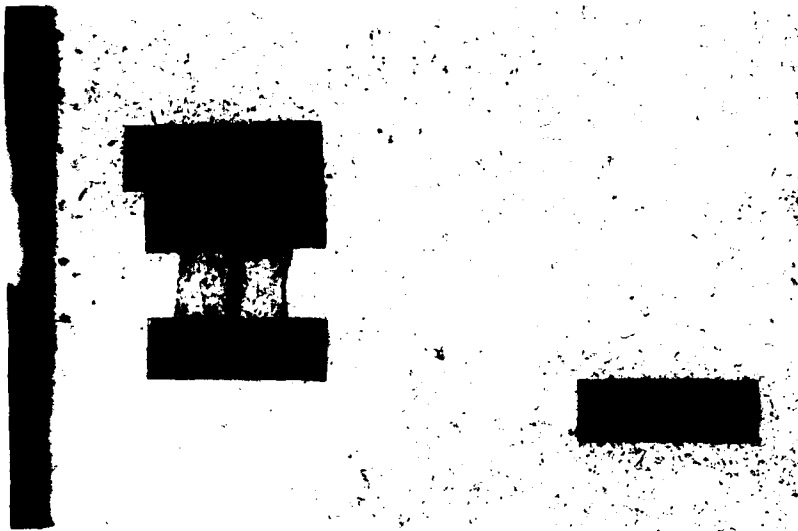


Figure 26

$\sigma = 34.09$ ksi, $R = 0.1$
 $N = 600,000$ cycles

X-RAY RADIOGRAPHS OF SPECIMEN NUMBER 8-32



Figure 28

$\sigma = 34.09$ ksi, $R = 0.1$
 $N = 1,000,000$ cycles

Figure 27

$\sigma = 34.09$ ksi, $R = 0.1$
 $N = 800,000$ cycles

X-RAY RADIOGRAPHS OF SPECIMEN NUMBER 10-26

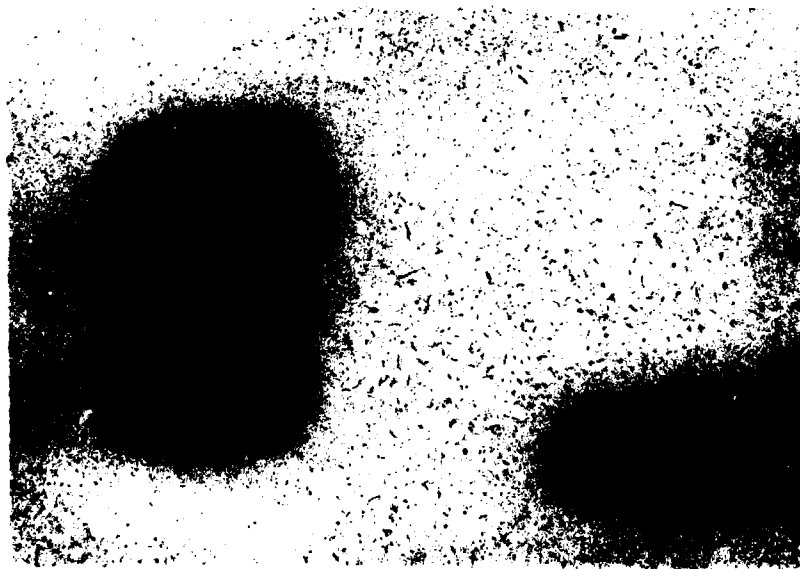


Figure 29

$\sigma = 0$, $R = 0$
 $N = 0$

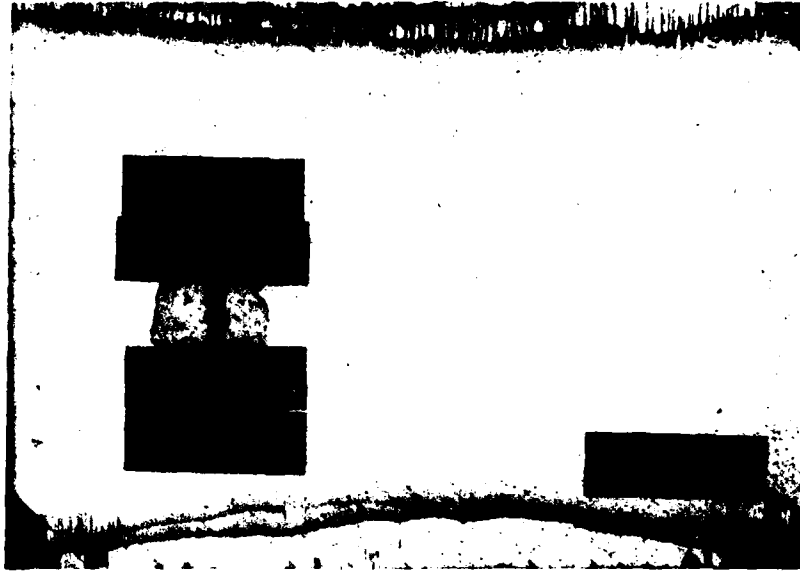


Figure 30

$\sigma = 35.81$ ksi, $R = 0.1$
 $N = 200,000$ cycles

X-RAY RADIOGRAPHS OF SPECIMEN NUMBER 10-26



Figure 31

$\sigma = 35.81$ ksi, $R = 0.1$
 $N = 400,000$ cycles

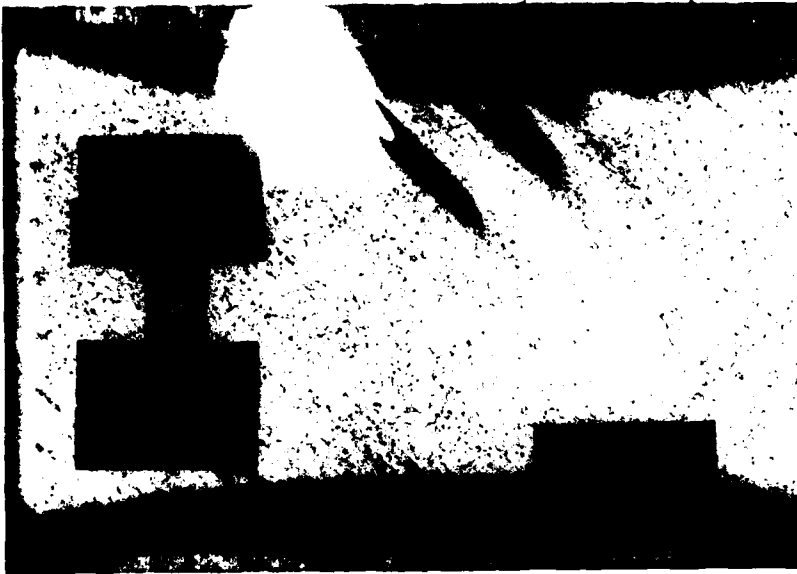


Figure 32

$\sigma = 35.81$ ksi, $R = 0.1$
 $N = 600,000$ cycles

X-RAY RADIOGRAPHS OF SPECIMEN NUMBER 10-26



Figure 33

$\sigma = 35.81$ ksi, $R = 0.1$
 $N = 800,000$ cycles



Figure 34

$\sigma = 35.81$ ksi, $R = 0.1$
 $N = 1,000,000$ cycles

X-RAY RADIOGRAPHS OF SPECIMEN NUMBER 5-10



Figure 35

$\sigma = 0$, $R = 0$
 $N = 0$



Figure 36

$\sigma = 63.74$ ksi, $R = 0.1$
 $N = 5,000$ cycles

X-RAY RADIOGRAPHS OF SPECIMEN NUMBER 5-10

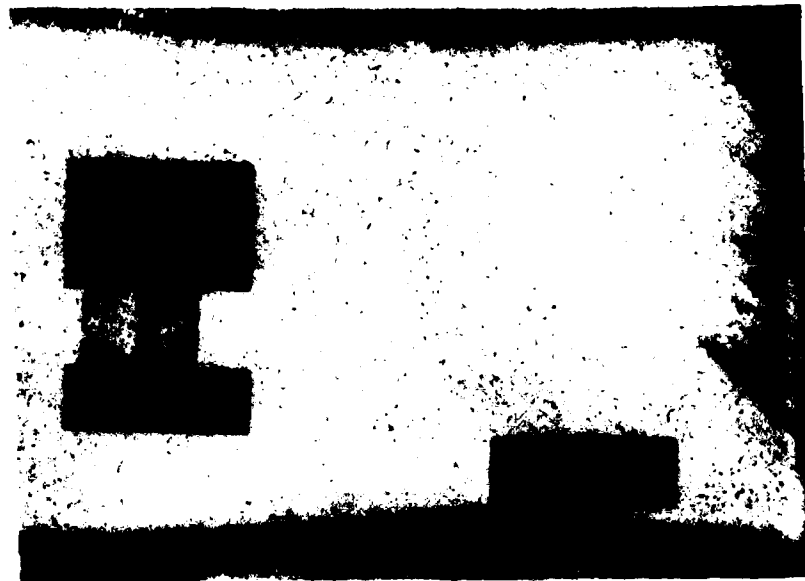
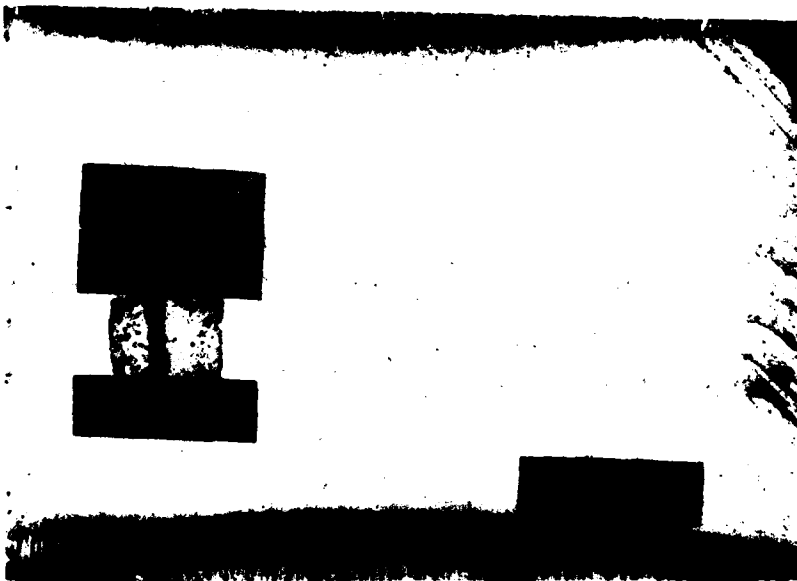


Figure 38

$\sigma = 63.74$ ksi, $R = 0.1$
 $N = 30,000$ cycles

Figure 37

$\sigma = 63.74$ ksi, $R = 0.1$
 $N = 15,000$ cycles

X-RAY RADIOGRAPHS OF SPECIMEN NUMBER 5-10

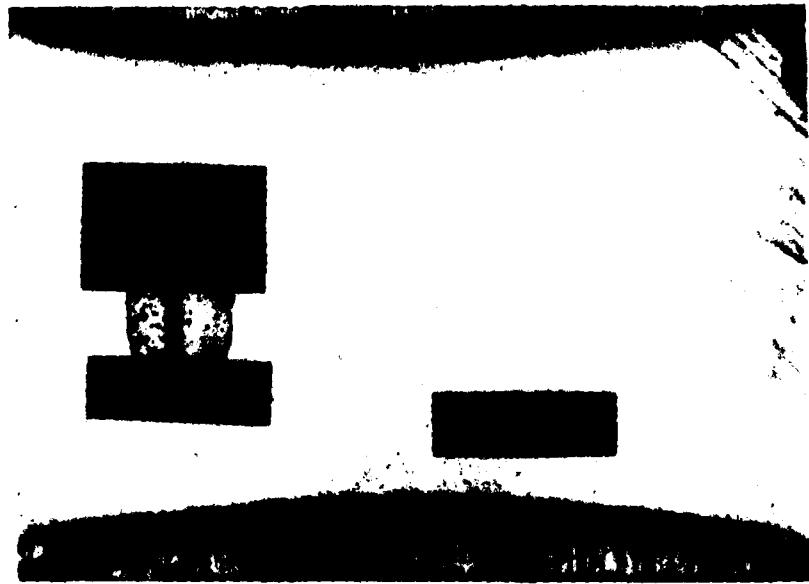


Figure 39

$\sigma = 63.74$ ksi, $R = 0.1$
 $N = 45,000$ cycles

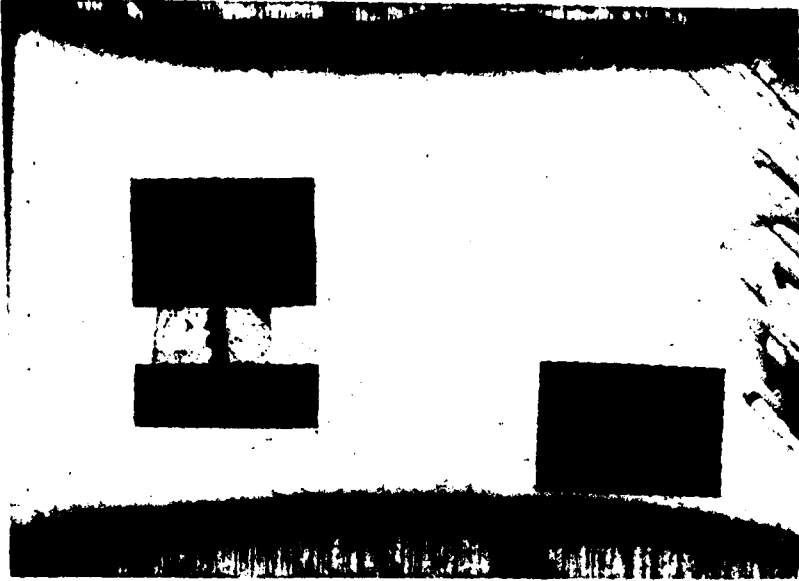


Figure 40

$\sigma = 63.74$ ksi, $R = 0.1$
 $N = 70,000$ cycles

X-RAY RADIOGRAPH OF SPECIMEN NUMBER 5-10



Figure 41

$\sigma = 63.74$ ksi, $R = 0.1$

$N = 120,000$ cycles

X-RAY RADIOGRAPHS OF SPECIMEN NUMBER 6-5

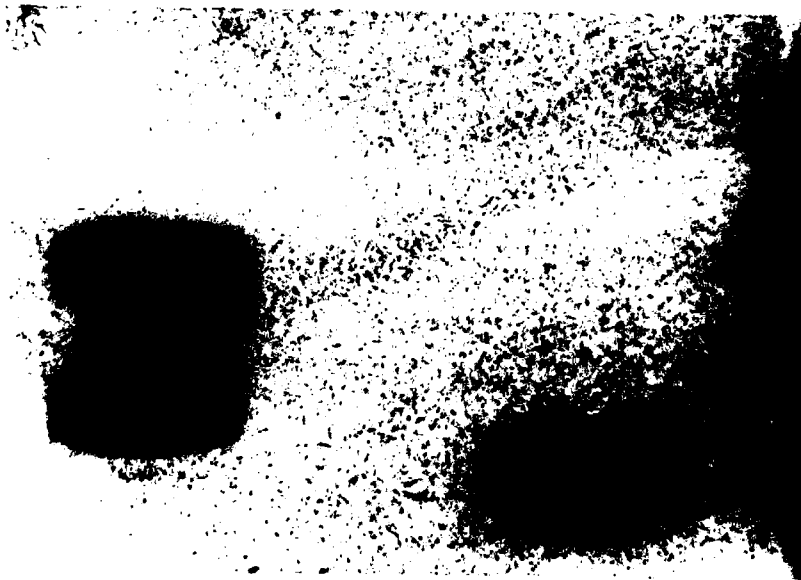


Figure 42

$\sigma = 0$, $R = 0$
 $N = 0$



Figure 43

$\sigma = 66.67$ ksi, $R = 0.1$
 $N = 5,000$ cycles

X-RAY RADIOGRAPHS OF SPECIMEN NUMBER 6-5

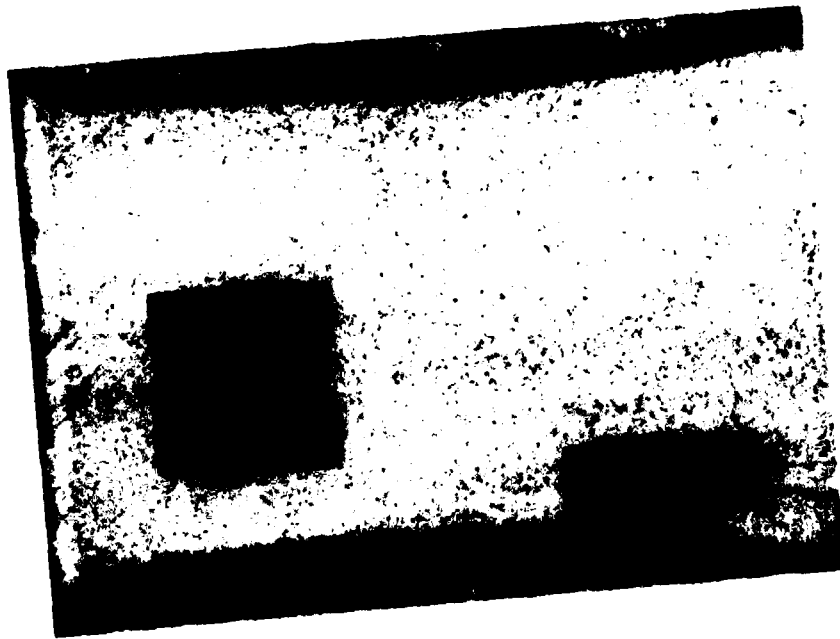


Figure 44

$\sigma = 66.67$ ksi, $R = 0.1$
 $N = 10,000$ cycles

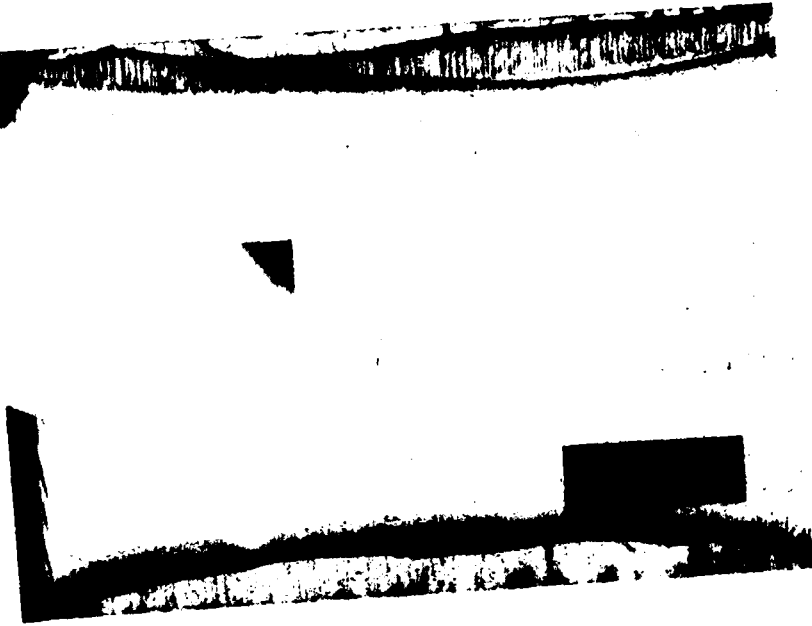


Figure 45

$\sigma = 66.67$ ksi, $R = 0.1$
 $N = 15,000$ cycles

are considered and they are shown in Figures 23 through 45. If the damage gets initiated on the left edge of the imaginary central vertical line (while facing the laminate plane), the tendency of the plies to delaminate on that side will be more compared to the other side.

Damage analysis of the specimen No. 10-26 shown in Figures 29 through 34 reveals the following:

Figure No.:

- 29 Radiograph of a typical virgin specimen.
- 30 Radiograph after completion of 200K cycles. Matrix cracking in both the 90° and $\pm 45^\circ$ plies may be seen. Delaminations at the free edges of the laminate may also be observed.
- 31 Radiograph taken after 400K cycles. Matrix cracking has increased considerably in the $\pm 45^\circ$ plies and delamination at the free edges appears to be identical in shape.
- 32 This radiograph shows the spreading of matrix cracking in $\pm 45^\circ$ plies after 600K cycles. (The white shaded area seen on the positive is due to a black spot formation in developing process, reason unknown).
- 33 This radiograph shows the appearance of damage after 800K cycles. The matrix cracking in the $\pm 45^\circ$ plies is widespread and distinct.
- 34 This view shows the damage after 1000K cycles. About 80% of the $\pm 45^\circ$ ply area appears to have extensive matrix cracking.

The radiographic technique as presented here needs to be improved further. One of the ways of improving the quality of the radiographs may be to apply the penetrant to the specimen while it is under a small load (to open the cracks, delaminations, etc., further). This technique, however, was not utilized in the present work.

4. Fatigue Tests With Notched Specimens

The results of the fatigue tests (Table 9) on specimens with a

centrally drilled hole show the effect of the applied stress and the number of fatigue cycles on the fatigue life of the specimen. These results are plotted as shown in Figure 46. This graph of the applied stress against the number of cycles reveals that the degradation of the fatigue lives due to fatigue loading is negligibly small up to a million cycles. The residual strength of the laminate is higher than the static ultimate strength of the notched laminate after a million cycles. From the three different load levels chosen for these tests, it is seen that the residual stress of the specimen after 10^6 cycles increases with the increase of the applied stress. For example, the average residual stress at an applied stress of 20.36 ksi is 40.81 ksi whereas that corresponding to an applied stress of 36 ksi is 47.85 ksi.

Some tests were performed to study the variation of the residual strength of the specimen with the number of fatigue cycles. The specimens were tested for their residual strength after each 200,000 cycles at three different applied stress levels. From the resulting experimental data obtained, it is seen that the variation of residual strength with the number of cycles is not significant. In other words, the degradation in strength of the specimen with the number of fatigue cycles, for a particular value of applied stress and within 10^6 cycles, is insignificantly small. These results are also shown in Fig. 46.

Radiographs of the specimens were taken at every 200,000 cycles to study the damage propagation in the material. In the radiographs of specimen No. 10-2, Figures 47(a) through 47(f), the failure of $\pm 45^\circ$ plies around the hole may be seen. The area of damage can be seen to

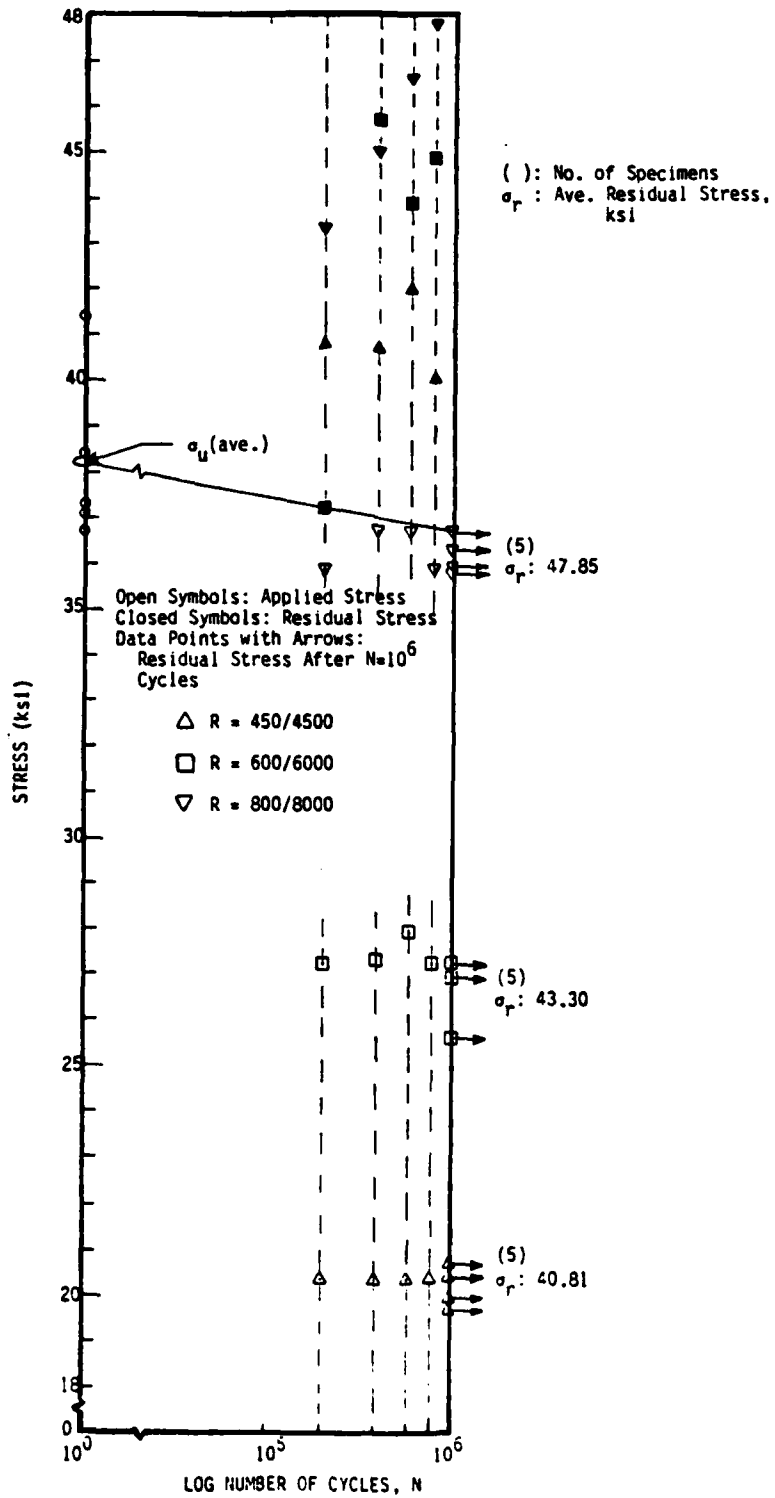


Figure 46. Stress Amplitude Vs Fatigue Life of Notched Laminate

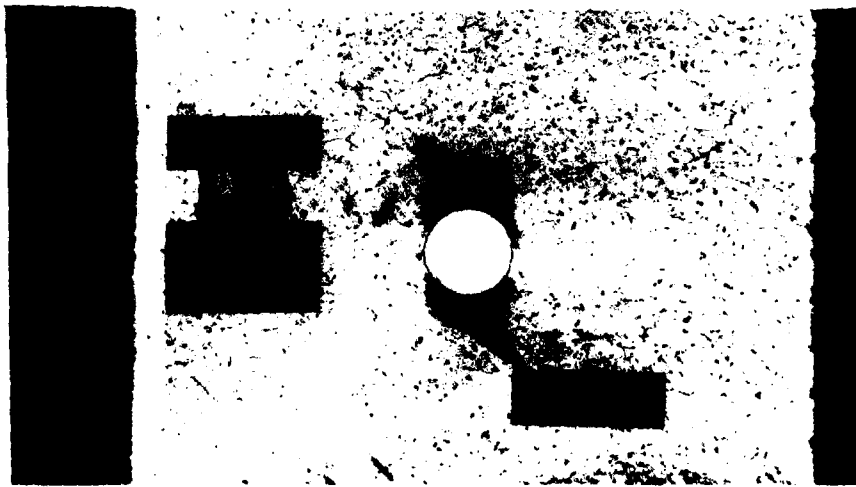


(a) N = 0



(b) N = 200,000 cycles

Figure 47. Radiograph of Specimen Number 10-2 Subjected to Cyclic Loading at $\sigma = 36.20$ ksi, $F = 10$ Hz, Stress Ratio, $R = 0.1$

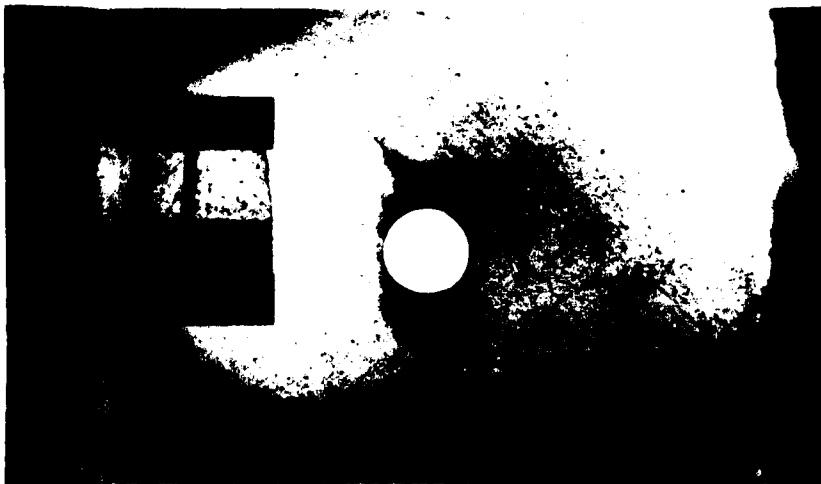


(c) N = 400,000 cycles

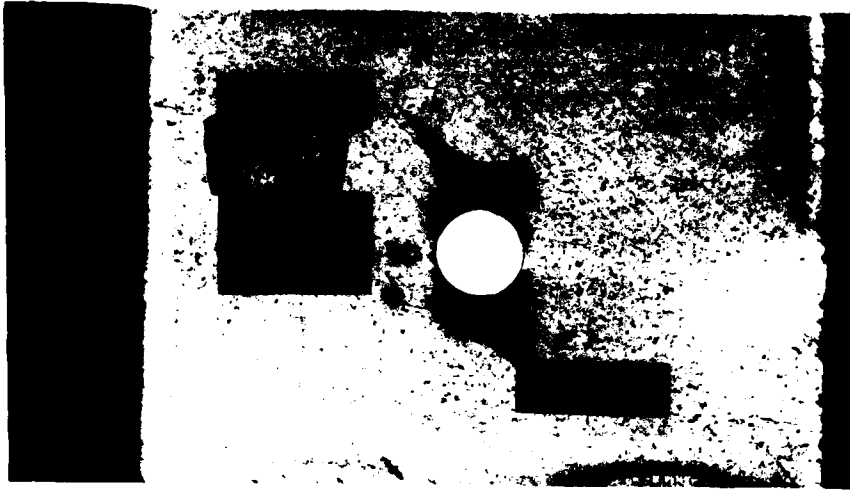


(d) N = 600,000 cycles

Figure 47. Radiograph of Specimen Number 10-2 Subjected to Cyclic Loading at $\sigma = 36.20$ ksi, $f = 10$ Hz, Stress Ratio, $R = 0.1$



(e) $N = 800,000$ cycles



(f) $N = 10^6$ cycles

Figure 47. Radiograph of Specimen Number 10-2 Subjected to Cyclic Loading at $\sigma = 36.20$ ksi, $f = 10$ Hz, Stress Ratio, $R = 0.1$

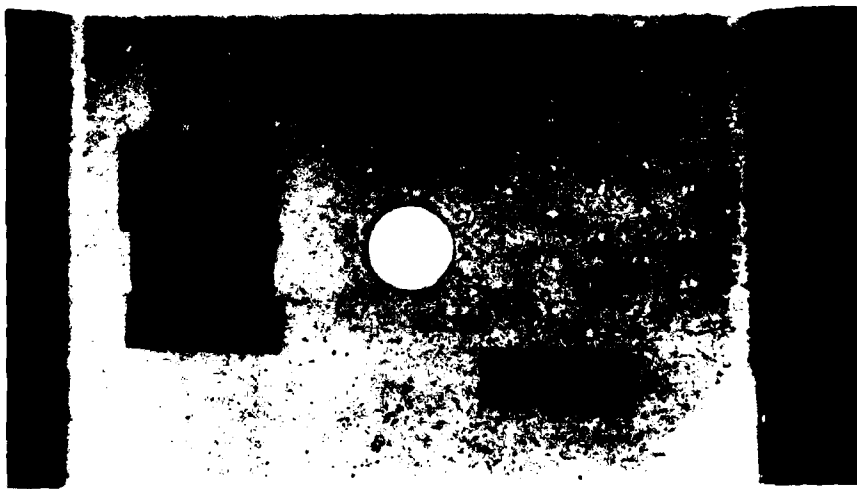
increase as the number of fatigue cycles increase. The delamination of 90° plies may also be seen along the edges of the specimen. In the radiographs of specimen No. 5-15, Figures 48(a) through 48(f), the gradual increase of the fiber fracture of +45° plies near the tabs, the delamination of 90° plies along the edges and the fracture of +45° plies around the hole may be seen.

E. Fatigue-Impact Tests

These tests were conducted in two ways: (a) the specimens were subjected to impact first followed by the fatigue cycling, and (b) the above sequence was reversed.

(a) Impact/Fatigue Tests

The objective of these tests was to find the effect of impact on the fatigue life of the specimens. The graphical representation of the resulting experimental data was expected to lie between the σ -N curve (Figure 46) corresponding to specimen with a clean hole (velocity = ∞) and the curve (Figure 18) corresponding to specimen subjected to fatigue loads alone (velocity = 0). Hence, the values of the applied stress and the impact velocity were chosen accordingly and the number of cycles the specimen could undergo after the impact was determined. In cases where the specimen survived a million fatigue cycles after impact, the test was stopped and the specimen was tested for its residual strength. The experimental data shown in Table X is plotted in Figure 49. This graph shows that most of the data points from the Impact/Fatigue tests do indeed lie in the region bounded by the notched and the unnotched σ -N curves.



(a) $N = 0$



(b) $N = 200,000$ cycles

Figure 48. Radiograph of Specimen Number 5-15 Subjected to Cyclic Loading at $\sigma = 35.87$ ksi, $F = 10$ Hz, Stress Ratio, $R = 0.1$

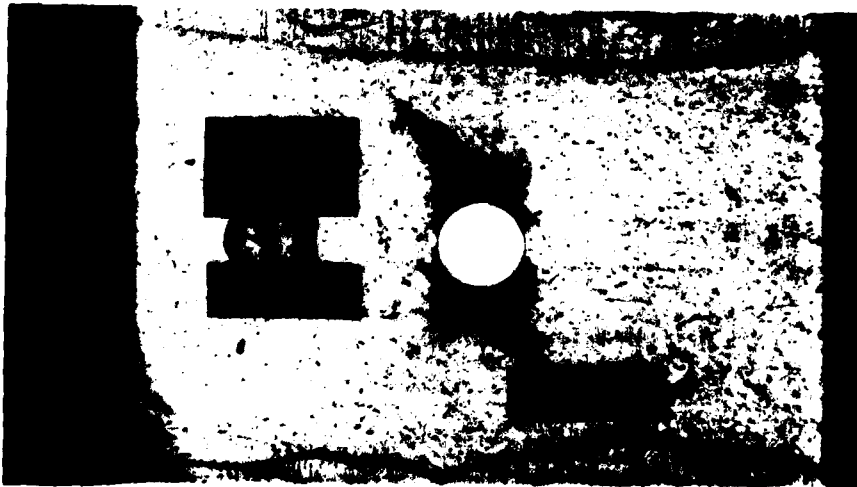


(c) N = 400,000 cycles

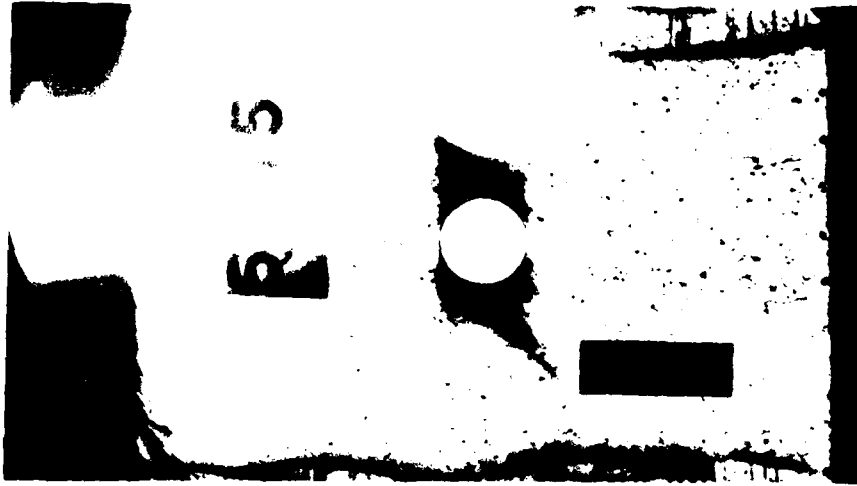


(d) N = 600,000 cycles

Figure 48. Radiograph of Specimen Number 5-15 Subjected to Cyclic Loading at $\sigma = 35.87$ ksi, $F = 10$ Hz, Stress Ratio, $R = 0.1$



(e) $N = 800,000$ cycles



(f) $N = 10^6$ cycles

Figure 48. Radiograph of Specimen Number 5-15 Subjected to Cyclic Loading at $\sigma = 35.87$ ksi, $F = 10$ Hz, Stress Ratio, $R = 0.1$

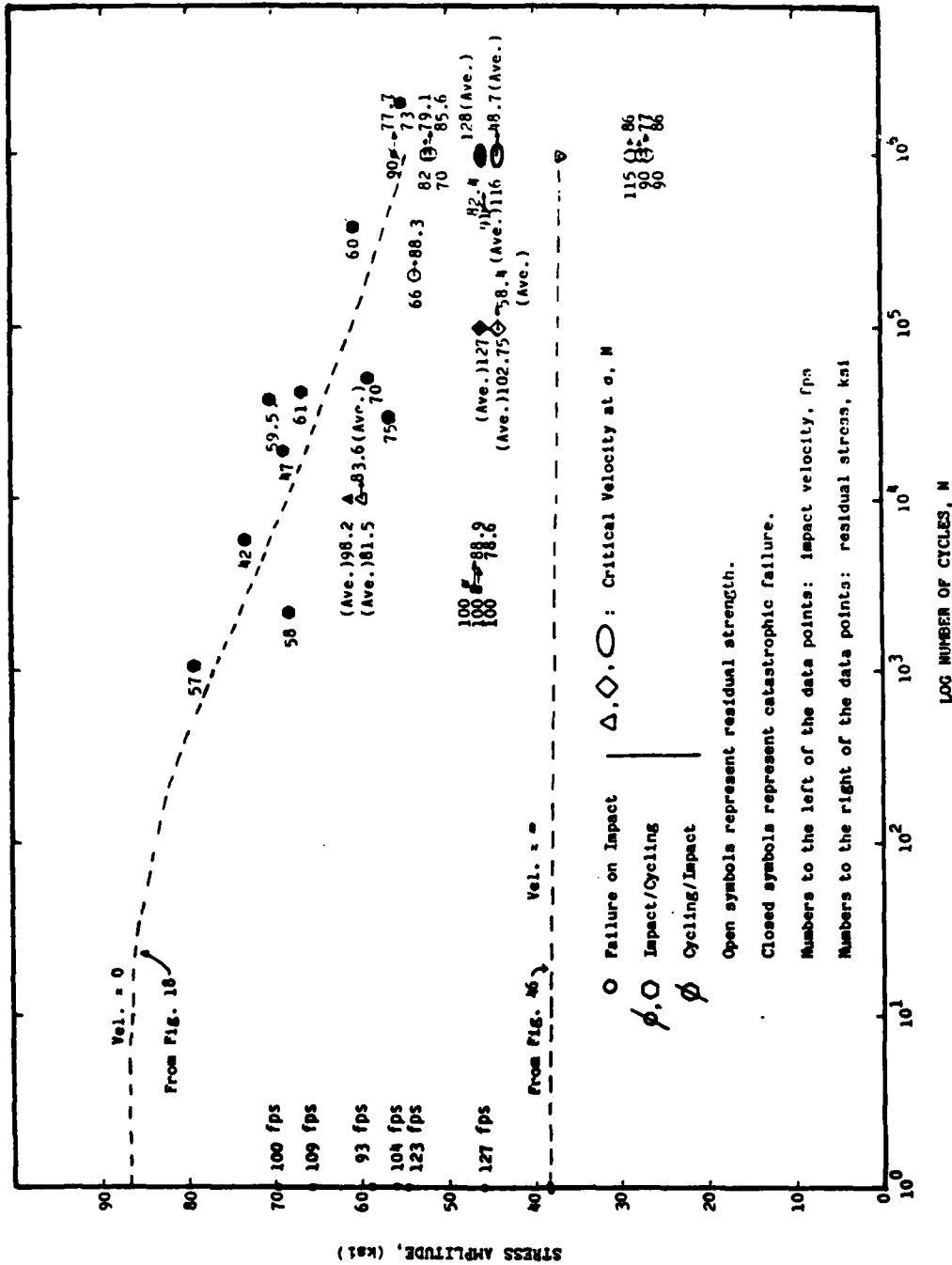


Figure 49. Impact/Fatigue, Fatigue/Impact, and Minimum Impact Velocity Studies.

As an extension of the above loading sequence (impact/cycle), it was decided to study the behavior of the laminate with reversed sequence of loading (cycle/impact/cycle, if necessary). Consequently, three combinations of the applied stress and velocity of impact values were selected. The specimen was first subjected to a predetermined number of fatigue cycles at which another specimen failed in a previous test. It was then impacted and the cyclic loading was continued if it did not fail on impact. Altogether three tests were conducted. It was found that the fatigue life is longer when the specimen is first subjected to cyclic loading and then impacted.

b. Fatigue/Impact Tests

These tests were conducted to determine the minimum velocity of impact which can cause catastrophic failure in a specimen at a particular applied stress level and after a particular number of fatigue cycles. Two stress levels, viz., 46 ksi (56% of σ_u) and 61 ksi (74% of σ_u) and three different number of cycles, viz., 10^4 , 10^5 and 10^6 up to which the specimen will be cyclic loaded were selected. On the average, about 7 specimens were tested for each test condition. Higher impact velocity was selected initially and then the velocity was gradually reduced to find the minimum velocity which could cause catastrophic failure of the specimen. The numerical results are shown in Table 11. The data points are plotted as shown in Figure 49.

The numerical values of the average minimum velocities are shown below:

<u>Applied Stress</u>	<u>No. of Cycles</u>	<u>Ave. Min. Velocity</u>
(ksi)	(N)	(ft/sec)
46	10^5	127
46	10^6	128
61	10^4	98.2

SECTION IX
CONCLUSIONS AND RECOMMENDATIONS

Based on the experimental work performed using a graphite/epoxy composite material system with an orientation and a stacking sequence of $(\pm 45, 0, 90)_2S$, the following conclusions may be drawn.

1. The residual strength of the impact-damaged laminates can be predicted using an analytical model. The correlation between the experimental and the analytical results was found to be good. Extensive experimental data is not necessary to use the analytical model.
2. Both the power law and the wearout models appear to be useful in predicting the fatigue life of the composite laminates. However, because of the slope parameter, the wearout model appears to have a slight edge over the power law model, particularly at low fatigue life and higher applied stress. The analytical and the experimental results were found to correlate well.
3. The strength degradation due to cyclic loading in notched laminates was found to be extremely small up to a million cycles. The residual strength of the fatigue-damaged laminates was found to increase (in proportion to the applied maximum stress with $R = 0.1$) after a million fatigue cycles.
4. Impact loading followed by cyclic loading was found to be more damaging (in reducing the life of the laminate) than the reversed sequence of loading.

5. The magnitude of the minimum projectile velocity causing catastrophic failure in the laminates tested was found as a function of the applied stress and the number of fatigue cycles.
6. The techniques used to document the damage in the impact- and fatigue-damaged specimens need further refinement.
7. The technique used to propel the projectile at a predetermined velocity needs further improvement.
8. The development of an analytical model is recommended to predict the minimum impact energy precipitating in a catastrophic failure of the composite materials subjected to cyclical loads.

REFERENCES

1. Reifsnider, K. L., "Fatigue of Composite Materials," ASTM Standardization News, p. 15, February 1980.
2. Ryder, J. T., "The Effect of Load History on Fatigue Life," Proceedings of the Fifth Annual Mechanics of Composites Review, AFWAL-TR-80-4020, p. 73, January 1980.
3. Ratwani, M. M., "Influence of Penetrants Used in X-Ray Radiography on Compression Fatigue Life of Graphite/Epoxy Laminates," Composites Technology Review, No. 1, Vol. 2, Winter, 1980.
4. Carlisle, J. G. "Hard Body Impact Damage Effects of Boron-Aluminum Composites," M.S. Thesis, USAF Institute of Technology, WPAFB, Ohio, March 1974.
5. Jaques, W., "Soft Body Impact Damage Effects on Boron-Aluminum Composites," M.S. Thesis, USAF Institute of Technology, WPAFB, Ohio, March 1974.
6. Husman, G. E., Whitney, J.M. and Halpin, J. C., "Residual Strength Characterization of Laminated Composites Subjected to Impact Loading," Foreign Object Impact Damage to Composites, STP 568, ASTM 1974, pp. 92-113.
7. Waddoups, M. E., Eisenmann, J. R., Kaminski, B. E., "Macroscopic Fracture Mechanics of Advanced Composite Materials," Journal of Composite Materials, Vol. 5, October 1971, pp. 446-454.
8. Nuismer, R. J. and Whitney, J. M., "Uniaxial Failure of Composite Laminates Containing Stress Concentrations," Fracture Mechanics of Composites, STP 593, ASTM, Philadelphia, 1975, pp. 117-142.
9. Yeow, Y. T., Morris, D. H. and Brinson, H. F., "A Correlative Study Between Analysis and Experiment on the Fracture Behavior of Graphite/Epoxy Composites," Journal of Testing and Evaluation, JTEVA, Vol. 7, No. 2, March 1979, pp. 117-125
10. Rhodes, M. D., "Impact Tests on Fibrous Composite Sandwich Structures," NASA TM-78719, National Aeronautics and Space Administration, Langley Research Center, Hampton, VA, October 1978.
11. Rhodes, M. D., "Impact Fracture of Composite Sandwich Structures," in Proceedings, ASME/AIAA/SAE, 16th Structural Dynamics and Materials Conference, Denver, CO, May 1975.

12. Sharma, A.V., "Effects of Low Velocity Projectile Impact on Strength of Composite Sandwich Structures," in Proceedings Fifth Inter-American Conference on Materials Technology, Sao Paulo, Brazil, November 1978.
13. Sharma, A.V., "Effects of Temperature on Composite Sandwich Structures Subject to Low Velocity Projectile Impact," Paper No. 78-WA/Aero-2, Winter Annual Meeting, The American Society of Mechanical Engineers, San Francisco, CA, December 1978.
14. Reifsnider, K. L., Stinchcomb, W. W. and O'Brien, T. K., "Frequency Effects on a Stiffness Based Fatigue Failure Criterion in Flawed Composite Specimens," Fatigue of Filamentary Composite Materials, ASTM STP 636, 1977, p. 171-184
15. Hahn, H. T. and Kim, R. Y. "Fatigue Behavior of Composite Laminates," J. Composite Materials, Vol. 10, April 1976.
16. Salkind, M. J., "Early Detection of Fatigue Damage in Composite Materials," J. Aircraft, Vol. 13, No. 10, 1973.
17. Dharan, C. K. H., "Fatigue Failure Mechanisms in an Unidirectionally Reinforced Composite Materials," ASTM STP 569, 1973.
18. Mullin, J., Berry, J. M., and Gatti, A., Journal of Composite Materials, Vol. 2, pp. 82-103, 1968.
19. Ryder, J. T., "The Effect of Compressive Loading on the Fatigue Lifetime of Graphite/Epoxy Laminates," Quarterly Progress Report No. 2, Contract No. F33(615)77-C-5045, Air Force Material Laboratory, 1977.
20. Street, K. W. and Ferle, J. P., Proceedings of 1975 International Conference on Composite Materials, Vol. 1, The Metallurgical Society of AIME, pp. 137-163, 1976.
21. Mills, G. J., Brown, G. and Waterman, D., Proceedings of 1975 International Conference on Composite Materials, Vol. 2, The Metallurgical Society of AIME, pp. 222-246, 1976.
22. Shimmin, K. D. and Toth, I. J. "On Failure Modes in Composites," Metallurgical Society of AIME, p. 357, 1973.
23. Scheirer, S. T. and Toth, I. J., "The Mechanical Behavior of Metal Matrix Composites," Technical Report AFML-TR-73-178, Air Force Materials Laboratory, 1973.
24. Swanson, G. D. and Hancock, J. R., Composite Materials Testing and Design (Second Conference) ASTM STP 497, American Society for Testing and Materials, pp. 469-482, 1972.

25. Hahn, H. T. "Fatigue Behavior and Life Prediction of Composite Laminates," April 1978, AD-4060 548 Air Force Materials Laboratory, Wright-Patterson AFB, Ohio.
26. Sturgeon, J. B., Proceedings of the 28th Annual Technical Conference, Society of Plastics Industry, December 12-13, 1973.
27. Sturgeon, J. B., "Fatigue Testing of Carbon Fiber Reinforced Plastics," Technical Report 75135, Royal Aircraft Establishment, England, 1975.
28. Halpin, J. C., Jerina, K. L. and Johnson, T. A., "Characterization of Composites for the Purpose of Reliability Function," Analysis of Test Methods for High Modulus Fiber and Composites, ASTM STP 521, American Society of Testing Materials, 1973, pp 5-64.
29. Hahn, H. T. and Kim, R. Y., "Proof Testing of Composite Materials," Vol. 9, 1975, pp 297-311.
30. Yang, J. N. and Lin, M. D., "Residual Strength Degradation Model and Theory of Periodic Proof Tests for Graphite/Epoxy Laminates," J. Composite Materials, Vol. 11, 1977, pp 176-203.
31. Hahn, H. T. and Tsai, S. W., "On the Behavior of Composite Laminates After Initial Failure," J. Composite Materials, Vol. 8, 1974, pp 288-305.
32. Tsai, S. W. and Hahn, H. T., "Failure Analysis of Composite Materials," Inelastic Behavior of Composite Materials, C. T. Harakovich, Ed., AMD, Vol. 13, ASME, 1975, pp 73-96.
33. Hahn, H. T., "Fatigue Behavior and Life Prediction of Composite Laminates," AFML-TR-78-43, April 1978.
34. Kim, R. Y., "Experimental Assessment of Static and Fatigue Damage of Graphite/Epoxy Laminates," Advances in Materials Proceedings 3rd Interconference on Composite Materials, Pergamon, 1980, pp 1015-1028.
35. Hahn, H. T. and Hwang, D. G., "Fatigue Behavior of Composite Laminates," November 1980, Washington University, St. Louis, Materials Research Laboratory.
36. Hashin, Z., "Fatigue Failure Criteria for Unidirectional Fiber Composites," AD-A088 733, NTIS, Pennsylvania University, Philadelphia, Department of Material Science and Engineering.

37. Sendeckyj, G. P., "Fitting Models to Composite Materials Fatigue Data," Test Methods and Design Allowables for Fibrous Composites, ASTM STP 734, C. C. Chamis, Ed., American Society for Testing and Materials, 1981, pp 245-260.
38. Yang, J. N. and Lin, M. D., "Residual Strength Degradation Model and Theory of Periodic Proof Tests for Graphite/Epoxy Laminates," AD-A040 077, NTIS, VPI & SU, Blacksburg, VA.
39. McLaughlin, P. V., Jr., Kulkarni, S. V., Huang, S. N. and Rosen, B. W., "Fatigue of Notched Fiber Composite Laminates," Part I: Analytical Model, NASA CR-132747, March 1975.
40. Ramkumar, R. L., Kulkarni, S. V. and Pipes, R. B., "Evaluation and Expansion of an Analytical Model for Fatigue of Notched Composite Laminates," Materials Sciences Corporation, Blue Bell, Pennsylvania, March 1978, p. 129.
41. Kulkarni, S. V., McLaughlin, P. V., Jr. and Pipes, R. B., "Fatigue of Notched Fiber Composite Laminates," Part II: Analytical and Experimental Evaluation, NASA CR-145039, April 1976.
42. Shutz, D., Gerharz, J. J. and Alschweig, E., "Fatigue Properties of Unnotched, Notched and Jointed Specimens of a Graphite/Epoxy Composite," Fatigue of Fibrous Composite Materials, ASTM STP 723, American Society for Testing and Materials, 1981, pp 31-47.
43. Whitney, J. M., Private Communication, Wright-Patterson Air Force Base, Ohio, 45433.
44. Avva, V. S., "Impact Initiated Damage in Laminated Composites," Final Report, September 30, 1982, AFOSR Contract No. F49620-80-C-0050, Department of Mechanical Engineering, North Carolina A&T State University, Greensboro, NC 27411.
45. Sendeckyj, G. P., "The Effect of Tetrabromoethane - Enhanced X-Ray Inspection on Fatigue Life of Resin-Matrix Composites," Composites Technology Review, No. 1, Vol. 2, Winter 1980.

APPENDIX A

IMPACT MODEL

In order to predict the residual strength of the impact-damaged laminates, the values of $2K$ and W_0 appearing in equation (e), p. 15 are to be evaluated using some of the experimental results. The equation (e),

$$(\sigma_r/\sigma_0) = [2K(W-W_0) + 1]^{-1/2}$$

may be re-written as

$$y = ax + b$$

where

$$y = (\sigma_0/\sigma_r)^2$$

$$x = W$$

$$a = 2K$$

$$b = (1 - 2K W_0)$$

By performing a few experiments with specimens subjected to impact at different velocities, the experimental values of the residual strength, σ_r , can be found. The stress ratio, σ_r/σ_u , was plotted as a function of the kinetic energy/unit laminate thickness of the projectile impact (forward velocity only) as shown in Figure 17. The notation used, σ_0 and σ_u , represent the same stress value (far-field or ultimate) in the laminate. Further, it may be remarked that the values of $2K$ and W_0 can be found by testing fewer specimens. The evaluation of the rebound velocities of the impacting projectile was not contemplated initially. However, as an after-thought, it was decided to apply the analytical model developed in another research project (44) to the current

experimental data. The graphical relationship between the forward and rebound velocities shown in Reference 44 is reproduced here shown as Figure 16 and the rebound velocities for the current results are estimated from this Figure 16. It may be noted that the rebound velocities shown in Figure 16 were obtained by testing a T300/5208 composite material with $(+45_2, -45_2, 0_2, 90_2)_s$ ply orientation and stacking sequence. Since the rebound velocity was observed to be about 10% of the magnitude of the forward velocity (44), the error introduced in assuming the rebound velocities as 10% of the forward velocities in the present results reported here was considered to be small.

The numerical values shown in the table below were obtained from the faired curve shown in Figure 17 .

REGRESSION TABLE TO EVALUATE CONSTANTS OF IMPACT MODEL

No.	$x = W$	$y = (\sigma_o/\sigma_r)^2$	x^2	xy
1	100	2.04	10,000	204
2	300	4.53	90,000	1,359
3	500	6.57	250,000	3,285
4	700	7.72	490,000	5,405
5	900	8.16	810,000	7,344
6	1,100	8.56	1,210,000	9,405
7	1,300	8.65	1,690,000	11,245
8	1,500	8.65	2,250,000	12,975
9	1,700	8.70	2,890,000	14,790
10	1,900	9.18	3,610,000	17,442
Σ	10,000	72.75	13,300,000	83,454

Using the method of least squares and linear regression analysis,
the following matrix representation is written:

$$\begin{vmatrix} \sum_1^n 1 & \sum_1^n x \\ \sum_1^n x & \sum_1^n x^2 \end{vmatrix} \begin{vmatrix} b \\ a \end{vmatrix} = \begin{vmatrix} \sum_1^n y \\ \sum_1^n (xy) \end{vmatrix}$$

Substituting numerical results from the table on the preceding page,
the above representation is written as,

$$\begin{vmatrix} 10 & 10 \times 10^3 \\ 10 \times 10^3 & 13.3 \times 10^6 \end{vmatrix} \begin{vmatrix} b \\ a \end{vmatrix} = \begin{vmatrix} 72.75 \\ 83,454 \end{vmatrix}$$

The above matrix results in the following equations:

$$b + 1000 a = 7.275$$

$$b + 1330 a = 8.345$$

Solving the above equations, the values of a and b are found to be

$$a = 0.0032 \text{ and } b = 4.075.$$

Using these values of a and b, the numerical values of 2K and W_0 are
found to be

$$2K = 0.032,$$

$$W_0 = -961 \text{ in-lb/in.}$$

The equation (e), p. 15, can now be re-written as

$$\sigma_r/\sigma_0 = [0.0032(W + 961) + 1]^{-1/2}$$

Knowing the values of σ_0 (far-field stress) and the kinetic energy of impact per unit laminate thickness, the residual strength of the laminate corresponding to any particular energy level of impact can be predicted. The analytical results thus obtained are represented in Figure 17.

APPENDIX B

FATIGUE MODEL

The wearout and the power law models discussed in detail in Reference 37 were briefly restated here on p. 16. The model parameters were calculated* using the present data (Table 8). A computer program (37) was used to perform the iterative computations. The seven columns in the data analysis tables (for both the wearout and power law models) refer to: data point number, maximum cyclic stress (SMAX), minimum cyclic stress (SMIN), number of cycles, residual strength (SRES), panel number, and test condition code (CODE). CODE = 1 designates static test data; CODE = 2 designates fatigue test data; and CODE = 1002 designates censored fatigue test data. The fatigue model parameters, given at the end of respective tables, were determined using two model fitting algorithms.

The probability of survival, $P(\sigma_e)$, as a function of the equivalent static strength, σ_e , data is shown in Figure 21 for the wearout model. The corresponding results for the power law model are shown in Figure 22. The basis in calculating the ordinates of the theoretical curve is equation (b), p. 16, in which the equivalent static strength, σ_e , values were assumed. On the other hand, equations (a) and (b), p. 16, were used (with $\sigma_r = \sigma_a$) to calculate the coordinates of the "experimental data" points shown in Figures 21 and 22. Appropriate numerical values (shown on the following pages) for the model parameters were utilized in using the equations (a) and (b), p. 16.

*The data reduction was performed by Dr. George P. Sendeckyj, Program Monitor for this contract.

Wearout Model: Data Tables

MATERIAL: T300/934 GRAPHITE-EPOXY

DATA FILE(S): AVVA

POINT	SMAX	SMIN	CYCLES	SRES	PANEL	CODE
1	77.96	0.00	1	77.96	12	1
2	83.21	0.00	1	83.21	12	1
3	93.17	0.00	1	93.17	12	1
4	80.03	0.00	1	80.03	10	1
5	73.04	0.00	1	73.04	11	1
6	87.70	0.00	1	87.70	13	1
7	79.50	0.00	1	79.50	7	1
8	71.84	0.00	1	71.84	9	1
9	94.05	0.00	1	94.05	12	1
10	92.27	0.00	1	92.27	7	1
11	76.69	0.00	1	76.69	5	1
12	34.09	3.41	1000000	71.18	9	2
13	33.94	3.39	800000	33.94	5	1002
14	34.09	3.41	1000000	93.20	8	2
15	34.09	3.41	1000000	84.81	12	2
16	34.09	3.41	1000000	87.25	9	2
17	40.72	4.07	1000000	73.67	6	2
18	40.36	4.04	1000000	78.37	7	2
19	40.72	4.07	1000000	82.29	9	2
20	40.18	4.02	1000000	80.59	1	2
21	40.36	4.04	1000000	84.94	10	2
22	44.84	4.43	1000000	58.57	13	1002
23	44.84	4.48	1000000	77.35	1	2
24	44.25	4.43	1000000	78.11	1	2
25	44.84	4.48	1000000	91.36	8	2
26	53.81	5.38	1000000	70.01	3	2
27	53.81	5.38	531500	53.31	1	2
28	52.40	5.24	106700	52.40	2	2
29	53.81	5.38	1000000	76.31	7	2
30	53.81	5.38	1000000	59.58	10	2
31	61.36	6.14	72730	61.36	12	2
32	59.73	5.97	187230	59.73	6	2
33	60.54	6.05	174370	60.54	10	2
34	59.73	5.97	264530	59.73	7	2
35	59.73	5.97	145360	59.73	7	2
36	63.74	6.37	122600	63.74	5	2
37	61.95	6.20	35400	61.95	1	2
38	61.95	6.20	23620	61.95	6	2
39	60.87	6.09	15140	60.87	13	2
40	63.35	6.34	4130	63.35	4	1002
41	66.67	6.67	18230	66.67	6	2
42	67.26	6.73	1040	67.26	2	2
43	67.26	6.73	23400	67.26	2	2
44	67.87	6.79	28340	67.87	3	2
45	67.37	6.79	8630	67.37	9	2

MATERIAL: T300/934 GRAPHITE-EPOXY Data File(s): Avva

POINT	SMAX	SMIN	CYCLES	SRES	PANEL	CODE
46	71.75	7.13	9870	71.75	3	2
47	71.75	7.13	2260	71.75	7	2
48	71.75	7.13	21670	71.75	2	2
49	71.75	7.13	5440	71.75	10	2
50	71.75	7.13	6720	71.75	5	2
51	76.92	7.69	160	76.92	13	2
52	76.23	7.62	200	76.23	3	2
53	76.23	7.62	1000	76.23	7	2
54	76.23	7.62	120	76.23	1	2
55	76.23	7.62	170	76.23	3	2
56	76.23	7.62	630	76.23	8	2
57	75.22	7.52	200	75.22	9	2
58	76.92	7.69	300	76.92	5	2
59	76.92	7.69	10	76.92	9	2
60	75.22	7.52	490	75.22	3	2
61	80.72	8.07	1000	80.72	5	2
62	80.72	8.07	310	80.72	9	2
63	81.82	8.18	330	81.82	3	2
64	79.65	7.97	10	79.65	3	2
65	81.45	8.15	710	81.45	9	2

Wearout Model: Parameter Estimates (Overall and panel-to-panel).

The parameters in the column, with heading least squares, were obtained by minimizing the sum of squares error for the equivalent static strength distribution. The parameters in the column, with heading max. shape, were obtained by maximizing the shape parameter. The same comments apply to the power law model parameters also. The values of the maximum shape parameters were used in plotting the numerical data.

WEAROUT MODEL - T-T, SMAX BASED WEIBULL PARAMETER ESTIMATES

	MAX SHAPE	LEAST SQUARES
"C" PARAMETER =	.010755	3.13163E-03
SLOPE PARAMETER =	.0499589	.0504578
SHAPE PARAMETER =	16.3578	15.2554
SCALE PARAMETER =	86.6087	83.9536
62 TH ROOT OF MAXIMUM LIKELIHOOD =	.0421038	.0416232
3 DATA POINTS CENSORED		

PANELS

MATERIAL: T300/934 GRAPHITE-EPOXY

DATA FILE(S): AVVA

POINT	SMAX	SMIN	CYCLES	SRES	PANEL	CODE
1	40.18	4.02	1000000	80.59	1	2
2	44.84	4.48	1000000	77.35	1	2
3	44.25	4.43	1000000	78.11	1	2
4	53.81	5.38	531500	53.81	1	2
5	61.95	6.20	35400	61.95	1	2
6	76.23	7.62	120	76.23	1	2

WEAROUT MODEL - T-T, SMAX BASED WEIBULL PARAMETER ESTIMATES

	MAX SHAPE	LEAST SQUARES
'C' PARAMETER =	5.24261E-03	4.64961E-03
SLOPE PARAMETER =	.0494278	.048161
SHAPE PARAMETER =	79.8717	71.1933
SCALE PARAMETER =	79.6417	79.1905
6 TH ROOT OF MAXIMUM LIKELIHOOD =	.21093	.203535
0 DATA POINTS CENSORED		

MATERIAL: T300/934 GEAPHITE-EPOXY

DATA FILE(S): AVVA

POINT	SMAX	SMIN	CYCLES	SRES	PANEL	CODE
1	53.81	5.38	1000000	70.01	3	2
2	67.87	6.79	28340	67.87	3	2
3	71.75	7.18	9870	71.75	3	2
4	76.23	7.62	200	76.23	3	2
5	76.23	7.62	170	76.23	3	2
6	75.22	7.52	490	75.22	3	2
7	81.82	8.18	330	81.82	3	2
8	79.65	7.97	10	79.65	3	2

WEAROUT MODEL - T-T, SMAX BASED WEIBULL PARAMETER ESTIMATES

	MAX SHAPE	LEAST SQUARES
'C' PARAMETER =	4.97722E-04	2.95288E-04
SLOPE PARAMETER =	.0642045	.0634608
SHAPE PARAMETER =	41.2883	36.6078
SCALE PARAMETER =	80.3002	79.1939
8 TH ROOT OF MAXIMUM LIKELIHOOD =	.106627	.106249
0 DATA POINTS CENSORED		

PANELS

MATERIAL: T300/934 GRAPHITE-EPOXY DATA FILE(S): AVVA

POINT	S _{MAX}	S _{MIN}	CYCLES	SRES	PANEL	CODE
1	76.69	0.00	1	76.69	5	1
2	33.94	3.39	800000	33.94	5	1002
3	63.74	6.37	122600	63.74	5	2
4	71.75	7.18	6720	71.75	5	2
5	76.92	7.69	300	76.92	5	2
6	80.72	8.07	1000	80.72	5	2

WEAROUT MODEL - T-T, S_{MAX} BASED WEIBULL PARAMETER ESTIMATES

	MAX SHAPE	LEAST SQUARES
"C" PARAMETER =	2.50924E-04	3.26514E-04
SLOPE PARAMETER =	.0669284	.0557165
SHAPE PARAMETER =	37.3759	35.023
SCALE PARAMETER =	79.6792	79.2594
5 TH ROOT OF MAXIMUM LIKELIHOOD =	.102861	.101277
1 DATA POINTS CENSORED		

MATERIAL: T300/934 GRAPHITE-EPOXY DATA FILE(S): AVVA

POINT	S _{MAX}	S _{MIN}	CYCLES	SRES	PANEL	CODE
1	40.72	4.07	1000000	73.67	6	2
2	59.73	5.97	187230	59.73	6	2
3	61.95	6.20	28620	61.95	6	2
4	66.67	6.67	18230	66.67	6	2

WEAROUT MODEL - T-T, S_{MAX} BASED WEIBULL PARAMETER ESTIMATES

	MAX SHAPE	LEAST SQUARES
"C" PARAMETER =	4.2885E-04	1.16348E-03
SLOPE PARAMETER =	.047989	.0396476
SHAPE PARAMETER =	78.2269	61.5504
SCALE PARAMETER =	73.563	74.2612
4 TH ROOT OF MAXIMUM LIKELIHOOD =	.190163	.17127
0 DATA POINTS CENSORED		

PANELS

MATERIAL: T300/934 GRAPHITE-EPOXY

DATA FILE(S): AVVA

POINT	S _{MAX}	S _{MIN}	CYCLES	SRES	PANEL	CODE
1	79.50	0.00	1	79.50	7	1
2	92.27	0.00	1	92.27	7	1
3	40.36	4.04	1000000	78.37	7	2
4	53.81	5.38	1000000	76.31	7	2
5	59.73	5.97	264530	59.73	7	2
6	59.73	5.97	145300	59.73	7	2
7	71.75	7.18	2260	71.75	7	2
8	76.23	7.62	1000	76.23	7	2

WEAROUT MODEL - T-T, S_{MAX} BASED WEIBULL PARAMETER ESTIMATES

	MAX SHAPE	LEAST SQUARES
"C" PARAMETER =	.0417203	7.53737E-03
SLOPE PARAMETER =	.046126	.0464321
SHAPE PARAMETER =	25.6053	18.6204
SCALE PARAMETER =	89.4583	85.3438
8 TH ROOT OF MAXIMUM LIKELIHOOD =	.0556201	.0514297
0 DATA POINTS CENSORED		

MATERIAL: T300/934 GRAPHITE-EPOXY

DATA FILE(S): AVVA

POINT	S _{MAX}	S _{MIN}	CYCLES	SRES	PANEL	CODE
1	71.84	0.00	1	71.84	9	1
2	34.09	3.41	1000000	71.18	9	2
3	34.09	3.41	1000000	87.25	9	2
4	40.72	4.07	1000000	82.29	9	2
5	67.87	6.79	8630	67.87	9	2
6	75.22	7.52	200	75.22	9	2
7	76.92	7.69	10	76.92	9	2
8	80.72	8.07	310	80.72	9	2
9	81.45	8.15	710	81.45	9	2

WEAROUT MODEL - T-T, S_{MAX} BASED WEIBULL PARAMETER ESTIMATES

	MAX SHAPE	LEAST SQUARES
"C" PARAMETER =	1.00593E-03	3.74908E-04
SLOPE PARAMETER =	.0887912	.0887696
SHAPE PARAMETER =	18.0711	16.9525
SCALE PARAMETER =	82.6004	81.1411
9 TH ROOT OF MAXIMUM LIKELIHOOD =	.0459475	.0459906
0 DATA POINTS CENSORED		

PANELS

MATERIAL: T300/934 GRAPHITE-EPOXY

DATA FILE(S): AVVA

POINT	S _{MAX}	S _{MIN}	CYCLES	SRES	PANEL	CODE
1	77.96	0.00	1	77.96	12	1
2	83.21	0.00	1	83.21	12	1
3	93.17	0.00	1	93.17	12	1
4	94.05	0.00	1	94.05	12	1
5	34.09	3.41	1000000	84.81	12	2
6	61.36	6.14	72730	61.36	12	2

WEAROUT MODEL - T-T, S_{MAX} BASED WEIBULL PARAMETER ESTIMATES

	MAX SHAPE	LEAST SQUARES
"C" PARAMETER =	.0625254	.135864
SLOPE PARAMETER =	.0468552	.0375061
SHAPE PARAMETER =	18.604	17.568
SCALE PARAMETER =	90.0365	89.2707
6 TH ROOT OF MAXIMUM LIKELIHOOD =	.0430665	.0425992
0 DATA POINTS CENSORED		

Power Law Model: Data Tables

MATERIAL: T300/934 GRAPHITE-EPOXY

DATA FILE(S): AVVA

POINT	SMAX	SMIN	CYCLES	SRES	PANEL	CODE
1	77.96	0.00	1	77.96	12	1
2	83.21	0.00	1	83.21	12	1
3	93.17	0.00	1	93.17	12	1
4	80.03	0.00	1	80.03	10	1
5	73.04	0.00	1	73.04	11	1
6	87.70	0.00	1	87.70	13	1
7	79.50	0.00	1	79.50	7	1
8	71.84	0.00	1	71.84	9	1
9	94.05	0.00	1	94.05	12	1
10	92.27	0.00	1	92.27	7	1
11	76.69	0.00	1	76.69	5	1
12	34.09	3.41	1000000	71.18	9	2
13	33.94	3.39	800000	33.94	5	1002
14	34.09	3.41	1000000	93.20	8	2
15	34.09	3.41	1000000	84.81	12	2
16	34.09	3.41	1000000	87.25	9	2
17	40.72	4.07	1000000	73.67	6	2
18	40.36	4.04	1000000	78.37	7	2
19	40.72	4.07	1000000	82.29	9	2
20	40.13	4.02	1000000	80.59	1	2
21	40.36	4.04	1000000	84.94	10	2
22	44.34	4.43	1000000	58.57	13	1002
23	44.34	4.43	1000000	77.35	1	2
24	44.25	4.43	1000000	78.11	1	2
25	44.24	4.43	1000000	91.36	8	2
26	53.31	5.33	1000000	70.01	3	2
27	53.31	5.38	531500	53.31	1	2
28	52.40	5.24	106700	52.40	2	2
29	53.31	5.38	1000000	76.31	7	2
30	52.31	5.33	1000000	59.53	10	2
31	61.36	6.14	72730	61.36	12	2
32	59.73	5.97	137230	59.73	6	2
33	60.54	6.05	174370	60.54	10	2
34	59.73	5.97	264530	59.73	7	2
35	59.73	5.97	145300	59.73	7	2
36	63.74	6.37	122600	63.74	5	2
37	61.95	6.20	35400	61.95	1	2
38	61.95	6.20	20620	61.95	6	2
39	60.37	6.09	15140	60.37	13	2
40	63.35	6.34	4130	63.35	4	1002
41	66.37	6.67	10220	66.37	6	2
42	67.23	6.73	1040	67.23	2	2
43	67.23	6.73	22400	67.23	2	2
44	67.37	6.79	20340	67.37	3	2
45	67.37	6.79	3630	67.37	9	2

MATERIAL: T300/934 GRAPHITE-EPOXY

POINT	SMAX	SMIN	CYCLES	SRES	PANEL	CODE
46	71.75	7.13	9870	71.75	3	2
47	71.75	7.13	2250	71.75	7	2
48	71.75	7.13	21670	71.75	2	2
49	71.75	7.13	5440	71.75	10	2
50	71.75	7.13	6720	71.75	5	2
51	76.92	7.69	160	76.92	13	2
52	76.23	7.62	200	76.23	3	2
53	76.23	7.62	1000	76.23	7	2
54	76.23	7.62	120	76.23	1	2
55	76.23	7.62	170	76.23	3	2
56	76.23	7.62	630	76.23	8	2
57	75.22	7.52	200	75.22	9	2
58	76.92	7.69	300	76.92	5	2
59	76.92	7.69	10	76.92	9	2
60	75.22	7.52	490	75.22	3	2
61	80.72	8.07	1000	80.72	5	2
62	80.72	8.07	310	80.72	9	2
63	81.82	8.18	330	81.82	3	2
64	79.65	7.97	10	79.65	3	2
65	81.45	8.15	710	81.45	9	2

Power Law Model: Parameter Estimates (Overall and panel to panel)

POWERLAW MODEL - T-T, SMAX BASED WEIBULL PARAMETER ESTIMATES

	MAX SHAPE	LEAST SQUARES
SLOPE PARAMETER =	.0270873	.023764
SHAPE PARAMETER =	14.6852	14.461
SCALE PARAMETER =	87.9372	86.405
62 TH ROOT OF MAXIMUM LIKELIHOOD =	.0363333	.0366253
3 DATA POINTS CENSORED		

SEQUIV = SAPPL*((SRES/SAPPL)^(1/SLOPE)+(CYCLES-1))^SLOPE

PANELS

MATERIAL: T300/934 GRAPHITE-EPOXY

DATA FILE(S): AVVA

POINT	S _{MAX}	S _{MIN}	CYCLES	SRES	PANEL	CODE
1	40.18	4.02	1000000	80.59	1	2
2	44.84	4.48	1000000	77.35	1	2
3	44.25	4.43	1000000	78.11	1	2
4	53.31	5.38	531500	53.31	1	2
5	61.95	6.20	35400	61.95	1	2
6	76.23	7.62	120	76.23	1	2

POWERLAW MODEL - T-T, S_{MAX} BASED WEIBULL PARAMETER ESTIMATES

	MAX SHAPE	LEAST SQUARES
SLOPE PARAMETER =	.0248156	.0262512
SHAPE PARAMETER =	22.4297	22.363
SCALE PARAMETER =	81.2131	81.7536
6 TH ROOT OF MAXIMUM LIKELIHOOD =	.0626938	.0624216
0 DATA POINTS CENSORED		

$$SEQUIV = SAPPL * ((SRES / SAPPL)^{(1/SLOPE)} + (CYCLES - 1))^{SLOPE}$$

MATERIAL: T300/934 GRAPHITE-EPOXY

DATA FILE(S): AVVA

POINT	S _{MAX}	S _{MIN}	CYCLES	SRES	PANEL	CODE
1	76.69	0.00	1	76.69	5	1
2	33.94	3.39	800000	33.94	5	1002
3	63.74	6.37	122600	63.74	5	2
4	71.75	7.18	6720	71.75	5	2
5	76.92	7.69	300	76.92	5	2
6	80.72	8.07	1000	80.72	5	2

POWERLAW MODEL - T-T, S_{MAX} BASED WEIBULL PARAMETER ESTIMATES

	MAX SHAPE	LEAST SQUARES
SLOPE PARAMETER =	6.85904E-03	.0120941
SHAPE PARAMETER =	17.4454	17.3143
SCALE PARAMETER =	79.6731	82.3739
5 TH ROOT OF MAXIMUM LIKELIHOOD =	.0474636	.046734
1 DATA POINTS CENSORED		

$$SEQUIV = SAPPL * ((SRES / SAPPL)^{(1/SLOPE)} + (CYCLES - 1))^{SLOPE}$$

PANELS

MATERIAL: T300/934 GRAPHITE-EPOXY

DATA FILE(S): AVVA

POINT	S _{MAX}	S _{MIN}	CYCLES	SRES	PANEL	CODE
1	79.50	0.00	1	79.50	7	1
2	92.27	0.00	1	92.27	7	1
3	40.36	4.04	1000000	78.37	7	2
4	53.81	5.38	1000000	76.81	7	2
5	59.73	5.97	264530	59.73	7	2
6	59.73	5.97	145300	59.73	7	2
7	71.75	7.18	2260	71.75	7	2
8	76.23	7.62	1000	76.23	7	2

POWERLAW MODEL - T-T, S_{MAX} BASED WEIBULL PARAMETER ESTIMATES

	MAX SHAPE	LEAST SQUARES
SLOPE PARAMETER =	.033313	.0263092
SHAPE PARAMETER =	18.5902	16.6156
SCALE PARAMETER =	90.6139	86.6707
8 TH ROOT OF MAXIMUM LIKELIHOOD =	.0427707	.0425711
0 DATA POINTS CENSORED		

$$SEQUIV = SAPPL * ((SRES / SAPPL)^{(1/SLOPE)} + (CYCLES - 1))^{SLOPE}$$